Single-Molecule Imaging of Active Mitochondrial Nitroreductases using a Photo-Crosslinking Fluorescent Sensor

Zacharias Thiel and Pablo Rivera-Fuentes*

Laboratorium für Organische Chemie, ETH Zürich, HCI G329, Vladimir-Prelog-Weg 3, 8093 Zürich (Switzerland).

pablo.rivera-fuentes@org.chem.ethz.ch

Abstract: Many biomacromolecules are known to cluster in microdomains with specific subcellular localization. In the case of enzymes, this clustering greatly defines their biological functions. Nitroreductases are enzymes capable of reducing nitro groups to amines and play a role in detoxification and pro-drug activation. Although nitroreductase activity has been detected in mammalian cells, the subcellular localization of this activity remains incompletely characterized. Here, we report a fluorescent probe that enables super-resolved imaging of pools of nitroreductase activity within mitochondria. This probe is activated sequentially by nitroreductases and light to give a photo-crosslinked adduct of active enzymes. In combination with a general photoactivatable marker of mitochondria, we performed two-color, three-dimensional, single-molecule localization microscopy. These experiments allowed us to image the sub-mitochondrial organization of microdomains of nitroreductase activity.

Fluorescence microscopy has become an indispensable tool for the study of intracellular localization and dynamics of enzymatic activity in living systems. Small-molecule fluorogenic probes for enzymatic activity usually consist of fluorescent dyes functionalized with groups that resemble the substrates of the enzyme and quench the fluorescence. Emission is restored upon enzymatic conversion of these functional groups, revealing the presence of active enzymes.[1,2] A commonly overlooked problem of these turn-on probes is the rapid diffusion of the fluorophores following enzymatic activation and the potential accumulation at intracellular locations that differ from the origin of activation. Hence, mapping the real subcellular distribution of enzymatic activity can be challenging and results can easily be misinterpreted. A possible way to minimize the unwanted diffusion of activated fluorophores and increasing the precision of localization of enzymatic activation is achieved by targeting the probe to certain organelles.[3–5] This strategy, however, assumes certain intracellular localization and enzymes that are active in other organelles might be neglected.

Another constraint of current fluorogenic probes is resolution, which is limited by diffraction of light. Even though super-resolution microscopy techniques such as stochastic optical reconstruction microscopy (STORM)[6] and photoactivation localization microscopy (PALM)[7] are well established, there is a lack of fluorescent sensors that are specifically optimized for

these techniques. We recently developed a sensing mechanism that is compatible with STORM.[8] We reported that photoactivatable diazoindanone-modified xanthene dyes bearing electron withdrawing substituents mainly form non-fluorescent photoproducts upon irradiation. Irradiation following enzymatic transformation of the substituent into an electron-donating group yields highly fluorescent photoproducts that display minimal diffusion.[8]

Herein, we apply this principle to develop a probe for the detection of nitroreductase activity in mammalian cells. Nitroreductases (NTRs) are a class of enzymes that catalyze the reduction of nitroaromatic compounds to their corresponding anilines.[9,10] NTRs are categorized into oxygen insensitive (Type I) and oxygen sensitive (Type II). These enzymes reduce nitro groups via an initial two electron or one electron step, respectively. The presence of Type II NTRs in tumors under hypoxic conditions is well established, and there are many fluorogenic methods for the detection of solid tumors based on this enzymatic activity.[11,12] Recently, probes were reported to detect mitochondrial NTR activity even under normoxic conditions, indicating the presence of Type I NTRs.[13] The role of NTRs in mammalian cells, however, remains unclear and their subcellular distribution is incompletely characterized. Some sources even report complete absence of NTR activity in non-cancerous cells.[14]

To characterize the subcellular distribution of NTR activity with nanometric precision, we designed photoactivatable probe **1** (Scheme 1). We envisioned that the nitro group of this diazoindanone-modified rhodamine analog would withdraw enough electron density to give mainly non-fluorescent products upon photoirradiation. Enzymatic conversion by NTRs, however, would produce the amino-substituted electron-rich xanthene derivative **2** (Scheme 1), which would yield a fluorescent product upon irradiation.

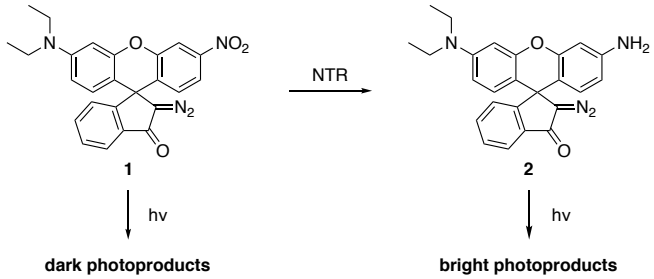

Scheme 1. Proposed mechanism for detecting NTR activity using photoactivatable probe **1**. NTR = nitroreductase.

We first tested the photochemistry of the probe before and after conversion of the nitro group, for which we prepared compounds **1** and **2** (Scheme S1 and S2). Solutions of **1** and **2** (10 µM in phosphate buffered saline (PBS), pH = 7.4/acetonitrile 1:1) did not display strong absorption

in the visible range or any fluorescence (Figures S1 and S2). These solutions were exposed to 350 nm light (8 lamps of 8 W each) for 15 min (Figure 1A and 1B). After irradiation, the solution of compound **1** did not display any measurable change in fluorescence (Figures 1B and S3), whereas a significant increase was observed when compound **2** was irradiated. The absorption and emission spectra of the irradiated solutions of compound **2** further confirmed the appearance of a prominent absorption band at 532 nm and a fluorescence emission band at 550 nm (Figures 1B and S4). These features suggest the formation of an emissive xanthene photoproduct. To confirm the identity of the putative photoproduct, we prepared compound **3** (Figure 1C), which we expected to be the major photoproduct.[8,15,16] Liquid chromatography coupled with mass spectrometry (LC-MS) confirmed that compound **3** is indeed the major photoproduct formed upon irradiation of **2** in water (Figure S5). Irradiation of **1**, however, produced a variety of unidentified non-fluorescent photoproducts (Figure S5) as indicated by the chromatogram of its irradiated solution. The photophysical properties and quantum yields of photoconversion are summarized in Table S1 and Figures S6 and S7. These data confirm that the formation of fluorescent photoproducts is strongly suppressed by the presence of the electron withdrawing nitro group.

Next, we tested the applicability of compound **1** as a probe for the detection of NTR activity in cuvettes using purified NTR from *E. coli* (NfsB, Figure 1D). A solution of **1** (10 μM in PBS, containing 500 μM NADH) was incubated with NTR (10 μg mL^{-1}) for 30 min and the fluorescence was determined before and after irradiation with 350 nm for 15 min. In presence of NTR, irradiation induces a significant increase in fluorescence. To exclude the possibility of the observed fluorescence increase arising from non-specific interactions with proteins,[17] **1** was treated with NTR in the absence of the cofactor NADH and with bovine serum albumin (10 μg mL^{-1}) prior to irradiation. No increase in fluorescence was detected in either case (Figure 1D). We also verified that the photoactivation outcome does not depend on the pH of the medium (Figure S8). The lack of fluorescence increase in absence of active NTR indicates that enzymatic transformation of **1** to **2** prior to photoactivation is necessary for fluorescence signal.

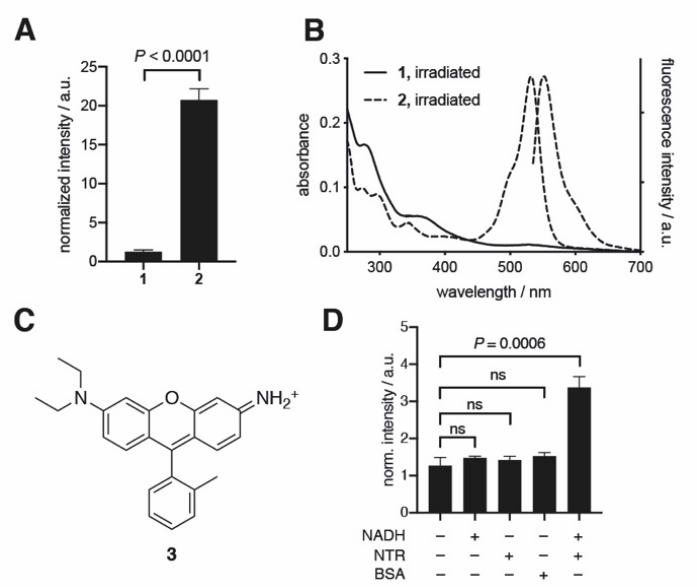

Figure 1. A) Fluorescence increase upon photoactivation of solutions of **1** and **2** in phosphate buffered saline pH = 7.4/acetonitrile 1:1. B) Absorbance and fluorescence emission spectra of irradiated (λ = 350 nm) solutions of **1** and **2.** C) Structure of the main fluorescent photoproduct formed by photolysis of **2**. D) Photoactivation of probe **1** in the presence of bacterial NTR, with and without the co-factor NADH, or only in the presence of BSA. In all cases bars are averages of independent measurements (*N* = 3) and error bars represent standard deviation. BSA = bovine serum albumin, ns: *P* > 0.05, NTR = nitroreductase.

Having confirmed the reactivity of compound **1** towards NTR, we evaluated its performance as a probe for NTR activity in live human embryonic kidney (HEK 293) cells using confocal fluorescence microscopy. Cells were incubated with compound **1** at a concentration of 10 μM for 10 min and subsequently exposed to 405 nm light (~80 mW, 10 s). Photoactivation led to a substantial increase in fluorescence signal (Figure 2A and 2B). Colocalization analysis using various genetically encoded organelle markers revealed that the signal obtained after photoactivation predominantly occurred in mitochondria (Figure 2C and S9), which agrees with previously reported targeted fluorescence reporters for NTR activity.[13]

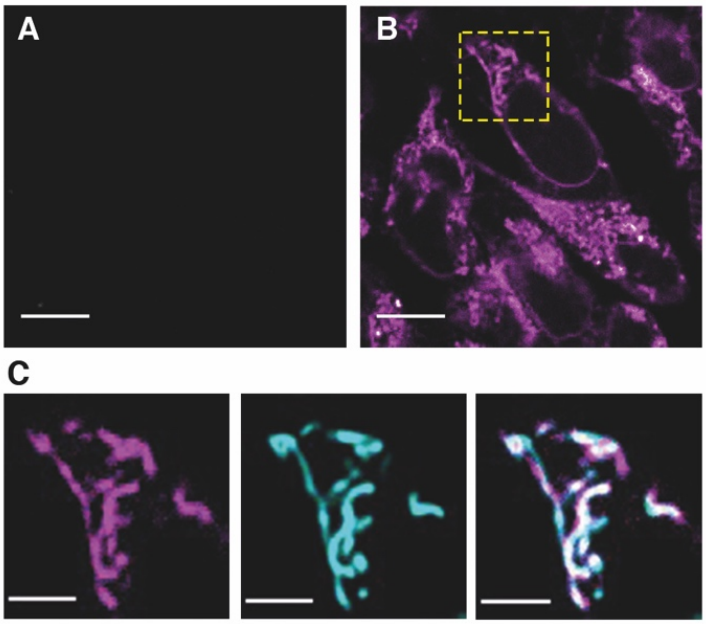

Figure 2 A) Live HEK 293 cells imaged with 561 nm excitation light after incubation with **1** (10 µM) for 10 min before photoactivation. B) Same cells as displayed in panel A imaged at 561 nm excitation light after exposure to 405 nm light (~80 mW, 10 s). C) Region of interest indicated with a yellow, dotted square in panel B. Imaged at 561 nm (photoactivated probe **1**, left), at 445 nm (mTurquoise2-COX8A, mitochondrial marker, center), and overlay of the photoactivated probe **1** and mitochondrial marker (right). Scale bars: 5 µm (panels A and B) and 2 µm (panels C).

The localization of enzymatic activity can be mistakenly assigned if the fluorogenic probe diffuses freely after enzymatic activation. Based on the mechanism of photoactivation of diazoindanones, we reasoned that the ketene intermediate that is formed during the photoinduced Wolff-rearrangement[16] could be readily trapped by nucleophilic side chains of proteins in its vicinity (Figure 3A). In order to validate this hypothesis, we investigated the propensity of **2** to form covalent adducts with amino acids upon irradiation in a cell-free environment. We irradiated **2** (100 µM in acetonitrile) in the presence of *N*-protected amino acids (5 mM). LC-MS analysis indicated that after 15 min of irradiation, compound **2** formed adducts with several amino acids bearing nucleophilic side chains, including cysteine, tyrosine, lysine, and histidine (Figure S10). Notably, when irradiated in aqueous solution, the reaction with amino acids was not observed because water is a competitive nucleophile that is present in large excess (Figure S10). Therefore, the ketene intermediate of compound **2** (Figure 3A) can only be trapped by nucleophiles that are present in close proximity immediately after photoactivation. We hypothesized that if the photochemical reaction occurs immediately after enzymatic conversion, the nitroreductase itself might be able to trap the ketene. To test this hypothesis, NTR from *E. coli* was incubated with **1** and immediately irradiated with 405 nm light. After

purification by gel electrophoresis, the band corresponding to NTR displays fluorescence at 602 ± 50 nm, whereas a non-irradiated control sample remains completely non-fluorescent. These data confirm that photoactivation immediately after the enzymatic transformation of **1** to **2** results in covalent modification of the activating enzyme with a fluorescent label.

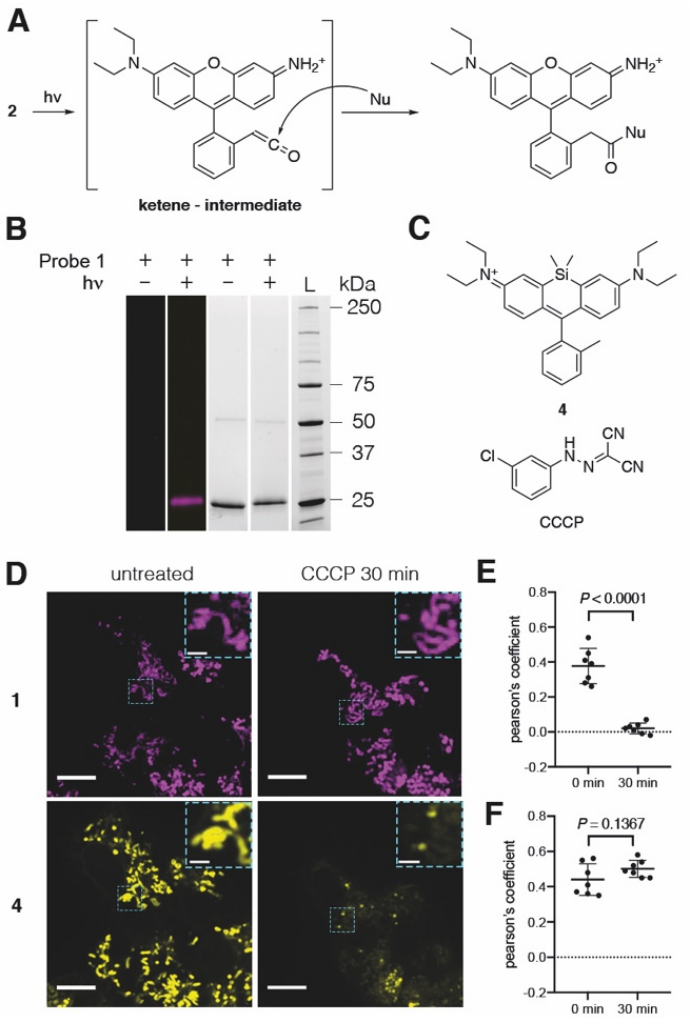

Figure 3. A) Proposed mechanism of photolysis of compound **2**, ketene formation and nucleophilic attack. B) Sodium dodecyl sulfate – polyacrylamide gel electrophoresis of NTR from *E. coli* crosslinked with fluorophores imaged at 602 ± 50 nm (dark lanes) and as stain-free gel image (white lanes). C) Structures of compound **4** and CCCP. D) Fluorescence images of live HEK 293 cells treated with compound **1** (10 µM, 10 min) imaged with 515 nm excitation light (magenta) and compound **4** (0.1 µM, 30 min) imaged with 640 nm excitation light (yellow) after exposure to 405 nm light (~80 mW, 10 s) before and 30 min after addition of CCCP (20 µM). Selected ROIs (dotted cyan squares) are displayed enlarged as insets. E) Colocalization between the signals obtained from compounds **1** and **4** in untreated cells before and 30 min after addition of CCCP (20 µM). F) Colocalization between the signals obtained from compounds **1** and **4** in control cells without addition of CCCP over a course of 30 min. Scale bars: 5 µm (panel D, insets: 1 µm). Graphs display individual values, averages, and standard deviations for $N = 7$ independent measurements from three biological replicates. Nu = nucleophile.

Although the probe is able to label the nitroreductase covalently, many molecules might still escape the proximity of the protein, react with water, and become a diffusible small molecule (Figure 3A). We noticed, however, that this small molecule has a very low quantum yield of emission in water. In contrast, the quantum yield of emission in apolar solvents is much higher (Figure S11). This fluorogenicity provides additional contrast for specific imaging of fluorophores covalently linked to proteins that provide an apolar environment.[18,19]

Encouraged by these results, we tested whether this covalent labeling also occurs in nitroreductases in live HEK 293 cells. We used 405 nm light to irradiate a small region of interest (ROI) within a cell that had been incubated with **1** and observed the diffusion of fluorescent molecules over a course of 10 min (Figure S12). Analysis of the signal revealed that the fluorescence stayed within the ROI, indicating minimal diffusion of the fluorophores formed by photoactivation of **2** within the cell. Lipophilic organic molecules carrying a permanent positive charge are known to be taken up and retained by mitochondria.[20,21] The fluorophore generated by photolysis of **2** carries a permanent positive charge, which makes it amenable for uptake and retention in mitochondria without covalent labeling. To exclude this possibility, we used the protonophore carbonyl cyanide *m*-chlorophenyl hydrazine (CCCP) to depolarize mitochondria, which induces dissipation of positively charged species.[22] Cells pretreated with **1** and the cationic dye **4**, which also localizes to mitochondria (Figure S13), were exposed to 405 nm light. Fluorescence images taken at 515 nm and 640 nm revealed that the signals of the two fluorophores colocalize with each other and with mitochondria (Figure 3D). Whereas addition of CCCP (20 μM) induced dissipation of compound **4** after 30 min, photoactivated compound **1** remained in mitochondria, resulting in a drastic decrease in the colocalization between compounds **1** and **4** (Figure 3E). Mitochondria of cells that were not treated with CCCP retained both compounds equally, resulting in no change in colocalization (Figure 3F). These data, together with the results of the previous experiments, confirm that **1** can be used to covalently label proteins in cells upon irradiation.

Photoactivatable probes that label proteins selectively are ideally suited for single-molecule localization microscopies such as STORM. Employing probe **1**, we set out to map the distribution of active nitroreductases within the mitochondria of live HEK 293 cells. In order to label mitochondria evenly and non-specifically, we prepared compound **5** (Figure 4A), a mitochondria-targeting,[23] far-red-emitting photoactivatable probe (Figure S14).[17] Using this compound and probe **1**, we performed two-color, three-dimensional STORM imaging. To minimize diffusion of compound **1** after enzymatic conversion and obtain super-imposable signals of the two imaging channels, we applied a 405 nm photoactivation pulse (100 μs),

followed by 40 alternating readout frames with 514 nm (50 ms) and 647 nm excitation (50 ms), respectively. This sequence was repeated every 4 s. From this acquisition, a super-resolved image of mitochondria as well as a super-resolved image of nitroreductase activity were reconstructed (Figure 4B) with average localization precisions of 40 ± 17 nm and 63 ± 18 nm, respectively. It must be mentioned that typical STORM experiments usually achieve better localization precisions (<20 nm), but most of these experiments employ fixed cells and do not report on the activity of the enzyme. In this case, imaging enzymatic activity requires live-cell STORM imaging and the localization precision in these experiments is generally eroded by motion blur. Nevertheless, our super-resolved images are able to distinguish domains of nitroreductase activity to a greater extent than diffraction-limited methods (Figure 4B).

These data revealed that nitroreductase activity occurs predominantly in mitochondria**.** This colocalization can be observed throughout the entire duration of image acquisition, even in moving mitochondria (Figure 4C – 4E). The enzymatic activity, however, does not appear to be evenly distributed within mitochondria but rather seems to cluster in certain regions. We used Voronoï tessellation[24] to identify clusters of active nitroreductases (Figure 4F and 4G) based on single-molecule signals. First, regions corresponding to mitochondria were identified using the signals generated by compound **5** (yellow regions in Figure 4H). Analysis of the signals generated by compound **1** (magenta regions in Figure 4H), gave clusters that overlap with the previously identified regions corresponding to mitochondria (white regions in Figure 4H). From these data, we conclude that nitroreductase activity is indeed mainly located within mitochondria, but it is not evenly distributed within these organelles. This experiment therefore reveals that mitochondrial nitroreductases cluster in domains of increased activity, and probe **1** is able to image these domains beyond the limit of diffraction of light.

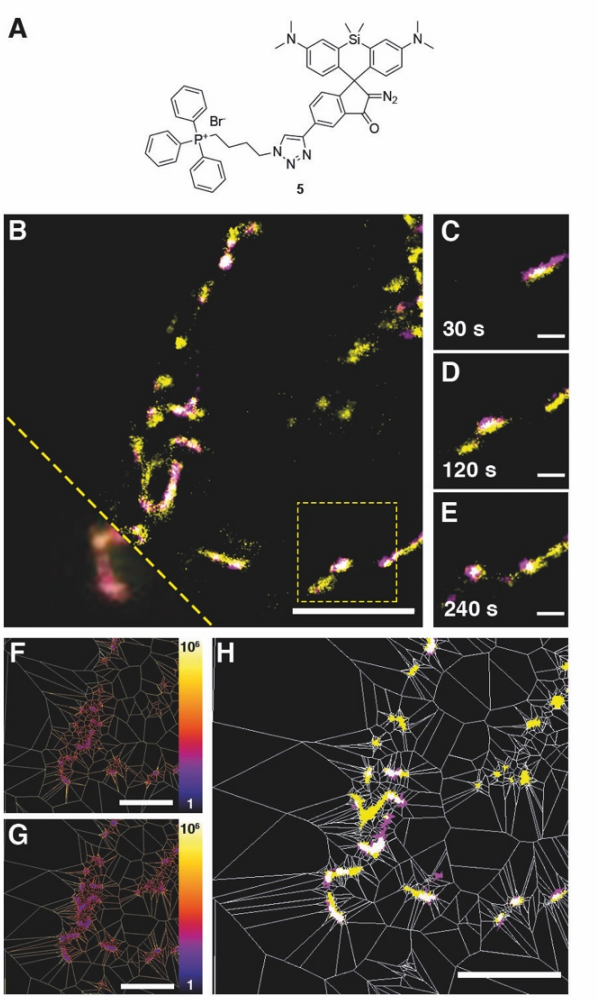

Figure 4. STORM super-resolution microscopy of nitroreductase activity in live HEK 293 cells. A) Structure of compound **5** used to label mitochondria evenly. B) Super-resolved image, reconstructed from 200 frames (20 s) of a cell treated with compound **1** (15 µM) in magenta and compound **5** (1 µM) in yellow. The image is displayed as a z-projection of the signals collected from a total depth of 1.6 µm. The diffraction limited counterpart is marked with the dashed yellow line in the lower left corner. C – D) Magnifications of the region outlined by the yellow rectangle in panel B at various time points. Each image was reconstructed from 100 frames (10 s). F) Voronoï tesselation of the signals obtained from compound **1** of the image displayed in panel B. G) Voronoï tesselation of the signals obtained from compound **5** of the image displayed in panel B. Polygons are colored according to their areas, see color bar (units: nm^2). H) Overlay of the identified clusters using the signals from compound **1** (magenta) and compound **5** (yellow). Scale bars = 5 µm (panels B, F, G, and H), 1 µm (panels C, D, and E).

In summary, we developed a probe that is activated by nitroreductases and generates a fluorescent photoproduct upon photoactivation. Furthermore, the probe covalently binds to

nucleophilic residues of proteins and does not diffuse freely during image acquisition. Using this photo-crosslinking, fluorogenic probe, we demonstrated that nitroreductase activity is observed in microdomains within mitochondria. It is not clear yet which enzymes display nitroreductase activity in mammalian mitochondria, but ongoing work in our lab is aimed at identifying them.

Acknowledgements

This work was supported by ETH Zurich. We thank Alina Tirla for the preparation of compound **4**, Dr. Nils Trapp for X-ray crystallography, and Dr. Dorothea Pinotsi for useful discussions.

Conflict of interest

The authors declare no conflicts of interest.

[1] J. B. Grimm, L. M. Heckman, L. D. Lavis, *Prog. Mol. Biol. Transl. Sci.* **2013**, *113*, 1–34.

[2] W. Chyan, R. T. Raines, *ACS Chem. Biol.* **2018**, *13*, 1810–1823.

[3] B. Huang, W. Chen, Y.-Q. Kuang, W. Liu, X.-J. Liu, L.-J. Tang, J.-H. Jiang, *Org. Biol. Chem.* **2017**, *15*, 4383–4389.

[4] R. S. Kathayat, P. D. Elvira, M. Z. Springer, L. E. Drake, *Nat. Commun.* **2018**, *9*, 334.

[5] M. N. Levine, T. T. Hoang, R. T. Raines, *Chem. Biol.* **2013**, *20*, 614–618.

[6] M. J. Rust, M. Bates, X. Zhuang, *Nat. Methods* **2006**, *3*, 793–795.

[7] E. Betzig, G. H. Patterson, R. Sougrat, O. W. Lindwasser, S. Olenych, J. S. Bonifacino, M. W. Davidson, J. Lippincott-Schwartz, H. F. Hess, *Science* **2006**, *313*, 1642–1645.

[8] E. A. Halabi, Z. Thiel, N. Trapp, D. Pinotsi, P. Rivera-Fuentes, *J. Am. Chem. Soc.* **2017**, *139*, 13200–13207.

[9] I. Oliveira, D. Bonatto, J. Antonio, P. Henriques, *Curr. Res., Technol. Ed. Top. Appl. Microbiol. Microb. Biotechnol.* **2010**, 1008–1019.

[10] M. D. Roldán, E. Pérez-Reinado, F. Castillo, C. Moreno-Vivián, *FEMS Microbiol Rev* **2008**, *32*, 474–500.

[11] L. Cui, Y. Zhong, W. Zhu, Y. Xu, Q. Du, X. Wang, X. Qian, Y. Xiao, *Org. Lett.* **2011**, *13*, 928–931.

[12] C. Xue, Y. Lei, S. Zhang, Y. Sha, *Anal. Methods* **2015**, *7*, 10125–10128.

[13] A. Chevalier, Y. Zhang, O. M. Khdour, J. B. Kaye, S. M. Hecht, *J. Am. Chem. Soc.* **2016**, *138*, 12009–12012.

[14] T. D. Gruber, C. Krishnamurthy, J. B. Grimm, M. R. Tadross, L. M. Wysocki, Z. J. Gartner, L. D. Lavis, *ACS Chem. Biol.* **2018**, *13*, 2888–2896.

[15] V. N. Belov, G. Y. Mitronova, M. L. Bossi, V. P. Boyarskiy, E. Hebisch, C. Geisler, K. Kolmakov, C. A. Wurm, K. I. Willig, S. W. Hell, *Chem. Eur. J.* **2014**, *20*, 13162–13173.

[16] V. N. Belov, C. A. Wurm, V. P. Boyarskiy, S. Jakobs, S. W. Hell, *Angew. Chem. Int. Ed.* **2010**, *49*, 3520–3523.

[17] J. B. Grimm, B. P. English, H. Choi, A. K. Muthusamy, B. P. Mehl, P. Dong, T. A. Brown, J. Lippincott-Schwartz, Z. Liu, T. Lionnet, L. D. Lavis, *Nat. Methods* **2016**, *13*, 985–988.

[18] B. E. Cohen, A. Pralle, X. Yao, G. Swaminath, C. S. Gandhi, Y. N. Jan, B. K. Kobilka, E. Y. Isacoff, L. Y. Jan, *Proc. Natl. Acad. Sci. U.S.A.* **2005**, *102*, 965–970.

[19] B. E. Cohen, T. B. McAnaney, E. S. Park, Y. N. Jan, S. G. Boxer, L. Y. Jan, *Science* **2002**, *296*, 1700–1703.

[20] R. W. Horobin, S. Trapp, V. Weissig, *J. Control. Release* **2007**, *121*, 125–136.

[21] S. Rin Jean, D. V. Tulumello, S. P. Wisnovsky, E. K. Lei, M. P. Pereira, S. O. Kelley, *ACS Chem. Biol.* **2014**, *9*, 323–333.

[22] R. C. Scaduto, L. W. Grotyohann, *Biophys. J.* **1999**, *76*, 469–477.

[23] J. Zielonka, J. Joseph, A. Sikora, M. Hardy, O. Ouari, J. Vasquez-Vivar, G. Cheng, M. Lopez, B. Kalyanaraman, *Chem. Rev.* **2017**, *117*, 10043–10120.

[24] F. Levet, E. Hosy, A. Kechkar, C. Butler, A. Beghin, D. Choquet, J.-B. Sibarita, *Nat. Methods* **2015**, *12*, 1065–1071.

Single-Molecule Imaging of Active Mitochondrial Nitroreductases using a Photo-Crosslinking Fluorescent Sensor

Supporting Information

Zacharias Thiel and Pablo Rivera-Fuentes*

Contents

General Methods

All reagents were purchased from commercial sources and used as received. Solvents were procured from Sigma-Aldrich and used as received. NMR spectra were acquired on Bruker AV300, Bruker 400 or Bruker 600 instruments. ^{1}H NMR chemical shifts are reported in ppm relative to $SiMe_4$ (δ = 0) and were referenced internally with respect to residual protons in the solvent (δ = 2.50 for $(CD_3)_2SO$, 7.24 for $CDCl_3$, and 3.35 for CD_3OD). Coupling constants are reported in Hz. ^{13}C NMR chemical shifts are reported in ppm relative to $SiMe_4$ (δ = 0) and were referenced internally with respect to solvent signal (δ = 39.5 for $(CD_3)_2SO$, 77.0 for $CDCl_3$, and 49.3 for CD_3OD). Peak assignments are based on calculated chemical shift, multiplicity, and 2D experiments. High-resolution mass spectrometry was conducted by staff at the Molecular and Biomolecular Analysis (MoBiAs) center (ETH Zurich) employing a Bruker maXIS ESI/NanoSpray-Qq-TOF-MS or a Bruker solariX ESI/MALDI-FTICR-MS instrument. Liquid Chromatography Mass Spectrometry experiments were performed on a Waters Acquity UPLC® with Zspray™ ESI SQ Detector 2. Solvent A: H_2O w. 0.1% HCOOH, Solvent B: acetonitrile. Linear gradient from A to B in 7 min. IUPAC names of all compounds are provided and were determined using CS ChemDraw Professional 16.0.

Optical Spectroscopy

Stock solutions in $(CH_3)_2SO$ were prepared at concentrations of 1 mM and stored at –20 °C in 0.1 mL aliquots and thawed immediately before each experiment. Spectroscopic measurements were conducted in phosphate-buffered saline (PBS) or PBS/acetonitrile 1:1. UV-visible spectra were acquired employing a Cary 500 Scan spectrometer using quartz cuvettes from ThorLabs (10 mm path length). Fluorescence spectra were acquired using a Fluorolog 3 fluorimeter (Horiba Jobin-Yvon) Plate reader experiments were carried out on a SPARK 10M, TECAN absorbance and fluorescence plate reader using black-wall, clear bottom, polystyrene costar® 96 Well Assay Plates with 100 µL volume (Corning Inc.). All measurements were conducted at room temperature and under red light ambient illumination to avoid unwanted photoactivation. Photoactivation was performed either on a custom-built transilluminator using 405 nm LEDs (2 mW cm^{-2}) or a Luzchem LZC-4V photoreactor with eight 350 nm lamps (each 8 W) and stirring. Fluorescence emission was measured before and after photoactivation and fluorescence intensity was obtained by integrating spectrum between 550 nm and 650 nm. The data were plotted as the fluorescence intensity normalized to the initial intensity (I = 1).

Quantum Yields of Photoactivation

Irradiations were performed in quartz cuvettes on 3 mL of 100 µM solutions of **1** and **2** in PBS/acetonitrile 1:1 under constant magnetic stirring. Every 10 minutes, the solutions were manually stirred by pipetting. An LED emitting at 405 nm (Roithner Lasertechnik, LED405-06V) was employed as light source. Light intensities were measured with a power-meter (Thorlabs, PM100D), equipped with a Si-photodiode detector (Thorlabs, S120VC). The light transmitted though the cuvette during the experiments was monitored. The number of absorbed photons was determined by the difference of the absorbed power measured for a blank sample and for the samples containing **1** and **2,** respectively, and the energy of a photon of 405 nm wavelength.

For HPLC analysis, 20 µL of the irradiated solution were diluted to 200 µL with PBS/acetonitrile 1:1, of which 100 µL were injected. A total of 6 time points with intervals of 20 min were taken during irradiation in order to build a trend line for the disappearance of starting materials and appearance of photoproducts. All measurements, as well as the calibration curves for the concentration of **1**, **2**, **3**, and **S12** were measured in triplicates.

The resulting chromatograms were exported as ASCII files and imported to Prism 8 (GraphPad). The area of the peaks was determined from which a baseline, obtained by injection of a blank sample, was subtracted. A linear fit of the areas obtained by injection of different concentrations of the known standards was calculated. The slope of this linear fit was

used to convert areas of the peaks obtained from the irradiation experiments into concentrations. The development of concentrations over time plotted and a linear fit was calculated to obtain rates in moles per minute. These rates were converted into molecules per minute and divided by the number of absorbed photons per minute to give the quantum yield of photoactivation $\Phi_{PA/DA}$.

Irradiation and Sodium Dodecylsulfate – Polyacrylamide Gel Electrophoresis of NTR

Stock solutions of nitroreductase from *E. coli* (NfsB, Sigma-Aldrich) were prepared in PBS at a concentration of 1 mg mL^{-1}, aliquoted, stored at –20 ºC, and thawed immediately before use. 500 µL solutions of NTR in PBS containing 500 µM NADH were prepared and incubated at 37 ºC for 10 min. The vials, containing the NTR were placed on a custom-built transilluminator (405 nm LEDs), positioned inside a thermocontrolled shaker (100 rpm) set to 37 ºC atmosphere. Compound **1** was added while illuminating the sample. The sample was irradiated for 20 min and immediately put on ice. The solution was transferred into Amicon® Ultra – 0.5 mL centrifugal filters equipped with Ultracel® 3K membranes and centrifuged at 15,000 g for 45 – 60 min until a final volume of approximately 50 µL was reached. The protein concentration was determined via a BCA assay. Aliquotes containing 5 µg protein were mixed with 12.5 µL 2x Laemmli sample buffer (Bio-Rad), containing 10% 2-mercaptoethanol and diluted with MilliQ H_2O to a final volume of 25 µL. These samples were incubated at 95 ºC for 5 min and loaded to Mini-Protean® TGX Stain-Free™ (Bio-Rad) 10-well comb precast gels. The gels were imaged using a ChemiDoc™ MP imaging system (Bio-Rad) with 602/50 nm fluorescence (green excitation) and stain-free imaging technology.

Cell Culture and Fluorescence Imaging

HEK 293 cells were grown in Dulbecco's Modified Eagle Medium (DMEM) supplemented with fetal bovine serum (FBS, 10%) and penicillin-streptomycin (1%) at 37 ºC in a 95% humidity atmosphere under 5% CO_2 environment. The cells were grown to 90% confluence before seeding at a density of 40,000 cells mL^{-1} onto Ibidi µ-Slide 8-well glass-bottom plates 48 h before the experiment. Prior to imaging, the growth medium was removed and the cells were rinsed with PBS (0.5 mL). A 10 µM solution of **1** in growth medium was added to the well and the cells were incubated for 10 min at 37 ºC. The solution was replaced with FluoroBrite™ DMEM (Thermo Fisher, 0.5 mL) and the cells imaged. Fluorescence images of cells were collected using a Nikon Eclipse T1 microscope equipped with a Yokogawa spinning-disk confocal scanner unit CSU-W1-T2, two sCMOS cameras (Orca Flash 4.0 V2) and a LUDL BioPrecision2 stage with piezo focus. The light sources were diode-pumped, solid-state lasers (DPSS): 405 nm (120 mW), 445 nm (100 mW), 515 nm (100 mW), and 651 nm (200 mW). All images were collected using a 100x CFI Apo TIRF (N. A. = 1.49) objective with oil-immersion. Emission was filtered using the following filters: DAPI (BP 450/50), CFP (BP 470/24), YFP (BP 535/ 0), RFP (BP 605/52), and mPlum (LP 655). The microscope was operated using VisiVIEW (Metamorph) software. The exposure time for acquisitions was kept constant for each series of images at each channel. Quantification of fluorescence intensity was performed using FIJI (ImageJ 1.51d, NIH). Fluorescence intensity was quantified by defining regions of interest (ROIs) comprising the whole cell body and recording the integrated intensity within this region. A ROI of the same size and shape was used to obtain the integrated intensity of the background (regions with no cells). This background was subtracted from the values obtained from the cell bodies. Significant outliers were identified by the ROUT method (Q = 1%) and excluded from further analysis. Data sets were analyzed by unpaired, two-tailed, Student's t-test. Results are presented as means, error bars represent standard deviations, and numerical *P* values are provided. Statistical analyses were carried out using Prism 8 (GraphPad).

Colocalization Experiments

HEK 293 cells were transfected using plasmids pmTurquoise2-ER, pmTurquoise2-Mito, or pmTurquoise2-Golgi (gift from Dorus Gadella, Addgene numbers 36204, 36208 and 36205, respectively).[7] Glycerol stocks of *E. coli* (DH5α) containing the desired plasmids were streaked on lysogeny broth (LB) agar plates containing kanamycin (50 mg mL^{-1}) and incubated for 24 h at 37 ºC. Single colonies were selected and inoculated in an LB liquid culture for 15 h. DNA plasmids were isolated using a QIAprep spin miniprep kit (Qiagen) using LyseBlue reagent. The identity of each plasmid was confirmed by DNA sequencing, which was performed by Microsynth AG (Balgach, Switzerland). Cells were transfected employing the jetPRIME kit (Polyplus) and incubated for 4 h at 37 ºC. Fresh growth medium was added after 5 h and incubated for 24 – 48 h. Compound **1** (10 µM) was added 10 min prior to photoactivation with 405 nm (120 mW, 70%, 10 s). Compound **4** (0.1 µM) was added 30 min prior to imaging. Pearson's correlation coefficients were determined using the plugin Colocalization Studio of the software ICY. A threshold was applied to exclude background and the colocalization was determined for each cell individually by selecting a region of interest ROI containing the whole cell. Notably, determination of colocalization was sometimes impaired by fast movement of the organelles between acquisition of the two channels resulting in decreased correlation coefficients.

Super-Resolution Microscopy and Image Analysis

HEK 293 cells were plated in phenol red-free medium (Gibco) three days before imaging. The medium was removed and refilled with phenol red-free medium (0.3 mL), containing compound **5** (1 µM). The cells were incubated for 10 min, washed with PBS (0.5 mL) and incubated with phenol red-free medium (0.15 mL). Compound **1** (30 µM in medium) was added to the cells (0.15 mL) 5 min prior to imaging. Cells were imaged using a Nikon N-STORM microscope (Nikon, UK Ltd.) equipped with an SR Apochromat TIRF 100x 1.49 N. A. oil immersion objective lens. Fluorescence was detected with a Hamamatsu Orca Flash 4 c3 (6.5 × 6.5 μm^2 pixel size). A built-in focus-lock system (perfect focus system) was used to prevent axial drift during data acquisition. The emission was collected and passed through a 514/640 TIRF-compatible dichroic filter cube that allows excitation at 514 nm and 640 nm and detection windows at 520–630 nm and 660–780 nm. The following laser powers were used: 405 nm (20 mW, 50%, 100 µs), 514 nm (23 mW, 80%, 50 ms) 647 nm (125 mW, 80%, 50 ms). An adaptive optics plug and play accessory MicAO 3dSR for SMLM (Imagine Optic, France) was inserted between the microscope side port and the camera. This unit was used to introduce a controllable and aberration-free astigmatism, which was used to perform 3D SMLM based on astigmatism based on the ellipticity of the point-spread function.[1] 3D calibration was performed with fluorescent 0.2 µm microspheres (TetraSpeck™, Invitrogen). Images were reconstructed using Thunderstorm[2] plugin of Fiji (ImageJ). Signals were detected searching the local intensity maxima in each frame, which were fit using an integrated Gaussian point spread function. Localizations with a localization precision above 100 nm were filtered out. A density filter regarding only those signals with at least 5 neighbors within the average localization precision was applied. Localizations with a z value higher than 800 nm and lower than –800 nm were filtered out. The remaining values were compressed to one plane for further analysis. The signals of 200 frames were exported as a text file and cluster (segmentation) analysis was performed using SR-Tesseler software.[3] Voronoï tessellation was applied to the image. Clusters were defined as regions with a local density δ^1_i (particles per unit of area) four times larger than the average density of the whole image.

Cell Viability Assay

Viability of HEK 293 cells after incubation with **1** was determined using a methylthiazolyldiphenyl-tetrazolium bromide (MTT) assay. Cells were seeded in a 96-well plate with each well containing 9,000 cells that were previously grown to 90% confluency. The cells were allowed to attach for 24 h in complete growth medium (containing 10% fetal bovine serum, FBS) prior to treatment with **1**. A solution of **1** (100 mM) in DMSO and diluted with growth medium, keeping the percentage of DMSO constant for each concentration (0.5%). Cells were treated with **1** at various concentrations between 150 µM

and 400 μM and incubated for 72 h at 37 °C under humidified atmosphere containing 5% CO_2. The cells were then treated with 10% MTT solution (5 g L^{-1}) in imaging medium (FluoroBrite) for 3 h. The supernatant was discarded and replaced with isopropanol (100 μL). The plates were shaken at 450 rpm in a microplate shaker and absorbance was recorded for each well using a plate reader. Duplicates of independent experiments with 6 individual replicates were measured. DMSO (0.5%) was used as positive control (100% viability). IC_{50} values were determined using PRISM 8 (GraphPad).

Supplementary Schemes

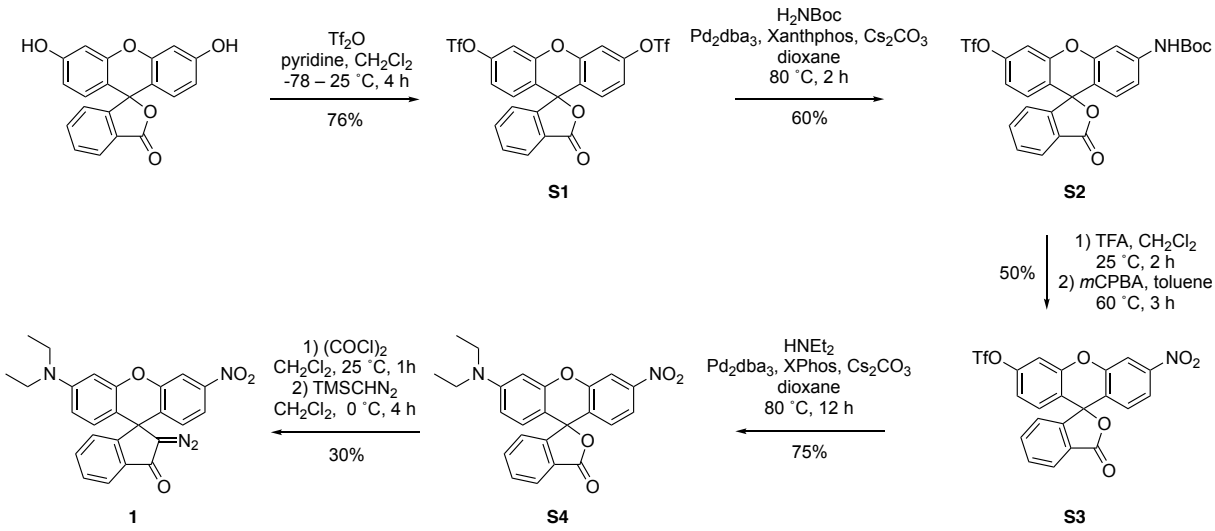

Scheme S1. Synthesis of probe **1.**

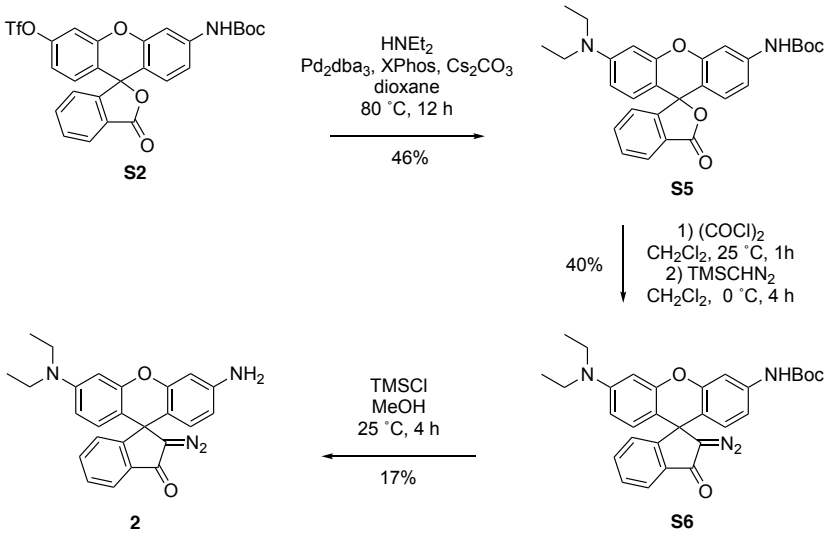

Scheme S2. Synthesis of probe **2.**

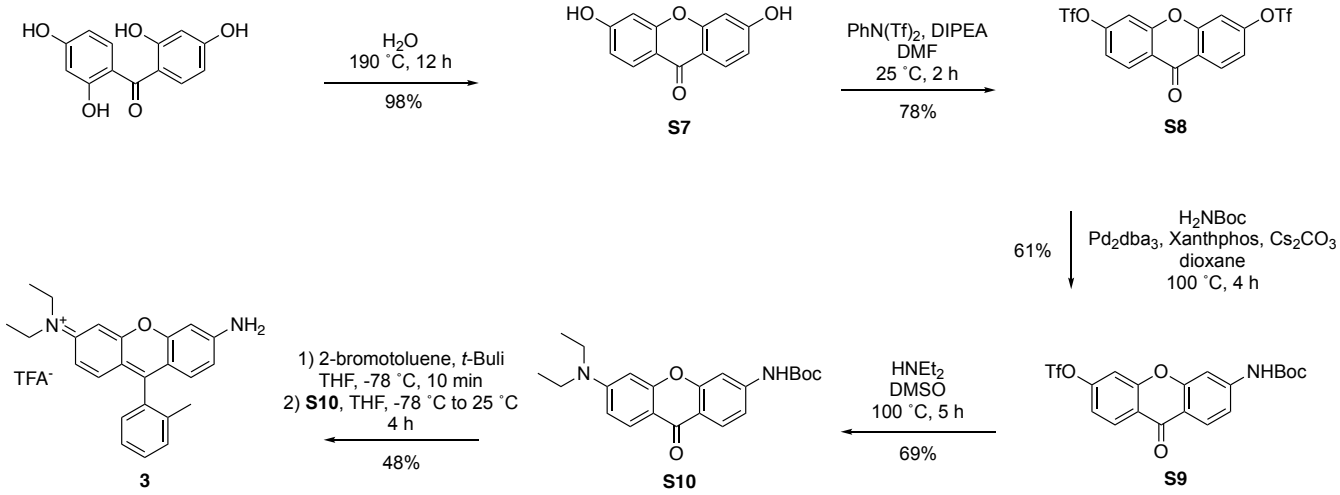

Scheme S3. Synthesis of probe **3.**

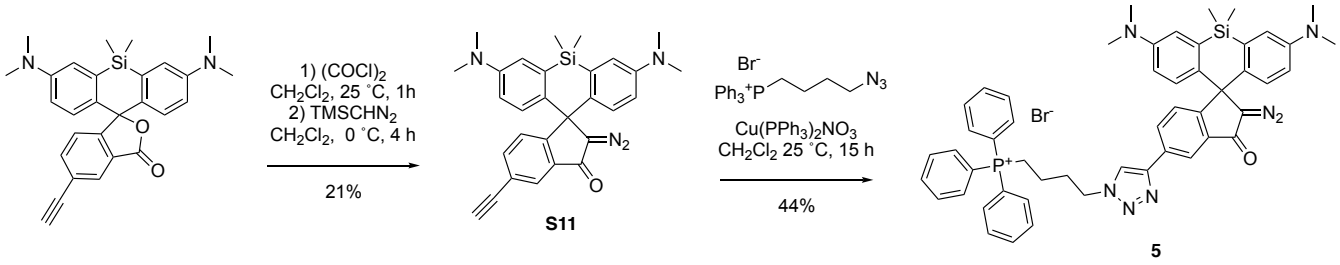

Scheme S4. Synthesis of probe **5**. The starting material was prepared as described before.[5]

Synthesis and Spectroscopic Characterization

Carbonyl cyanide *m*-chlorophenyl hydrazone (CCCP) is commercially available and compound **4** was prepared according to a published procedure.[4]

2-Diazo-3'-(diethylamino)-6'-nitrospiro[indene-1,9'-xanthen]-3(2*H*)-one (1)

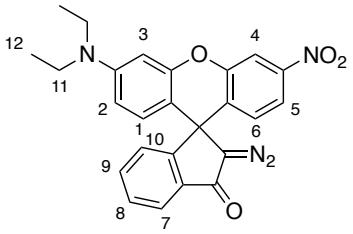

Compound **S4** (260 mg, 0.63 mmol), was dissolved in dry CH_2Cl_2 (2 mL) and oxalyl chloride (2 M in CH_2Cl_2, 470 µL, 0.94 mmol) was added. The reaction was stirred at 25 °C for 1 h and the volatiles were removed under vacuum. The residue was dissolved in dry CH_2Cl_2 (2 mL) and cooled to 0 °C in an ice bath. Triethylamine (125 µL, 0.94 mmol) and trimethylsilyl diazomethane (2 M in diethylether, 1.5 mL, 3.1 mmol) were added. The reaction was stirred at 0 °C for 4 h and the volatiles were removed under vacuum. The crude was purified via reverse phase column chromatography (H_2O/acetonitrile 1:1 to H_2O/acetonitrile 5:95) to give **1** as a dark yellow solid. (80 mg, 30%). ^{1}H NMR (400 MHz, $CDCl_3$) δ = 8.06 (d, *J* = 2.3 Hz, 1H, H4), 7.92 – 7.86 (m, 1H, H7), 7.80 (dd, *J* = 8.7 Hz, 2.3 Hz, 1H, H5), 7.60 – 7.41 (m, 2H, H8, H9), 7.15 – 7.02 (overlapping signals, 2H, H6 and H10), 6.71 (d, *J* = 8.8 Hz, 1H, H1), 6.45 (s, 1H, H3), 6.40 (s, 1H, H2), 3.36 (q, *J* = 7.1 Hz, 4H, H11), 1.19 (t, *J* = 7.1 Hz, 6H, H12). ^{13}C NMR (126 MHz, $CDCl_3$) δ = 186.5, 155.0, 151.8, 151.8, 149.1, 148.2, 135.1, 134.6, 129.8, 129.5, 129.2, 129.2, 128.7, 125.5, 122.9, 118.2, 113.1, 109.5, 105.6, 98.2, 49.3, 44.6, 12.7. HRMS (ESI) calcd. for $[C_{25}H_{21}N_4O_4]^+$, $[M + H]^+$: 441.1557, found: 441.1569

3'-Amino-2-diazo-6'-(diethylamino)spiro[indene-1,9'-xanthen]-3(2*H*)-one (2)

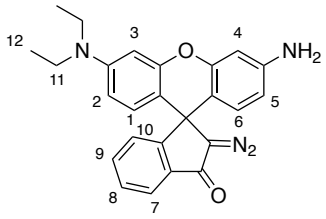

Compound **S6** (35 mg, 0.07 mmol), was dissolved in CH_3OH (1 mL) and chlorotrimethylsilane (8 µL, 0.06 mmol) was added. The reaction was stirred at 25 °C for 4 h. The reaction was stopped by addition of saturated aqueous $NaHCO_3$ (500 µL) and extracted with CH_2Cl_2. The organic phase was dried over anhydrous $MgSO_4$ and the volatiles were removed under vacuum. The residue was purified via flash column chromatography (SiO_2; CH_2Cl_2 100% to CH_2Cl_2/ethyl acetate 8:2) to give **2** as an orange solid (5 mg, 17%).^{1}H NMR (500 MHz, CD_3OD) δ = 8.55 (d, *J* = 7.5 Hz, 1H, H7), 8.40 (t, *J* = 7.6 Hz, 1H, H9), 8.30 (t, *J* = 7.5 Hz, 1H, H8), 7.83 (d, *J* = 7.7 Hz, 1H, H10), 7.42 (d, *J* = 9.4 Hz, 1H, H1), 7.33 (d, *J* = 8.5 Hz, 1H, H6), 7.25 – 7.16 (overlapping signals, 3H, H2, H3, H4), 7.08 (dd, *J* = 8.5 Hz, 2.3 Hz, 1H, H5), 4.12 (q, *J* = 7.1 Hz, 4H, H11), 1.88 (t, *J* = 7.0 Hz, 6H, H12). ^{13}C NMR (126 MHz, CD_3OD) δ = 195.8, 165.7, 161.3, 161.1, 159.1, 157.6, 144.8, 143.1, 138.2, 137.9, 137.7, 134.8, 131.4, 120.7, 117.8, 117.2, 109.7, 107.2, 84.0, 58.3, 53.2, 22.0. HRMS (ESI) calcd. for $[C_{25}H_{23}N_4O_2]^+$, $[M + H]^+$: 411.1816, found: 411.1821

3-Oxo-3*H*-spiro[isobenzofuran-1,9'-xanthene]-3',6'-diyl bis(trifluoromethanesulfonate) (S1)

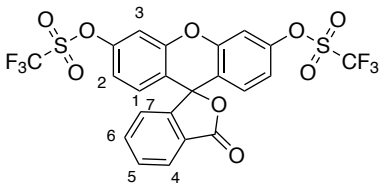

Fluorescein (3 g, 9 mmol) was dispersed in CH_2Cl_2 (200 mL) and cooled to –78 °C. Pyridine (3 mL) and triflic anhydride (4.5 g, 27 mmol) were added and the reaction was allowed to warm to 25 °C. The reaction was stirred for 4 h at 25 °C and washed three times with aqueous HCl (1 M, 50 mL). The organic phase was dried over anhydrous $MgSO_4$ and the volatiles were removed in vacuum, giving **S1** (4.1 g, 76%), which was used without further purification. ^{1}H NMR (400 MHz, $CDCl_3$) δ = 8.08 (ddd, *J* = 7.3 Hz, 1.4 Hz, 0.8 Hz, 1H, H4), 7.86 – 7.63 (m, 2H, H5, H6), 7.30 (dd, *J* = 2.4, 0.4 Hz, 2H, H3), 7.19 (ddd, *J* = 7.5 Hz, 1.2 Hz, 0.8 Hz, 1H, H7), 7.03 (dd, *J* = 8.8 Hz, 2.4 Hz, 2H, H2), 6.96 (dd, *J* = 8.8 Hz, 0.4 Hz, 2H, H1). ^{13}C NMR (101 MHz, $CDCl_3$) δ =

168.6, 152.3, 151.5, 150.4, 136.0, 130.8, 130.1, 125.9, 125.7, 123.9, 120.4, 119.4, 117.8, 117.2, 110.8, 80.2. LRMS (ESI) calcd. for $[C_{21}H_{11}F_3N_1O_8S_1]^+$, $[M + H]^+$: 597.0, found: 597.2

3'-((*tert*-Butoxycarbonyl)amino)-3-oxo-3*H*-spiro[isobenzofuran-1,9'-xanthen]-6'-yl trifluoromethanesulfonate (S2)

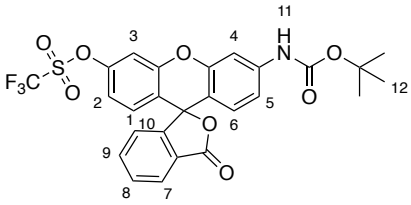

Compound **S1** (750 mg, 1.26 mmol), *tert*-butyl carbamate (73 mg, 0.63 mmol), tris(dibenzylideneacetone)dipalladium(0)·$CHCl_3$ (130 mg, 0.13 mmol), Xantphos (218 mg, 0.38 mmol), and Cs_2CO_3 (1147 mg, 3.50 mmol) were dissolved in dry dioxane and purged with N_2 for 15 min. The mixture was stirred at 80 °C for 2 h, cooled to room temperature and filtered over Celite. The filtrate was purified by flash column chromatography (SiO_2; CH_2Cl_2 100% to CH_2Cl_2/ethyl acetate = 9:1) to give **S1** as brown solid (425 mg, 60%) ^{1}H NMR (400 MHz, $CDCl_3$) δ = 8.13 – 7.98 (m, 1H, H7), 7.75 – 7.62 (m, 2H, H8 and H9), 7.59 (d, *J* = 2.2 Hz, 1H, H4), 7.23 (d, *J* = 2.4 Hz, 1H, H3), 7.15 (m, 2H, H10), 7.04 – 6.85 (overlapping signals, 3H, H1, H2, and H5), 6.72 (d, *J* = 8.6 Hz, 1H, H6), 6.61 (s, 1H, H11), 1.53 (s, 12H, H12). ^{13}C NMR (101 MHz, $CDCl_3$) δ = 169.1, 152.9, 152.3, 152.2, 151.5, 150.2, 141.1, 135.5, 130.3, 130.1, 128.7, 126.2, 125.5, 124.0, 120.4, 119.8, 117.2, 116.9, 114.9, 112.7, 110.7, 106.1, 81.5, 28.4. ^{19}F NMR (377 MHz, $CDCl_3$) δ = –72.7. HRMS (ESI) calcd. for $[C_{26}H_{21}F_3N_1O_8S_1]^+$, $[M + H]^+$: 564.0934, found: 564.0935

3'-Nitro-3-oxo-3*H*-spiro[isobenzofuran-1,9'-xanthen]-6'-yl trifluoromethanesulfonate (S3)

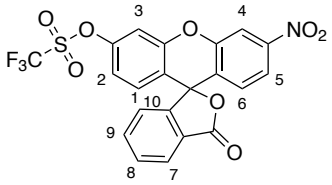

Compound **S2** (950 mg, 1.69 mmol) was dissolved in CH_2Cl_2 (3 mL) and trifluoroacetic acid (1 mL) was added. The mixture was stirred at room temperature for 2 h. Toluene (1 mL) was added and the volatiles were removed under vacuum. The crude solid was dissolved in toluene (10 mL) and 3-chloroperoxybenzoic acid (1460 mg, 8.4 mmol) was added. The mixture was stirred at 60 °C for 3 h. The volatiles were removed and the residue was purified by flash column chromatography (SiO_2; CH_2Cl_2/hexane = 7:3) to give **S3** as yellow solid (415 mg, 50%). ^{1}H NMR (300 MHz, $CDCl_3$) δ = 8.22 (d, *J* = 2.3 Hz, 1H, H4), 8.14 – 8.06 (m, 1H, H7), 7.94 (dd, *J* = 8.7 Hz, 2.3 Hz, 1H, H5), 7.81 – 7.64 (m, 2H, H8 and H9), 7.38 – 7.32 (m, 1H, H3), 7.20 – 7.14 (m, 1H, H10), 7.11 – 6.96 (overlapping signals, 3H, H1, H2, H6). ^{13}C NMR (101 MHz, $CDCl_3$) δ = 168.5, 152.5, 151.4, 150.8, 150.5, 149.3, 136.1, 131.0, 130.0, 129.4, 126.1, 125.3, 125.3, 123.7, 119.2, 119.1, 118.1, 113.3, 111.0, 79.9. ^{19}F NMR (282 MHz, $CDCl_3$) δ = –72.6. HRMS (ESI) calcd. for $[C_{21}H_{11}F_3N_1O_8S_1]^+$, $[M + H]^+$: 494.0152, found: 494.0142

3'-(Diethylamino)-6'-nitro-3*H*-spiro[isobenzofuran-1,9'-xanthen]-3-one (S4)

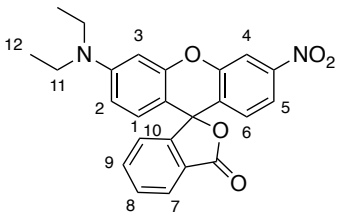

Compound **S3** (100 mg, 0.20 mmol), diethylamine (1.5 mL, 14.75 mmol), tris(dibenzylideneacetone)dipalladium(0)·$CHCl_3$ (21 mg, 0.02 mmol), XPhos (29 mg, 0.06 mmol), and Cs_2CO_3 (184 mg, 0.57 mmol) were dissolved in dry dioxane and purged with N_2 for 15 min. The mixture was stirred at 80 °C for 12 h in a sealed microwave flask, cooled to room temperature and filtered over Celite. The filtrate was purified by flash column chromatography (SiO_2; CH_2Cl_2 100%) to give **S4** as red solid (63 mg, 75%). ^{1}H NMR (300 MHz, $CDCl_3$) δ = 8.14 (d, *J* = 2.2 Hz, 1H, H4), 8.09 – 7.95 (m, 1H, H7), 7.82 (dd, *J* = 8.7 Hz, 2.3 Hz, 1H, H5), 7.76 – 7.57 (m, 2H, H8, H9), 7.22 – 7.13 (m, 1H, H10), 6.96 (d, *J* = 8.7 Hz, 1H, H6), 6.61 (d, *J* = 8.9 Hz, 1H, H1), 6.51 (s, 1H, H3), 6.42 (d, *J* = 9.3 Hz, 1H, H2), 3.38 (q, *J* = 7.1 Hz, 4H, H11), 1.19 (t, *J* = 7.0 Hz, 6H, H12). ^{13}C NMR (126 MHz, $CDCl_3$) δ = 169.2, 152.7, 152.6, 152.0, 148.9, 135.4, 130.2, 129.5, 129.3, 129.0, 127.4, 126.8, 126.2, 125.5, 124.0, 117.7, 113.0, 68.1, 44.8, 25.8, 24.0, 17.6, 12.6. HRMS (ESI) calcd. for $[C_{24}H_{21}N_2O_5]^+$, $[M + H]^+$: 417.1445, found: 417.1455

tert-Butyl (3'-(diethylamino)-3-oxo-3*H*-spiro[isobenzofuran-1,9'-xanthen]-6'-yl)carbamate (S5)

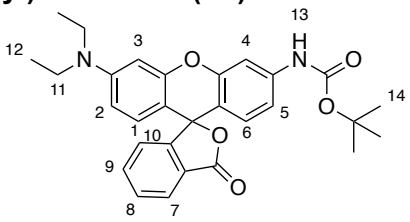

Compound **S2** (50 mg, 0.09 mmol), diethylamine (46 µL, 0.44 mmol), tris(dibenzylideneacetone)dipalladium(0)·$CHCl_3$ (10 mg, 0.01 mmol), XPhos (13 mg, 0.03 mmol), and Cs_2CO_3 (58 mg, 0.18 mmol) were dissolved in dry dioxane (2 mL) and purged with N_2 for 15 min. The mixture was stirred at 80 °C for 12 h in a sealed microwave flask, cooled to room temperature and filtered over Celite. The filtrate was purified by flash column chromatography (SiO_2; hexane/ethyl acetate 9:1 to hexane/ethyl acetate 3:1) to give **S5** as red solid (27 mg, 62%). ^{1}H NMR (400 MHz, $CDCl_3$) δ = 8.03 – 7.95 (m, 1H, H7), 7.64 (td, *J* = 7.4 Hz, 1.3 Hz, 1H, H9), 7.58 (td, *J* = 7.4 Hz, 1.1 Hz, 1H, H8), 7.48 (d, *J* = 2.2 Hz, 1H, H4), 7.21 – 7.14 (m, 1H, H10), 6.84 (dd, *J* = 8.6 Hz, 2.2 Hz, 1H, H5), 6.65 (d, *J* = 8.5 Hz, 1H, H6), 6.56 (d, *J* = 8.9 Hz, 1H, H1), 6.56 (s, 1H, H13), 6.43 (d, *J* = 2.6 Hz, 1H, H3), 6.35 (dd, *J* = 8.9 Hz, 2.6 Hz, 1H, H2), 3.36 (q, *J* = 7.1 Hz, 4H, H11), 1.52 (s, 9H, H14), 1.17 (t, *J* = 7.1 Hz, 6H, H12). ^{13}C NMR (101 MHz, $CDCl_3$) δ = 169.7, 153.2, 153.0, 152.4, 152.3, 149.6, 140.2, 134.7, 129.4, 128.8, 128.7, 127.2, 124.8, 124.1, 113.8, 113.6, 108.4, 106.0, 105.2, 97.7, 81.0, 44.5, 28.3, 12.5. HRMS (ESI) calcd. for $[C_{29}H_{30}N_2NaO_5]^+$, $[M + Na]^+$: 509.2047, found: 509.2043

tert-Butyl (2-diazo-3'-(diethylamino)-3-oxo-2,3-dihydrospiro[indene-1,9'-xanthen]-6'-yl)carbamate (S6)

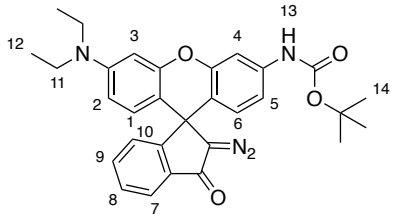

Compound **S5** (480 mg, 0.99 mmol), was dissolved in dry CH_2Cl_2 (5 mL) and oxalyl chloride (2 M in CH_2Cl_2, 740 µL, 1.48 mmol) was added. The reaction was stirred at 25 °C for 1 h and the volatiles were removed under vacuum. The residue was dissolved in dry CH_2Cl_2 (5 mL) and cooled to 0 °C in an ice bath. Trimethylsilyl diazomethane (2 M in diethylether, 3 mL, 6.0 mmol) was added. The reaction was stirred at 0 °C for 4 h and the volatiles were removed under vacuum. The crude was purified via flash column chromatography (SiO_2; hexane/CH_2Cl_2 2:8 to CH_2Cl_2 100%) to give **S6** as a dark yellow solid. (200 mg, 40%). ^{1}H NMR (400 MHz, $CDCl_3$) δ = 7.88 – 7.79 (m, 1H, H7), 7.53 – 7.36 (overlapping signals, 3H, H8, H9, H4), 7.11 – 7.02 (m, 1H, H10), 6.82 (dd, *J* = 8.6 Hz, 2.1 Hz, 1H, H5), 6.78 (d, *J* = 8.5 Hz, 1H, H6), 6.68 (d, *J* = 8.8 Hz, 1H, H1), 6.49 (s, 1H, H13), 6.38 (d, *J* = 2.6 Hz, 1H, H3), 6.32 (dd, *J* = 8.8 Hz, 2.6 Hz, 1H, H2), 3.34 (q, *J* = 7.1 Hz, 4H, H11), 1.52 (s, 9H, H14), 1.17 (t, *J* = 7.0 Hz, 6H, H12). ^{13}C NMR (101 MHz, $CDCl_3$) δ = 187.3, 156.1, 152.6, 152.3, 152.1, 148.7, 139.1, 134.8, 134.7, 128.8, 128.7, 128.6, 125.6, 122.4, 116.1, 114.1, 108.6, 107.1, 106.7, 98.4, 81.1, 77.4, 49.2, 44.5, 28.4, 12.8. HRMS (ESI) calcd. for $[C_{30}H_{31}N_4O_4]^+$, $[M + H]^+$: 511.2340, found: 511.2337

3,6-Dihydroxy-9*H*-xanthen-9-one (S7)

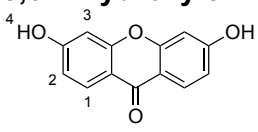

2,2',4,4'-Tetrahydroxybenzophenone (800 mg, 3.25 mmol) was dispersed in H_2O (5 mL) and heated to 190 °C for 12 h using a microwave reactor. The resulting solid was filtered, washed with hot water, and dried under vacuum to give **S7** as a pale-yellow solid (725 mg, 98%). ^{1}H NMR (400 MHz, $(CD_3)_2SO$) δ = 10.82 (s, 2H, H4), 7.98 (d, *J* = 8.7 Hz, 2H, H1), 6.86 (dd, *J* = 8.7 Hz, 2.2 Hz, 2H, H2), 6.82 (d, *J* = 2.2 Hz, 2H, H3). ^{13}C NMR (101 MHz, $(CD_3)_2SO$) δ = 173.92, 163.38, 157.48, 127.78, 114.00, 113.67, 102.10. HRMS (ESI) calcd. for $[C_{13}H_9O_4]^+$, $[M + H]^+$: 229.0495, found: 229.0497

9-Oxo-9*H*-xanthene-3,6-diyl bis(trifluoromethanesulfonate) (S8)

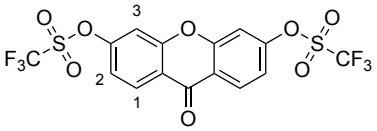

Compound **S7** (400 mg, 1.75 mmol) and 1,1,1-trifluoro-*N*-phenyl-*N*-((trifluoromethyl)sulfonyl)methanesulfonamide (1566 mg, 4.39 mmol) were dissolved in anhydrous DMF and (3 mL) and *N,N*-diisopropylethylamine (1.2 mL, 7 mmol) was added. The reaction was stirred for 2 h at 25 °C and diluted with CH_2Cl_2 (20 mL). The organic phase was washed with water (3 × 40 mL) and dried over anhydrous $MgSO_4$. The volatiles were removed under vacuum and the residue was purified via flash column chromatography (SiO_2; CH_2Cl_2/hexane 8:2) to give **S8** as a pale-yellow solid (670 mg, 78%). ^{1}H NMR (400 MHz, $CDCl_3$) δ = 8.44 (d, *J* = 8.8 Hz, 2H, H1), 7.49 (d, *J* = 2.3 Hz, 2H, H3), 7.35 (dd, *J* = 8.8 Hz, 2.3 Hz, 2H, H2). ^{13}C NMR (101 MHz, $CDCl_3$) δ = 174.67, 156.72, 153.49, 129.76, 121.52, 118.32, 111.57. ^{19}F NMR (377 MHz, $CDCl_3$) δ = –72.5. HRMS (ESI) calcd. for $[C_{15}H_7F_6O_8S_2]^+$, $[M + H]^+$: 492.9481, found: 492.9482.

6-((*tert*-Butoxycarbonyl)amino)-9-oxo-9*H*-xanthen-3-yl trifluoromethanesulfonate (S9)

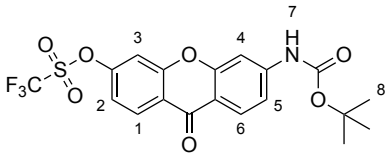

Compound **S8** (670 mg, 1.36 mmol), tris(dibenzylideneacetone)dipalladium(0)·$CHCl_3$ (12 mg, 0.01 mmol), Xanthphos (24 mg, 0.05 mmol) Cs_2CO_3 (881 mg, 2.72 mmol), and *tert*-butyl carbamate (159 mg, 1.36 mmol) were dissolved in anhydrous dioxane (3 mL) and stirred at 100 °C for 4 h. The reaction was diluted with CH_2Cl_2 and filtered over Celite. The volatiles were removed under vacuum and the residue was purified via flash column chromatography (SiO_2; CH_2Cl_2 100% to CH_2Cl_2/CH_2OH 95:5) to give **S9** as a pale-yellow solid (280 mg, 61%). ^{1}H NMR (400 MHz, $CDCl_3$) δ = 8.41 (d, *J* = 8.8 Hz, 1H, H1), 8.22 (d, *J* = 8.7 Hz, 1H, H6), 7.87 (d, *J* = 2.1 Hz, 1H, H4), 7.41 (d, *J* = 2.4 Hz, 1H, H3), 7.30 – 7.23 (dd, *J* = 8.7 Hz, 2.1 Hz, 1H, H2), 7.16 (dd, *J* = 8.7 Hz, 2.1 Hz, 1H, H5), 6.95 (s, 1H, H7), 1.55 (s, 12H, H8). ^{13}C NMR (101 MHz, $CDCl_3$) δ = 175.02, 157.68, 156.76, 152.89, 151.97, 145.27, 129.43, 128.00, 121.87, 117.30, 116.89, 115.30, 111.32, 105.42, 82.12, 28.38. ^{19}F NMR (377 MHz, $CDCl_3$) δ = –72.6. HRMS (ESI) calcd. for $[C_{19}H_{17}F_3NO_7S]^+$, $[M + H]^+$: 460.0672, found: 460.0676.

tert-Butyl (6-(diethylamino)-9-oxo-9*H*-xanthen-3-yl)carbamate (S10)

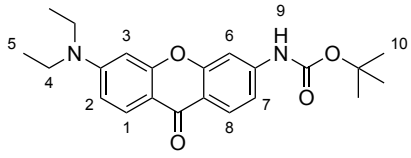

Compound **S9** (250 mg, 0.76 mmol) was dissolved in anhydrous dimethylsulfoxide (1.5 mL) and diethylamine (1 mL, 9.8 mmol) was added. The reaction was stirred at 100 °C in a sealed microwave flask for 5 h, cooled to 25 °C and diluted with CH_2Cl_2 (10 mL). The organic phase was washed with water (3 × 10 mL) and brine (10 mL) and dried over anhydrous $MgSO_4$. The volatiles were removed under vacuum and the residue was purified via flash column chromatography (SiO_2; CH_2Cl_2 100% to CH_2Cl_2/CH_3OH 98:2) to give **S10** as a pale-yellow solid (201 mg, 69%). ^{1}H NMR (400 MHz, $CDCl_3$) δ = 8.19 (d, *J* = 8.6 Hz, 1H, H8), 8.11 (d, *J* = 9.1 Hz, 1H, H2), 7.72 (d, *J* = 2.1 Hz, 1H, H6), 7.06 (dd, *J* = 8.7 Hz, 2.1, 1H, H7), 6.77 (s, 1H, H9), 6.68 (dd, *J* = 9.1 Hz, 2.5, 1H, H2), 6.46 (d, *J* = 2.5 Hz, 1H, H3), 3.47 (q, *J* = 7.1 Hz, 4H, H4), 1.55 (s, 9H, H10), 1.25 (t, *J* = 7.1 Hz, 6H, H5). ^{13}C NMR (101 MHz, $CDCl_3$) δ = 175.0, 158.8, 157.2, 152.6, 152.0, 143.3, 128.0, 127.4, 117.6, 113.8, 111.3, 109.2, 105.3, 96.3, 81.4, 44.8, 28.3, 12.5. HRMS (ESI) calcd. for $[C_{22}H_{26}N_2NaO_4]^+$, $[M + Na]^+$: 405.1785, found: 405.1787.

N-(6-Amino-9-(*o*-tolyl)-3*H*-xanthen-3-ylidene)-*N*-ethylethanaminium 2,2,2-trifluoroacetate (3)

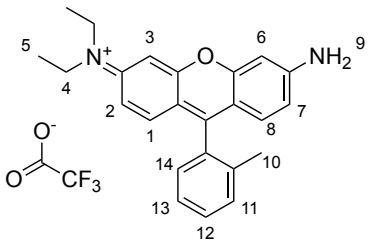

2-Bromotoluene (8 µL, 0.63 mmol) was dissolved in anhydrous tetrahydrofuran (3 mL) and cooled to –78 °C. *tert*-Butyllithium (1.7 M in pentane, 0.79 mL, 1.33 mmol) was added and the reaction stirred for 10 min. A solution of **S10** (60 mg, 0.16 mmol) in anhydrous tetrahydrofuran (3 mL) was added dropwise and the reaction was allowed to warm to 25 °C and stirred for 4 h. The reaction was diluted with aqueous HCl (1 N, 2 mL) and CH_2Cl_2 (10 mL). The organic phase was washed with brine and dried over anhydrous $MgSO_4$. The volatiles were removed under vacuum and the residue was dissolved in CH_2Cl_2 (5 mL). Trifluoroacetic acid (2 mL) was added and the reaction was stirred for 4 h at 25 °C. The volatiles were removed under vacuum and the residue was purified by reverse phase column chromatography (H_2O/acetonitrile + 0.1% trifluoroacetic acid 1:1 to 100% acetonitrile) to give **3** as a dark red solid (35 mg, 48%).^{1}H NMR (400 MHz, $(CD_3)_2SO$) δ = 8.18 (s, 2H, H9), 7.54 (m, 2H, H11, H12), 7.46 (td, *J* = 7.3 Hz, 1.5 Hz, 1H, H13), 7.28 (dd, *J* = 7.6 Hz, 1.3, 1H, H14), 7.12 (dd, *J* = 9.5 Hz, 2.5, 1H, H2), 7.06 (d, *J* = 2.4 Hz, 1H, H3), 7.03 (d, *J* = 5.7 Hz, 1H, H8), 7.01 (d, *J* = 6.0 Hz, 1H, H1), 6.89 (dd, *J* = 9.1 Hz, 2.1, 1H, H7), 6.83 (d, *J* = 2.1 Hz, 1H, H6), 3.65 (q, *J* = 7.1 Hz, 4H, H4), 2.01 (s, 3H, H10), 1.21 (t, *J* = 7.0 Hz, 6H, H5). ^{13}C NMR (101 MHz, $(CD_3)_2SO$) δ = 159.7, 157.7, 157.3, 156.8, 155.2, 135.4, 131.8, 131.7, 131.1, 130.5, 129.9, 128.9, 126.1, 117.2, 114.7, 113.0, 112.5, 97.1, 96.1, 45.3, 19.1, 12.5. ^{19}F NMR (377 MHz, $(CD_3)_2SO$) δ = –73.4. HRMS (ESI) calcd. for $[C_{24}H_{25}N_2O]^+$, $[M]^+$: 357.1961, found: 357.1962.

2'-Diazo-3,7-bis(dimethylamino)-5'-ethynyl-5,5-dimethyl-5*H*-spiro[dibenzo[*b*,*e*]siline-10,1'-inden]-3'(2'*H*)-one (S11)

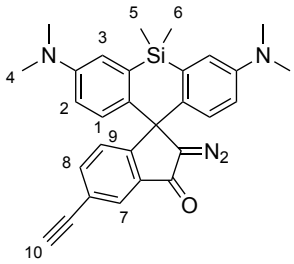

3,7-Bis(dimethylamino)-5'-ethynyl-5,5-dimethyl-3'*H*,5*H*-spiro[dibenzo[*b*,*e*]siline-10,1'-isobenzofuran]-3'-one (70 mg, 0.15 mmol), was dissolved in dry CH_2Cl_2 (2 mL) and oxalyl chloride (2 M in CH_2Cl_2, 110 µL, 0.23 mmol) was added. The reaction was stirred at 25 °C for 1 h and the volatiles were removed under vacuum. The residue was dissolved in dry CH_2Cl_2 (2 mL) and cooled to 0 °C in an ice bath. Triethylamine (30 µL, 0.23 mmol) and trimethylsilyl diazomethane (2 M in diethylether, 0.58 mL, 1.2 mmol) were added. The reaction was stirred at 0 °C for 4 h and the volatiles were removed under vacuum. The crude was purified via flash column chromatography (SiO_2; CH_2Cl_2 100% to CH_2Cl_2/ethyl acetate 9:1) to give **S11** as a dark yellow solid. (15 mg, 21%). ^{1}H NMR (500 MHz, $CDCl_3$) δ = 7.97 (d, *J* = 1.6, 1H, H7), 7.51 (dd, *J* = 8.0 Hz, 1.6 Hz, 1H, H8), 6.87 (d, *J* = 8.0 Hz, 1H, H9), 6.85 (d, *J* = 2.9 Hz, 2H, H3), 6.82 (d, *J* = 9.0 Hz, 2H, H1), 6.64 (dd, *J* = 9.0 Hz, 3.0 Hz, 2H, H2), 3.11 (s, 1H, H10), 2.97 (s, 12H, H4), 0.60 (s, 3H, H5 or H6), 0.49 (s, 3H, H5 or H6). ^{13}C NMR (126 MHz, $CDCl_3$) δ = 187.3, 157.9, 148.5, 138.0, 135.3, 134.7, 132.5, 130.2, 126.4, 125.5, 122.0, 115.6, 115.3, 82.8, 57.3, 40.4, 1.1, 0.3. HRMS (ESI) calcd. for $[C_{29}H_{29}N_4OSi]^+$, $[M+H]^+$: 477.2105, found: 477.2104.

(4-(4-(2'-Diazo-3,7-bis(dimethylamino)-5,5-dimethyl-3'-oxo-2',3'-dihydro-5*H*-spiro[dibenzo[*b*,*e*]siline-10,1'-inden]-5'-yl)-1*H*-1,2,3-triazol-1-yl)butyl)triphenylphosphonium bromide (5)

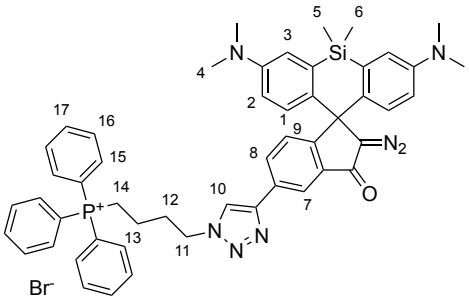

Compound **S11** (10 mg, 0.02 mmol), (4-azidobutyl)triphenylphosphonium bromide (8.8 mg, 0.02 mmol) and $[Cu(PPh_3)_2]NO_3$ (13 mg, 0.02 mmol) were dissolved in anhydrous CH_2Cl_2 (1 mL) and stirred at 25 °C for 15 h. The solution was washed with water (3 × 1 mL) and the volatiles were removed under vacuum. The residue was purified via reverse phase column chromatography (H_2O/acetonitrile 1:1 to acetonitrile 100%) to give **5** as a brown solid. (8 mg, 44%). ^{1}H NMR (300 MHz, $CDCl_3$) δ = 8.44 (s, 1H, H10), 8.27 (d, *J* = 1.5 Hz, 1H, H7), 7.96 (dd, *J* = 8.1 Hz, 1.7 Hz, 1H, H8), 7.85 – 7.49 (m, 15H, H15, H16, H17), 7.08 (d, *J* = 2.7 Hz, 2H, H3), 6.97 (d, *J* = 8.2 Hz, 1H, H9), 6.93 (d, *J* = 9.0 Hz, 2H, H1), 6.80 (dd, *J* = 9.0 Hz, 2.8 Hz, 2H, H2), 4.73 (t, *J* = 5.7 Hz, 2H, H11), 3.86 (m, 2H, H13), 3.01 (s, 12H, H4), 2.43 (t, *J* = 5.7 Hz, 2H, H12), 1.60 (m, 2H, H14), 0.64 (s, 3H, H5 or H6), 0.52 (s, 3H, H5 or H6). ^{13}C NMR (126 MHz, $CDCl_3$) δ = 187.82, 156.80, 146.73, 135.72, 135.26, 135.24, 135.13, 133.84, 133.76, 132.72, 131.27, 130.68, 130.58, 130.52, 125.99, 121.97, 119.78, 118.40, 117.72, 116.52, 79.27, 57.24, 48.86, 41.49, 29.93, 29.79, 22.19, 21.78, 19.09, 1.15, 0.21. ^{31}P NMR (202 MHz, $CDCl_3$) δ = 24.50. HRMS (ESI) calcd. for $[C_{51}H_{51}N_7OPSi]^+$, $[M]^+$: 836.3656, found: 836.3659.

11-Amino-7-(diethylamino)-14*H*-dibenzo[*b*,*f*]indeno[1,2-*d*]oxepin-14-one (S12)

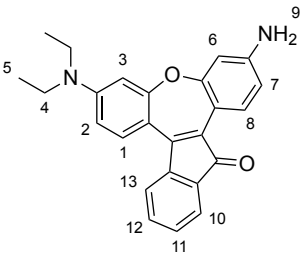

Compound **S12** was isolated as a side product during the preparation of **2** (4 mg, 15%). ^{1}H NMR (500 MHz, $CDCl_3$) δ = 7.77 (dd, *J* = 8.3 Hz, 0.4, 1H, H8), 7.63 (d, *J* = 8.6 Hz, 1H, H1), 7.56 (ddd, *J* = 7.1 Hz, 1.2 Hz, 0.6 Hz, 1H, H10), 7.48 – 7.42 (m, 1H, H13), 7.38 (td, *J* = 7.5 Hz, 1.2 Hz, 1H, H12), 7.26 (ddd, *J* = 7.6 Hz, 7.0 Hz, 0.9 Hz, 1H, H11), 6.64 – 6.53 (m, 4H, H1, H3, H6, H7), 3.45 (q, *J*= 7.1 Hz, 4H, H4), 1.25 (t, *J* = 7.1 Hz, 6H, H5). ^{13}C NMR (126 MHz, $CDCl_3$) δ = 195.5, 159.8, 158.0, 151.8, 151.0, 148.5, 143.9, 132.8, 132.7, 130.0, 128.5, 128.3, 126.6, 122.4, 121.1, 116.3, 113.8, 112.1, 108.0, 107.4, 104.4, 44.7, 29.7, 12.6. HRMS (ESI) calcd. for $[C_{25}H_{23}N_2O_2]^+$, $[M + H]^+$: 383.1754, found: 383.1753.

Supplementary Figures and Table

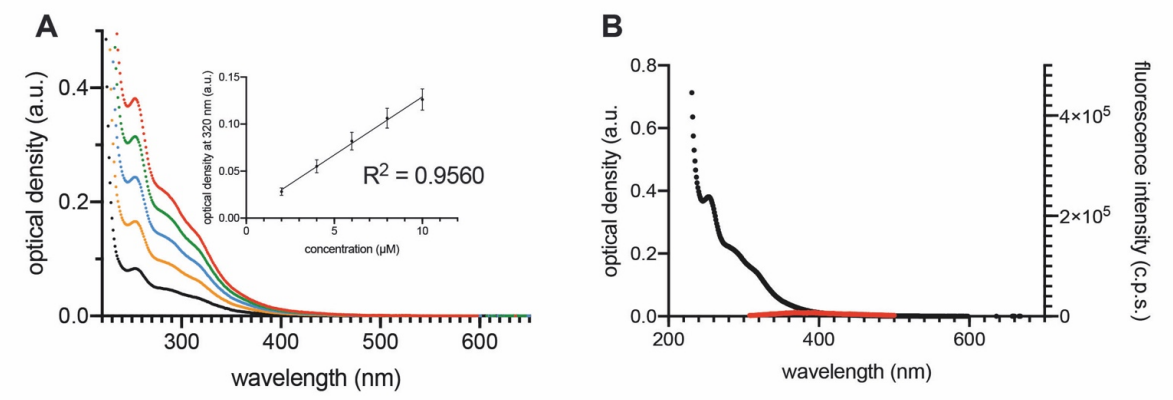

Figure S1. Absorbance and fluorescence emission spectra of **1** in PBS/acetonitrile 1:1. A) Absorbance at various concentrations ranging from 2 μM (black data points) to 10 μM (red data points). Insert: Plot of absorbance at 320 nm against concentration. B) Absorbance spectrum (10 μM) and fluorescence emission spectrum (5 μM, λ_{ex} = 320 nm).

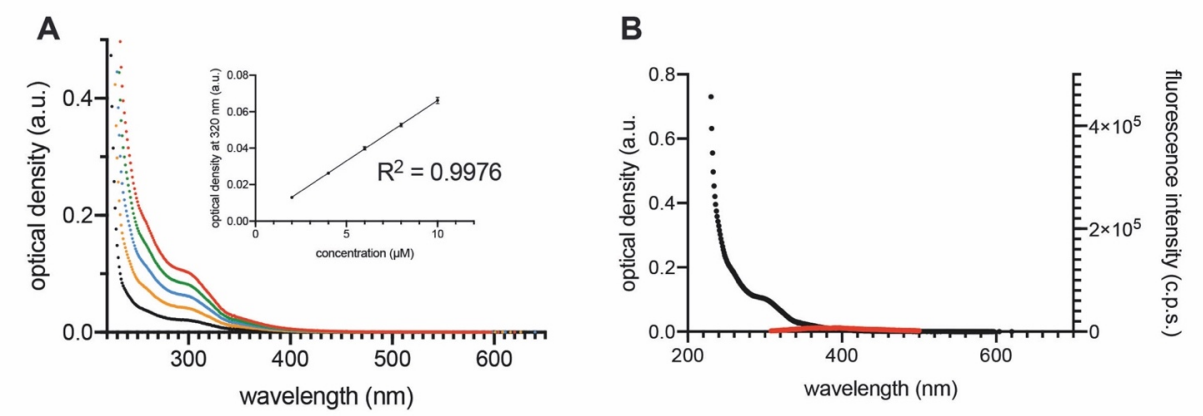

Figure S2. Absorbance and fluorescence emission spectra of **2** in PBS/acetonitrile 1:1. A) Absorbance at various concentrations ranging from 2 μM (black data points) to 10 μM (red data points). Insert: Plot of absorbance at 320 nm against concentration. B) Absorbance spectrum (10 μM) and fluorescence emission spectrum (5 μM, λ_{ex} = 320 nm).

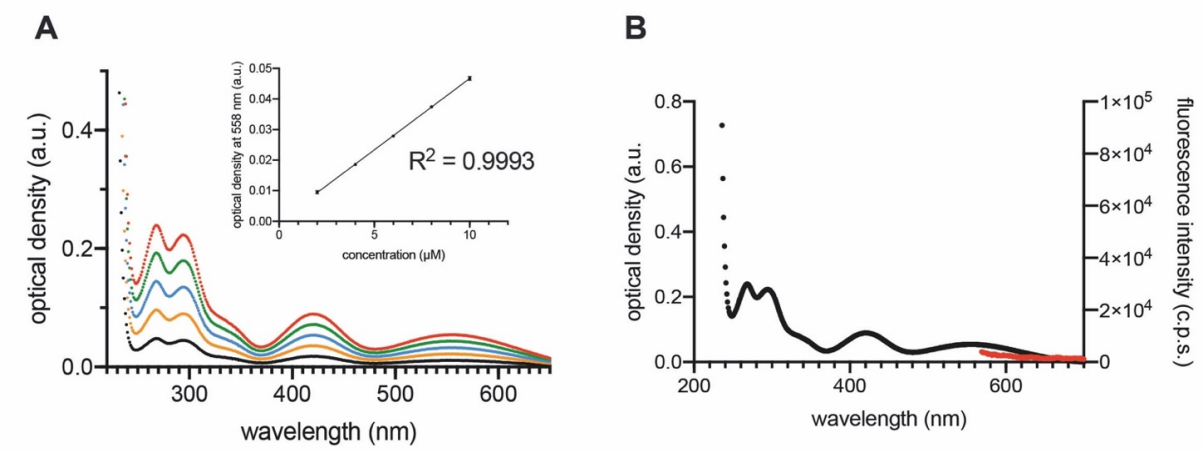

Figure S3. Absorbance and fluorescence emission spectra of **S12** in PBS/acetonitrile 1:1. A) Absorbance at various concentrations ranging from 2 μM (black data points) to 10 μM (red data points). Insert: Plot of absorbance at 555 nm against concentration. B) Absorbance spectrum (10 μM) and fluorescence emission spectrum (5 μM, λ_{ex} = 555 nm).

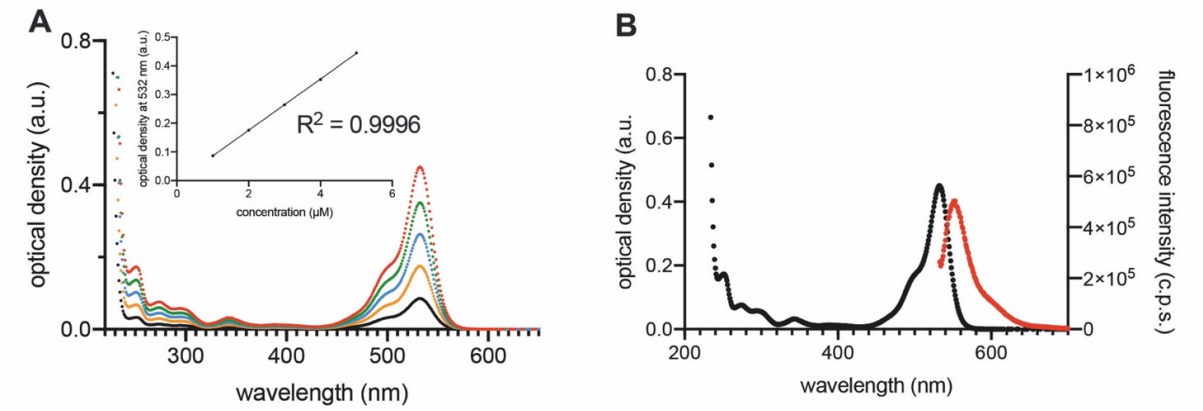

Figure S4. Absorbance and fluorescence emission spectra of **3** in PBS/acetonitrile 1:1. A) Absorbance at various concentrations ranging from 1 μM (black data points) to 5 μM (red data points). Insert: Plot of absorbance at 532 nm against concentration. B) Absorbance spectrum (5 μM) and fluorescence emission spectrum (0.5 μM, λ_{ex} = 532 nm).

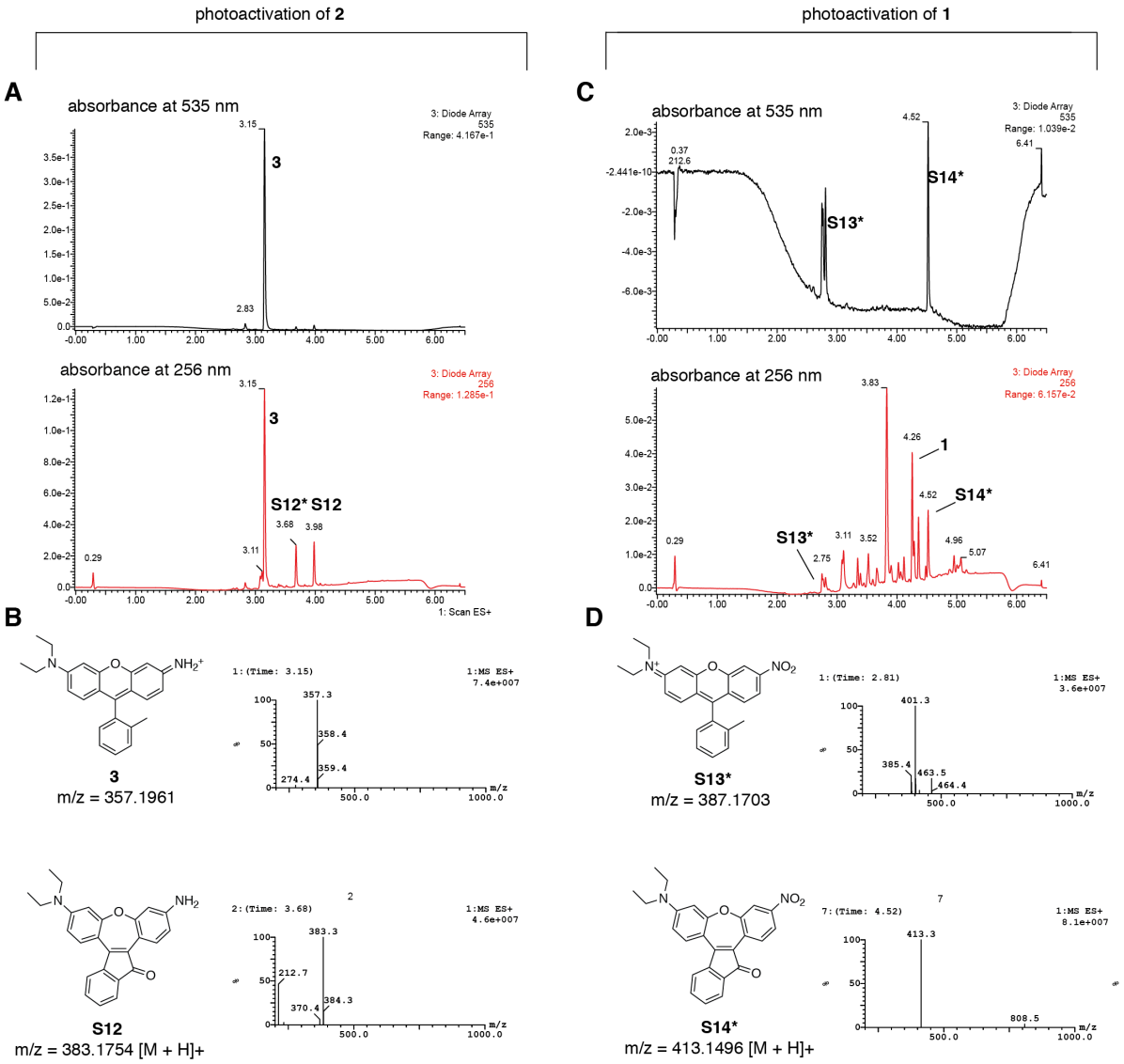

Figure S5. Photoactivation and LC-MS analysis of 1 and 2. Solutions of **1** and **2** (100 µM in PBS/acetonitrile 1:1) were irradiated with 350 nm light for 60 min and then subjected to LC-MS analysis. A) LC-MS chromatogram at λ_{abs} = 535 nm and λ_{abs} = 256 nm of an irradiated solution of **2**. B) Structures and corresponding traces of identified products of the photolysis of **2**. Compound **S12** can exist as two isomers with the carbonyl group pointing in the direction of either the free amine or the diethylamine. Only one of these two possible isomers was characterized unambiguously (see Figure S17). C) LC-MS chromatogram at λ_{abs} = 535 nm and λ_{abs} = 256 nm of an irradiated solution of **1**. D) Structures and corresponding traces of identified products of the photolysis of **2**. Compound **S14** can display isomerism similar to compound **S12**. *compound only identified by mass spectrometry.

Table S1. Photophysical properties of starting materials and photoproducts in PBS (pH = 7.4).

	$\varepsilon \times 10^4$ (M^{-1} cm^{-1})	$\lambda_{max,\ abs}$ (nm)	Φ_{em} (%)	$\lambda_{max,\ em}$ (nm)	$\varepsilon \times \Phi$ (M^{-1} cm^{-1})	$\Phi_{PA/DA}$
1	1.23(7)	320	0	-	0	0.37(9)
2	0.663(9)	320	0	-	0	0.7(1)
3	8.94(5)	532	2.95(2)	550	264(3)	0.043(7)
3* [a]	-	-	-	-	-	0.104(9)
S12	0.466(3)	555	0	-	0	0.06(1)
S12* [b]	-	-	-	-	-	0.084(7)

[a] Photophysical properties were not determined for this compound. Compound **3** was used for building the calibration curve for the determination of $\Phi_{PA/DA}$. [b] Photophysical properties were not determined for this compound. Compound **S12** was used for building the calibration curve for the determination of $\Phi_{PA/DA}$. Numbers indicate average over three independent runs (N = 3) and number in parenthesis indicates standard deviation (±) of the last significant figure.

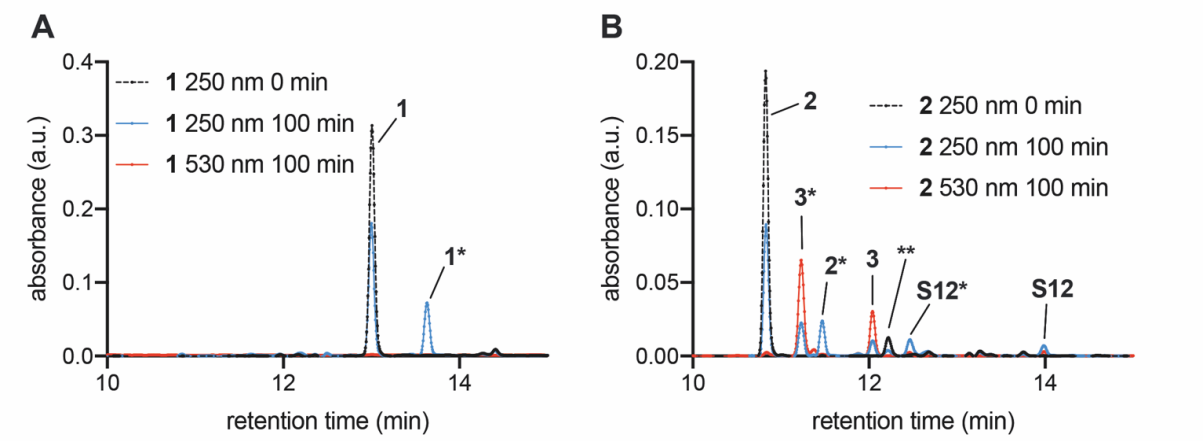

Figure S6. Representative HPL-chromatograms of irradiated solutions of compounds **1** and **2** (100 µM in PBS/acetonitrile 1:1) used for the determination of photoactivation quantum yields. A) Compound **1** before irradiation (black line: absorbance at λ = 250 nm) and after irradiation with a 405 nm LED for 100 min (blue line: absorbance at λ = 250, red line: absorbance at λ = 530 nm). B) Compound **2** before irradiation (black line: absorbance at λ = 250 nm) and after irradiation with a 405 nm LED for 100 min (blue line: absorbance at λ = 250 nm, red line: absorbance at λ = 530 nm). The peaks associated with **1*** and **2*** likely correspond to isomers of the starting materials **1** and **2**, respectively, formed by light-induced isomerization of the diazo group to a diazirine.[6] The peaks associated with the photoproducts **3** and **S12** were assigned by injection of synthetic standards. The peaks associated with the photoproducts **3*** and **S12*** were assigned by LC-MS analysis of the irradiated solution. Compound **3*** is the product of water addition to the ketene intermediate prior to decarboxylation. **Uncharacterized impurity of the starting material.

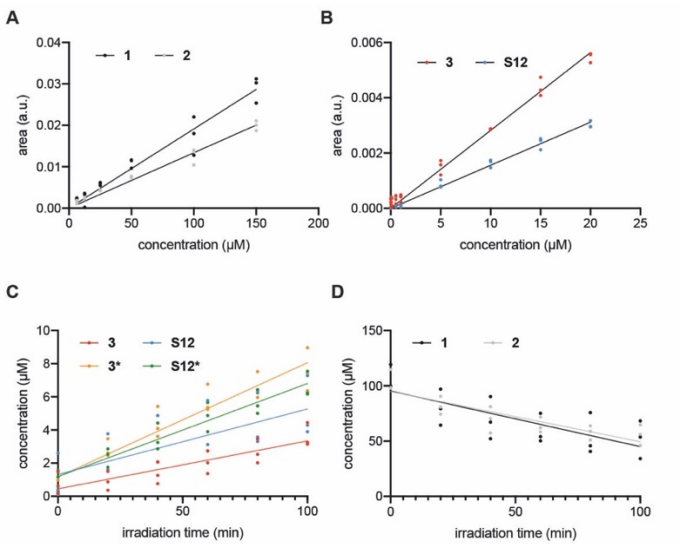

Figure S7. A) Calibration curves and linear regression of starting materials **1** and **2**. B) Calibration curves and linear regression of photoproducts **3** and **S12.** Evolution of concentrations of photoproducts after irradiation of a solution of **2** (100 μM in PBS/acetonitrile 1:1) with a 405 nm LED for 100 min. C) Evolution of concentrations of starting materials after irradiation of solutions of **1** and **2** 100 μM in PBS/acetonitrile 1:1) with a 405 nm LED for 100 min. Relative fits are represented as solid lines. Compound **3*** is the product of water addition to the ketene intermediate prior to decarboxylation.

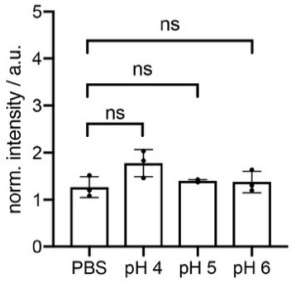

Figure S8. Dependence of fluorescence increase after photoactivation on pH. 10 μM solutions of **1** irradiated in PBS and various buffers with different pH values. The solutions were incubated at 37 °C for 30 min. Fluorescence was recorded before and after exposure to 350 nm light for 15 min. In all cases bars are averages of independent measurements (*N* = 3) and error bars represent standard deviation. ns *P* > *0.05.*

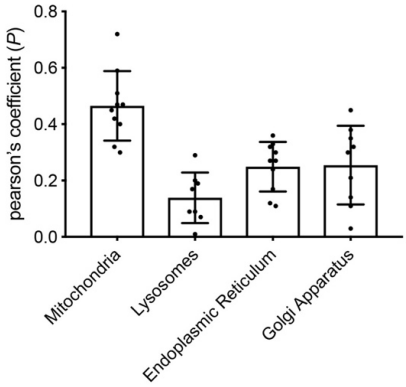

Figure S9. Colocalization experiments of **1** with various genetically encoded organelle markers. Compound **1** was photoactivated with 405 nm (120 mW, 70%, 10 s) and imaged with 561 nm (200 mW, 60%, 500 ms). Imaging of mTurquoise2 fusion proteins was performed with 445 nm (100 mW, 20%, 100 ms). In all cases bars are averages of independent measurements and error bars represent standard deviation.

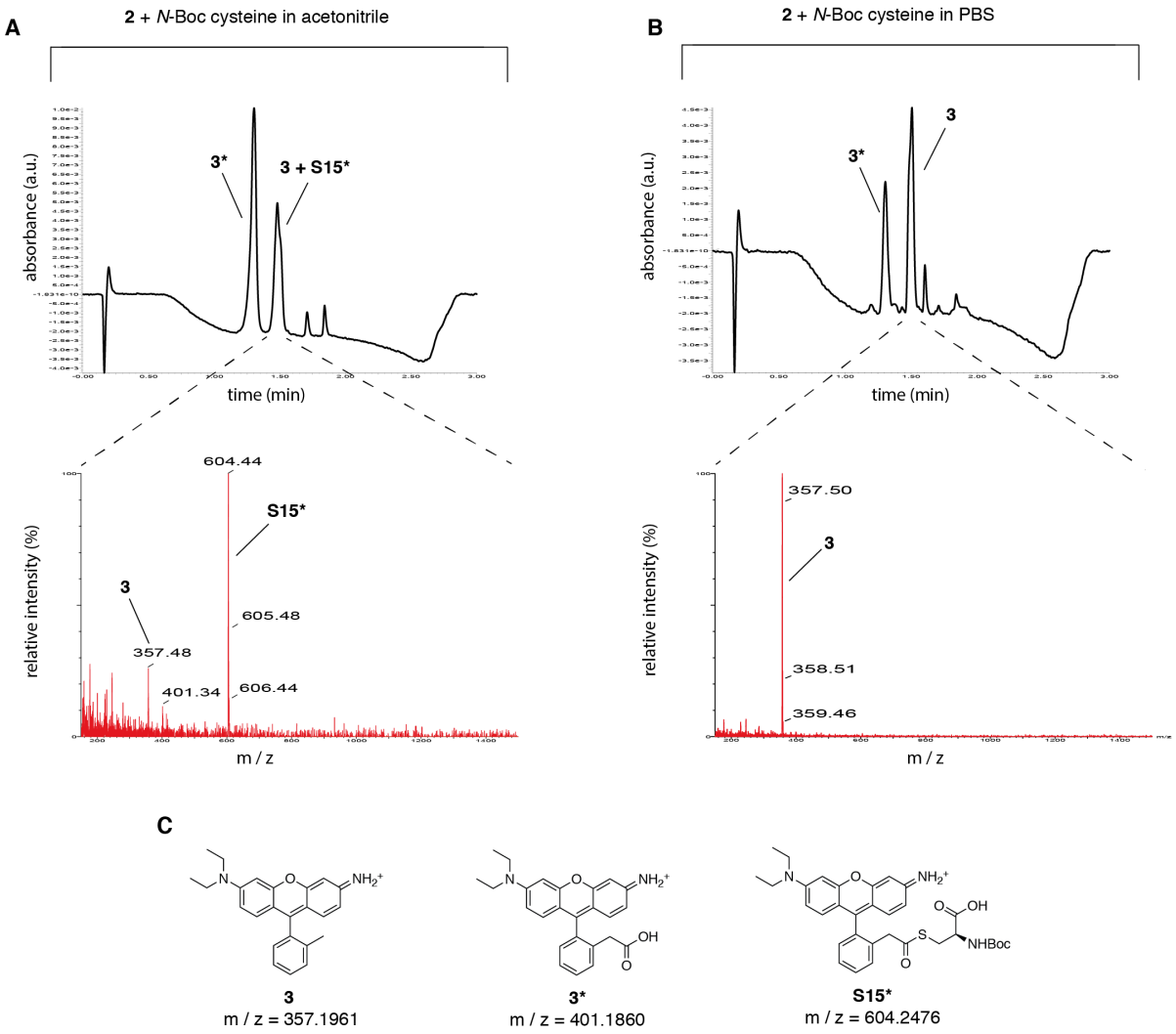

Figure S10. Characterization of amino acid specificity *in vitro*. As previously reported, diazoindanone modified xanthene dyes form an electrophilic xanthene intermediate upon irradiation.[8] To assess whether amino acids can form covalent adducts with the photoproduct of **2**, we performed 40 separate irradiation experiments *in vitro* with each of the amino acids in acetonitrile and PBS, respectively. *N*-Boc protected amino acids were used to exclude reaction between the potential ketene intermediate and the primary amine of the *N*-terminus. Solutions of **2** (100 µM) were therefore irradiated in presence of the amino acids (5 mM) with 350 nm light for 15 min and subjected to LC-MS analysis. Representative chromatograms of the reaction of **2** with *N*-Boc cysteine in acetonitrile and PBS are shown in panel (A) and (B), respectively. The proposed photoproducts that were observed are shown in panel (C). **S3*** is the primary photoproduct that forms after addition of H_2O to the ketene, prior to decarboxylation.[8] When irradiated in acetonitrile the formation of the photoproducts **S15*** as well as **3** and **3*** and is observed. The latter presumably form with trace amounts of H_2O present in the solution. When **2** was irradiated in aqueous buffer only the photoproducts **3** and **3*** could be identified. Of the 20 canonical amino acids, only adducts of cysteine, tyrosine, lysine, and histidine were observed (data are only shown for cysteine). *Compound was identified only by mass spectrometry.

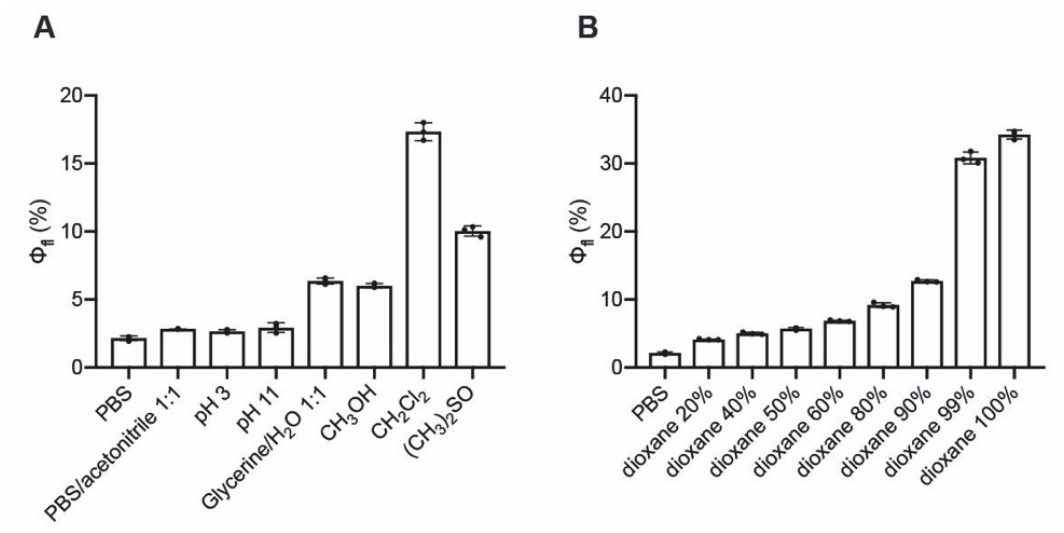

Figure S11. A) Fluorescence quantum yields (Φ_{fl}) of **3** in various solvents. B) Fluorescence quantum yields (Φ_{fl}) of **3** in mixtures of PBS/dioxane at different ratios. In all cases bars are averages of independent measurements (N = 3) and error bars represent standard deviation.

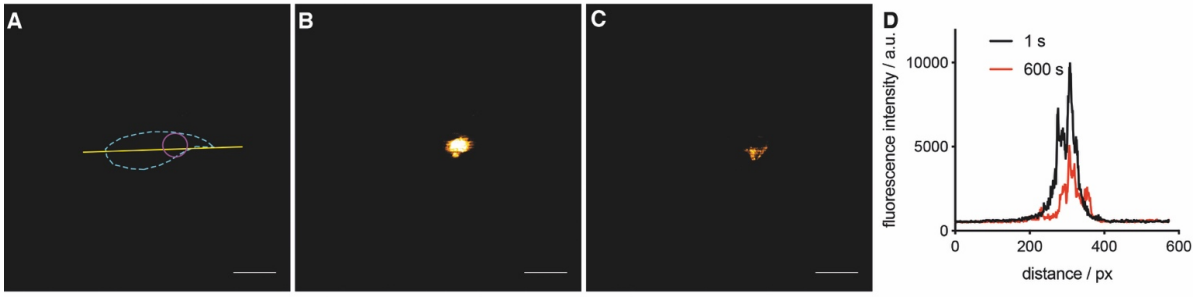

Figure S12. Intracellular diffusion of signal after photoactivation. Compound **1** (10 μM) was incubated in live cells for 10 min. A) Cell imaged with 561 nm (200 mW, 60%, 500 ms) before photoactivation. The cell is outlined with a dashed, cyan line. A region of interest (ROI) depicted by a magenta circle was then irradiated with 405 nm (120 mW, 70%, 2 ms px^{-1}). The same cell was imaged with 561 nm (200 mW, 60%, 500 ms) immediately after photoactivation (B) and 600 s after photoactivation (C). D) Fluorescence profile along a line (yellow line in panel A). Scale bars = 10 μm.

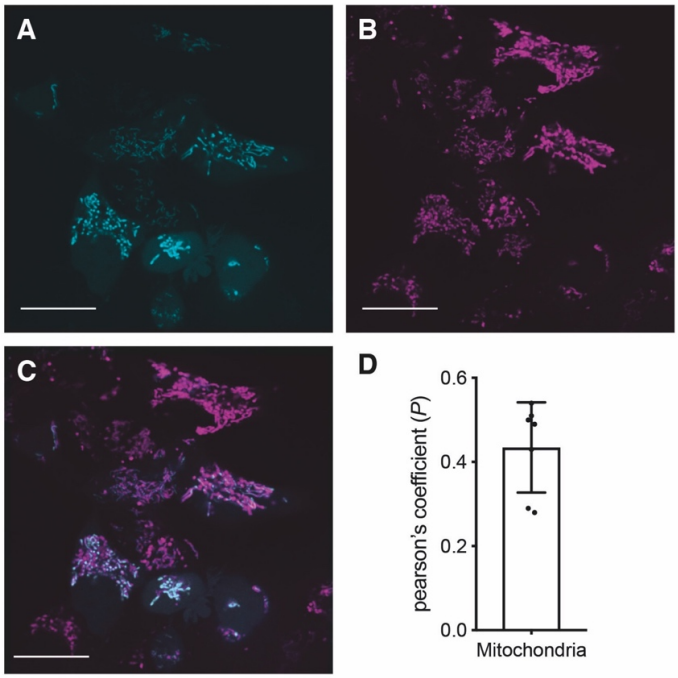

Figure S13. Colocalization experiments of **4** with mTurquoise2-COX8A (mitochondrial marker). A) Localization of mTurquoise2-COX8A, imaged with 445 nm laser (100 mW, 20%, 100 ms). B) Localization of **4,** imaged with 640 nm laser (150 mW, 10%, 100 ms). C) Overlay of the channels, displayed in panels A and B. D) Pearson's correlation coefficient (*P*) of the signals obtained from **4** and mTurquoise2-COX8A. In all cases bars are averages of independent measurements and error bars represent standard deviation.

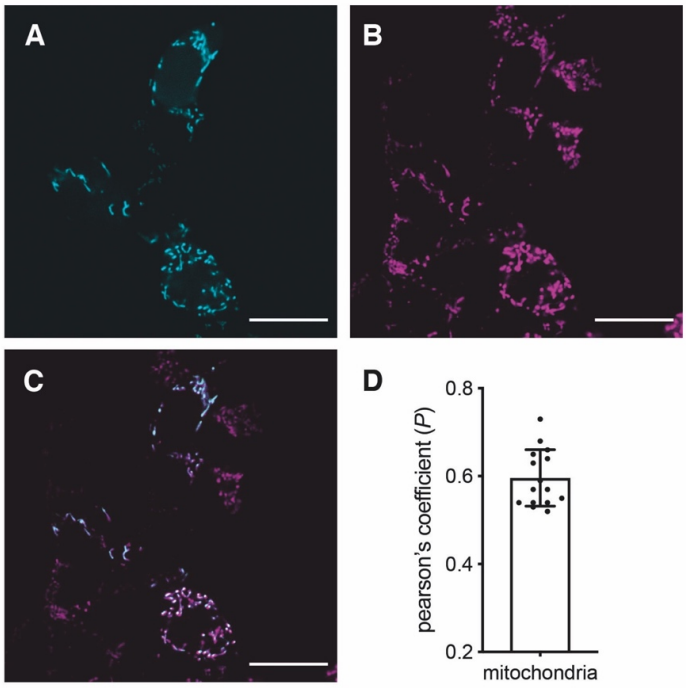

Figure S14. Colocalization experiments of **5** with mTurquoise2-COX8A. A) Localization of mTurquoise2-COX8A, imaged with 445 nm laser (100 mW, 20%, 100 ms). B) Localization of **5,** imaged with 640 nm laser (150 mW, 10%, 100 ms). C) Overlay of the channels, displayed in panels A and B. D) Pearson's correlation coefficient (*P*) of the signals obtained from **5** and mTurquoise2-COX8A. In all cases bars are averages of independent measurements and error bars represent standard deviation.

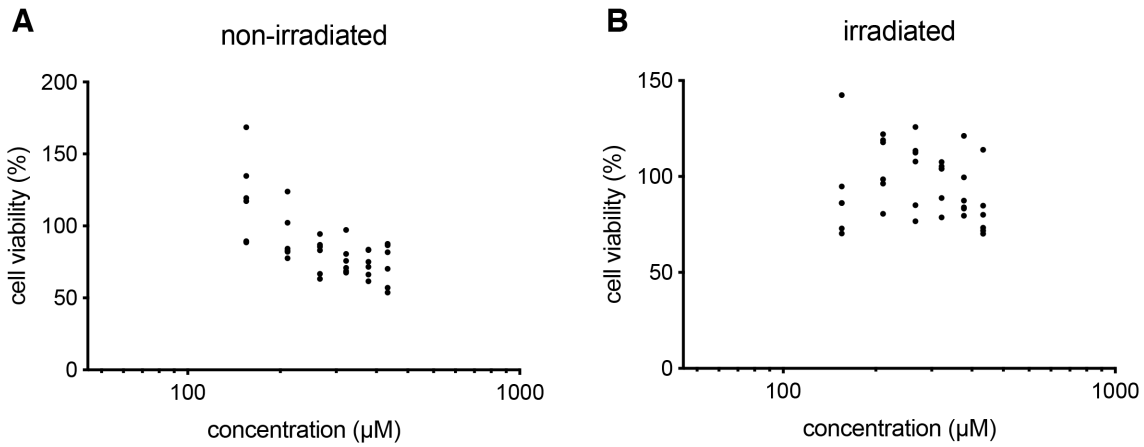

Figure S15. MTT cell viability assay of compound 1. HEK293-1 cells were incubated with **1** at various concentrations (150 μM – 400 μM) for 72 h without (A) and with (B) irradiation at 405 nm for 10 min. IC_{50} values could not be determined due to limited solubility at concentrations above 400 μM.

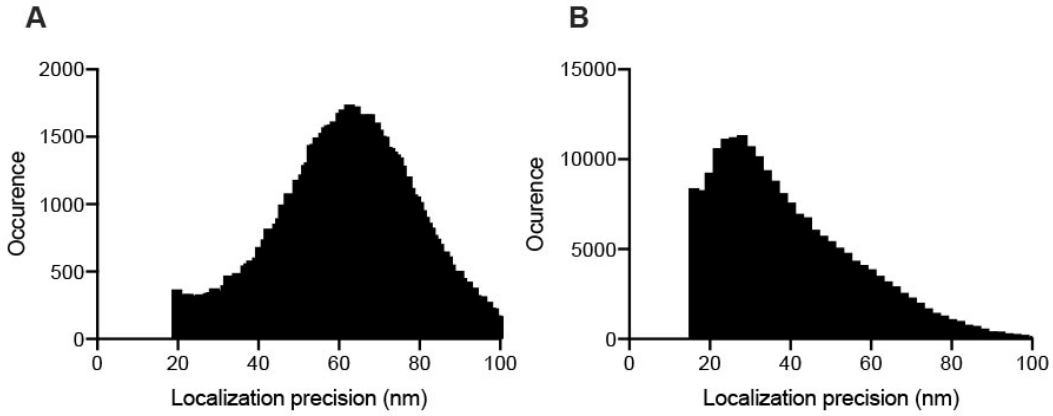

Figure S16. A) Histogram of localization precision for single-molecule localizations used to reconstruct the super-resolved image obtained with compound **1**. B) Histogram of localization precision for single-molecule localizations used to reconstruct the super-resolved image obtained with compound **5.**

Crystallographic Data

Black crystals of compound **S12** $C_{25}H_{22}N_2O_2$ (M = 382.44 g mol^{-1}, CCDC 1909731) were obtained (approximate size 0.197 × 0.119 × 0.052 mm) by slow evaporation of H_2O/acetonitrile 1:2 at 25 °C. The monoclinic crystal system belongs to the space group $P2_1/c$ a = 18.6212(2) Å, b = 10.59290(10) Å, c = 19.6163(2) Å, β = 90.2150(10)°, V = 3869.34(7) $Å^3$, Z = 8, T = 100.0(1) K, μ (CuKα) = 0.665 mm^{-1}, *Dcalc* = 1.313 g/cm^3. 52182 reflections were measured (4.746° ≤ 2Θ ≤ 160.11°) out of which 8307 unique (R_{int} = 0.0391, R_{sigma} = 0.0248) which were used in all calculations. The final R_1 was 0.0385 (I > 2σ(I)) and wR_2 was 0.1002 (all data).

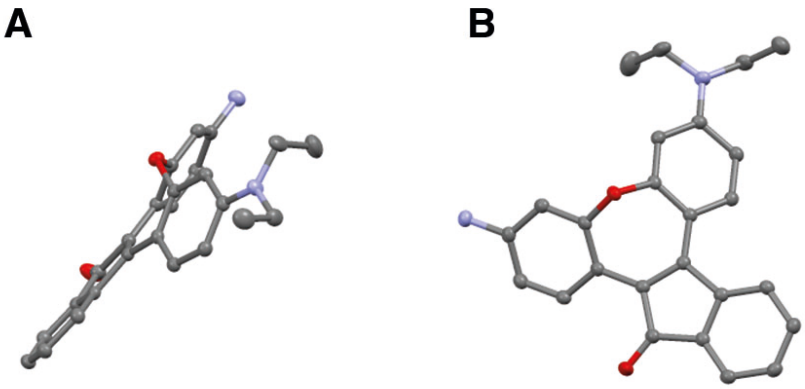

Figure S17. Solid-state structure of **S12** obtained by single-crystal X-ray crystallography. A) Side view. B) Front view. H-Atoms are omitted for clarity. Atomic displacement parameters at 100 K are drawn at 50% probability level.

References

[1] B. Huang, W. Wang, M. Bates, X. Zhuang, *Science* **2009**, *319*, 5864.

[2] M. Ovesný, P. Křížek, J. Borkovec, Z. Švindrych, G. M. Hagen, *Bioinformatics* **2014**, *30*, 2389–2390.

[3] F. Levet, E. Hosy, A. Kechkar, C. Butler, A. Beghin, D. Choquet, J.-B. Sibarita, *Nat. Methods* **2015**, *12*, 1065–1071.

[4] X. Chai, X. Cui, B. Wang, F. Yang, Y. Cai, Q. Wu, T. Wang, *Chem. Eur. J.* **2015**, *21*, 16754–16758.

[5] A. Tirla, P. Rivera-Fuentes, *Biochemistry* **2019**, *58*, 1184–1187.

[6] E. A. Halabi, Z. Thiel, N. Trapp, D. Pinotsi, P. Rivera-Fuentes, *J. Am. Chem. Soc.* **2017**, *139*, 13200–13207.

[7] J. Goedhart, D. von Stetten, M. Noirclerc-Savoye, M. Lelimousin, L. Joosen, M. A. Hink, L. van Weeren, T. W. J. Gadella, A. Royant, *Nat. Commun.* **2012**, *3*, 751.

[8] V. N. Belov, C. A. Wurm, V. P. Boyarskiy, S. Jakobs, S. W. Hell, *Angew. Chem. Int. Ed.* **2010**, *49*, 3520–3523; *Angew. Chem.* **2010**, *122*, 3598–3602.

NMR Spectra

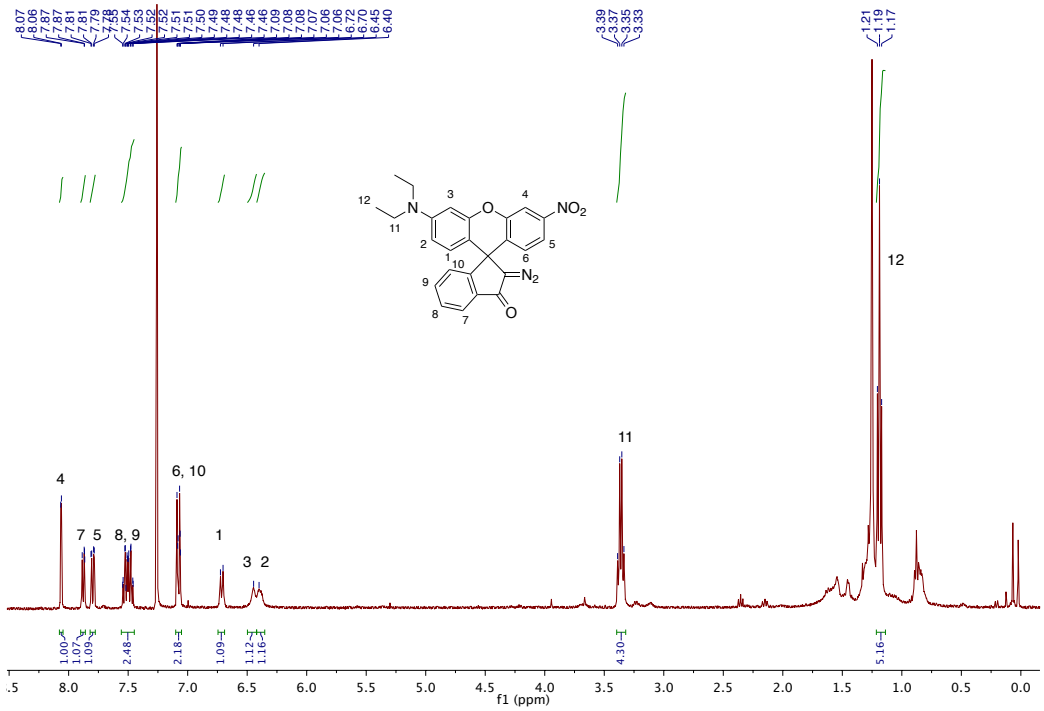

^{1}H NMR (400 MHz) of **1** in $CDCl_3$.

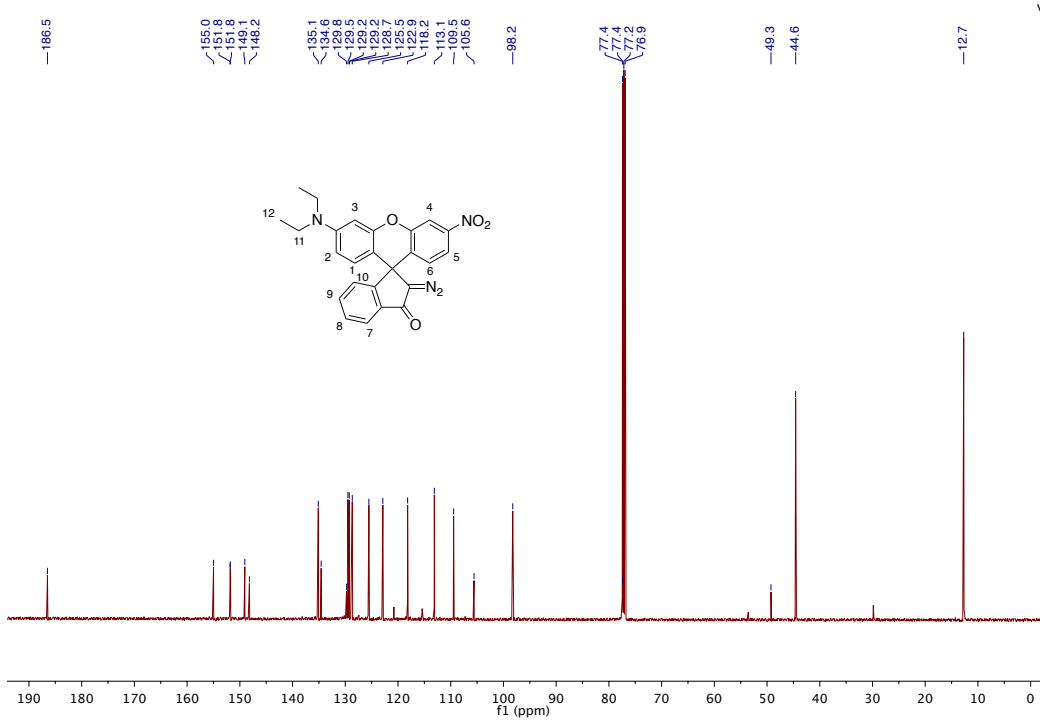

^{13}C NMR (126 MHz) of **1** in $CDCl_3$.

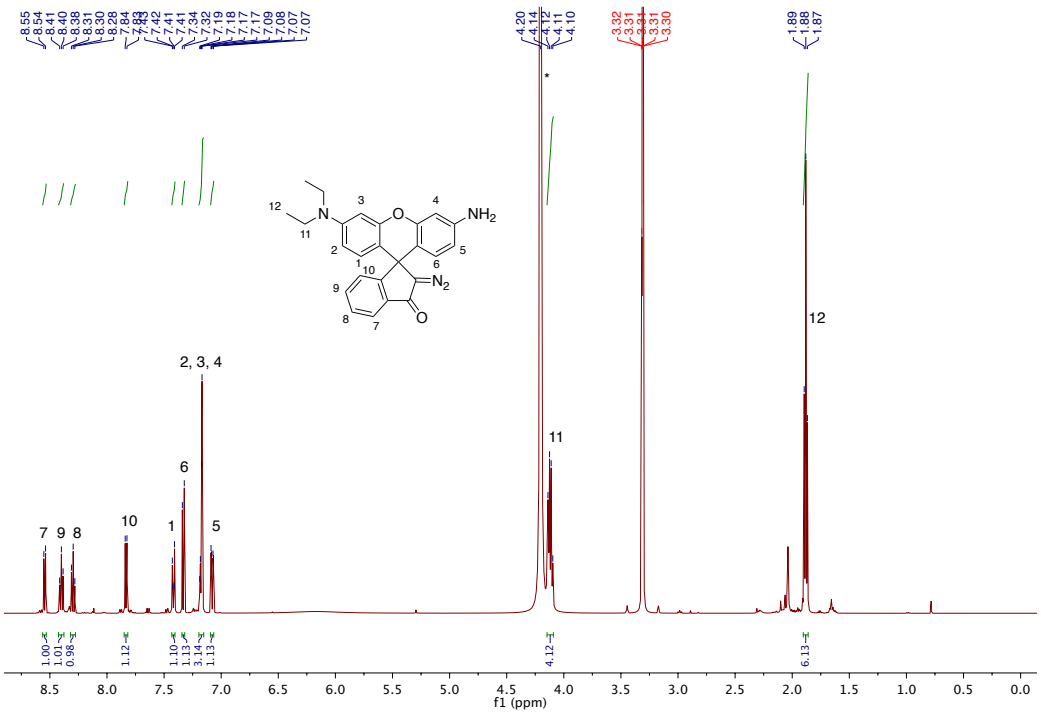

^{1}H NMR (500 MHz) of **2** in CD_3OD.

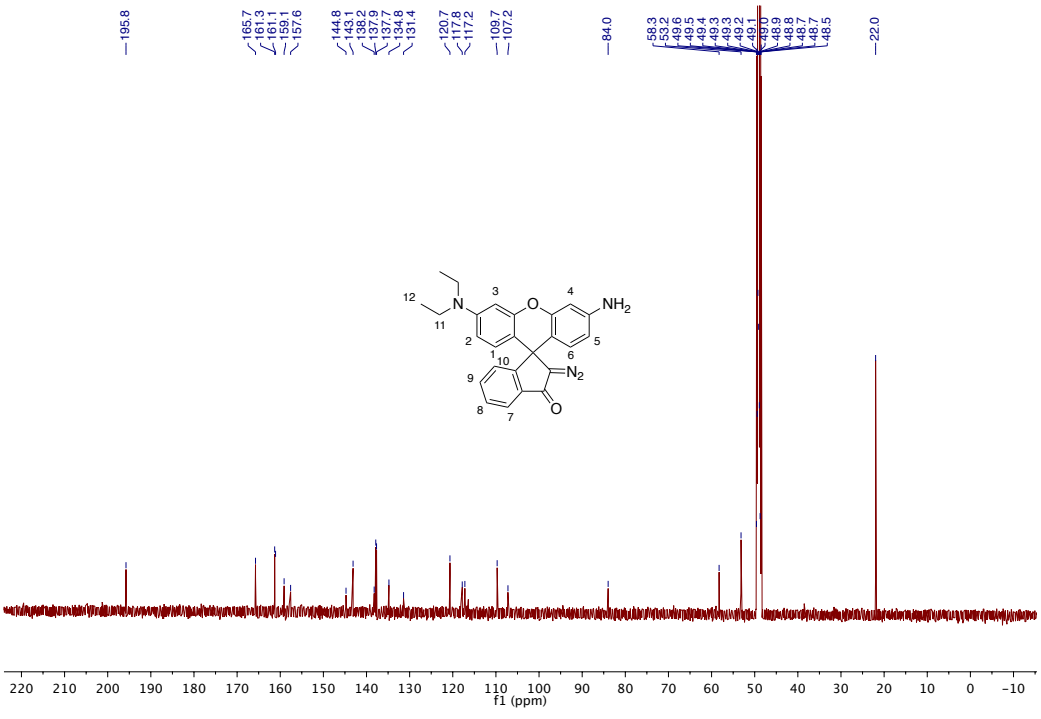

^{13}C NMR (126 MHz) of **2** in CD_3OD.

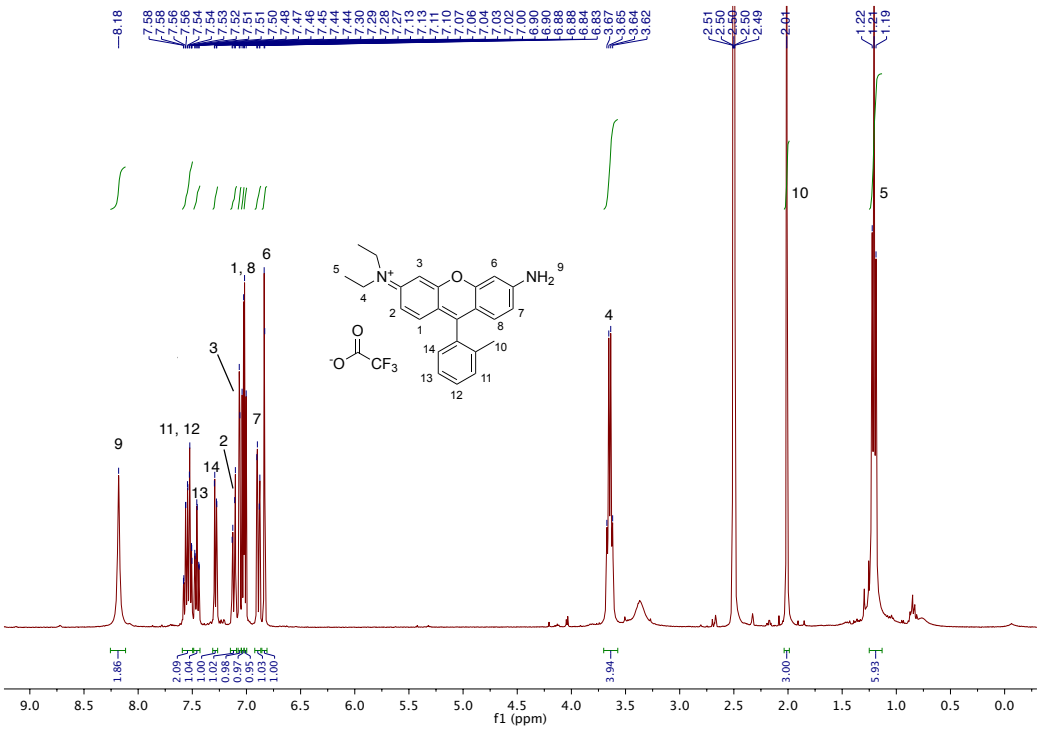

^{1}H NMR (400 MHz) of **3** in $(CD_3)_2SO$.

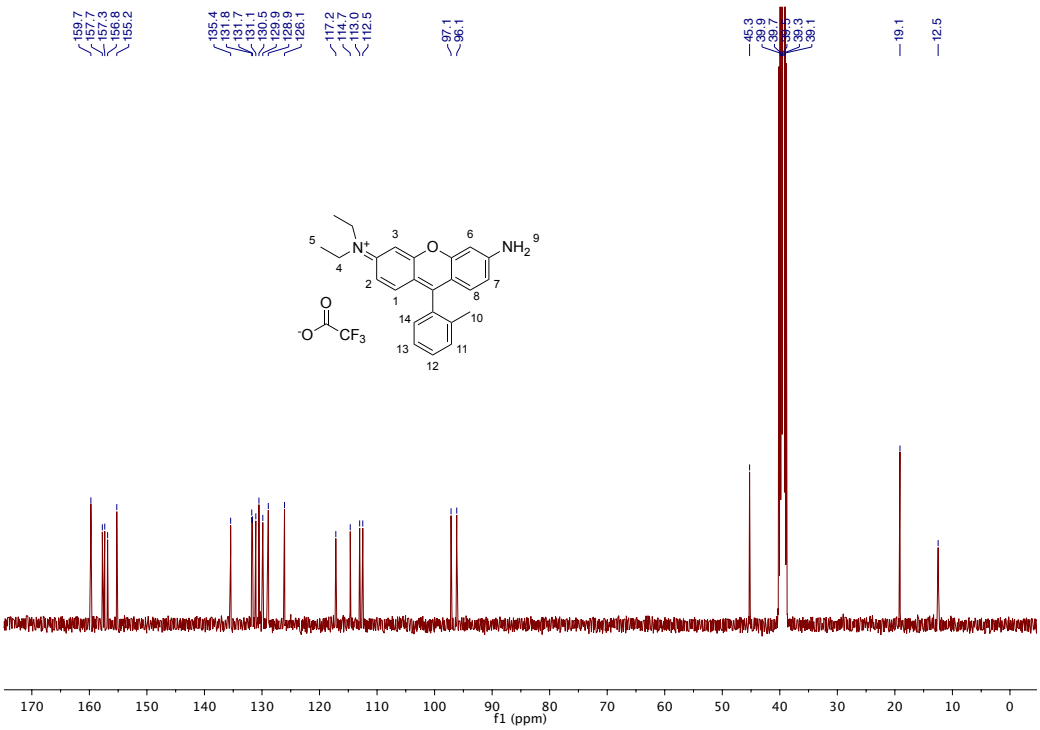

^{13}C NMR (101 MHz) of **3** in $(CD_3)_2SO$.

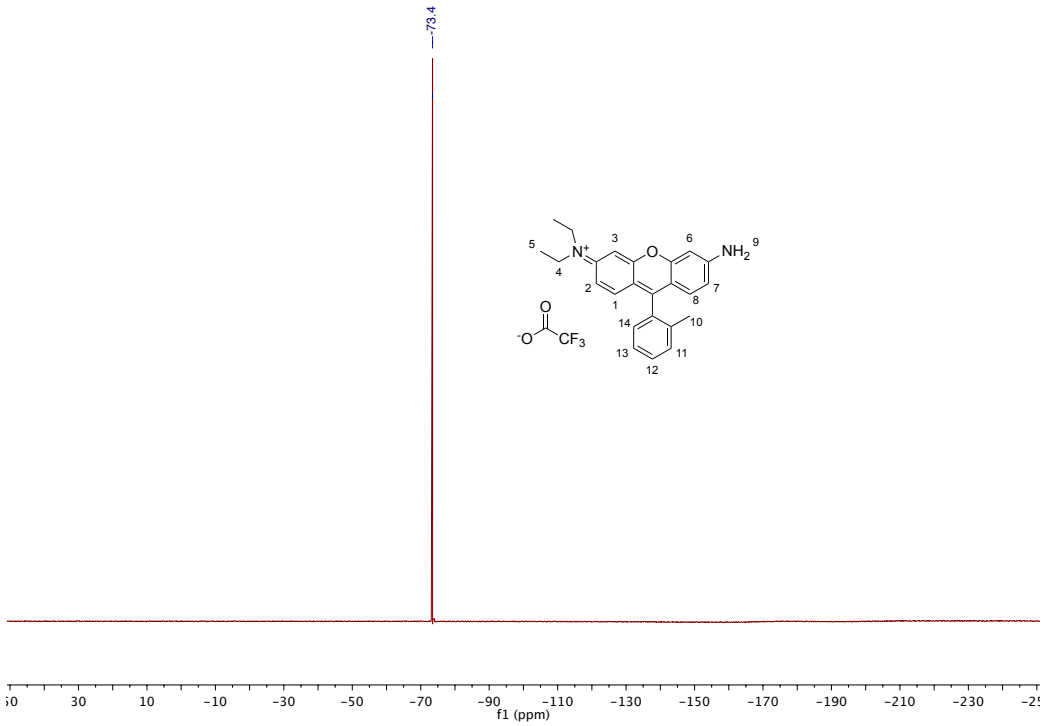

^{19}F (377 MHz) of **3** in $(CD_3)_2SO$.

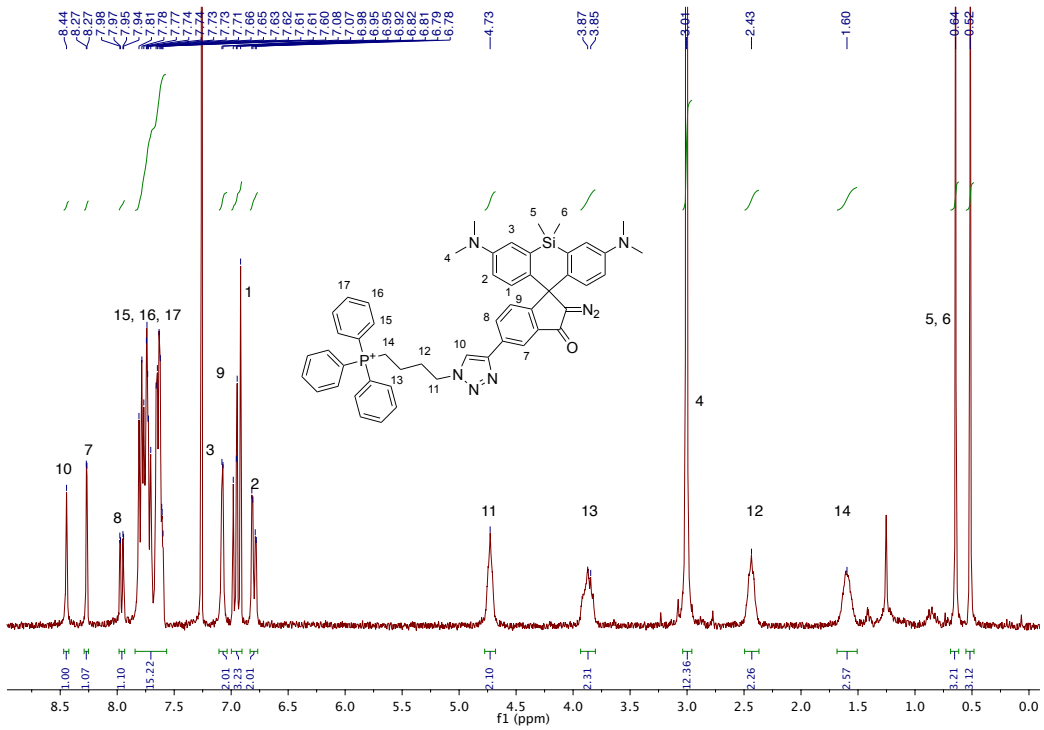

^{1}H NMR (500 MHz) of **5** in $CDCl_3$.

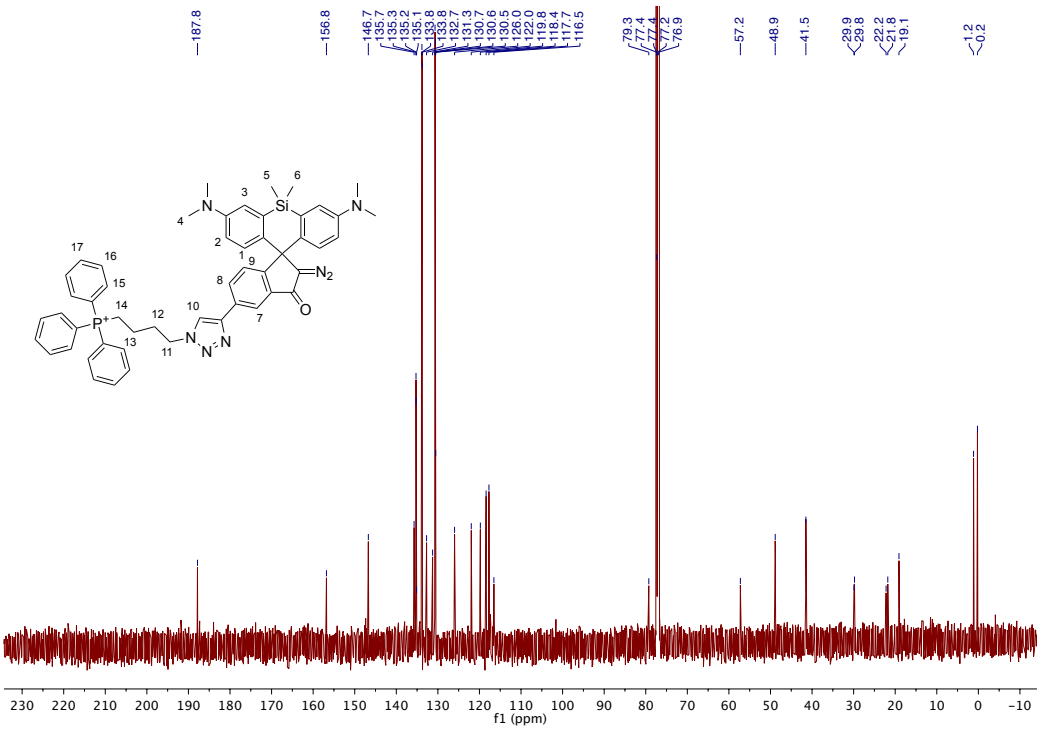

^{13}C NMR (126 MHz) of **5** in $CDCl_3$.

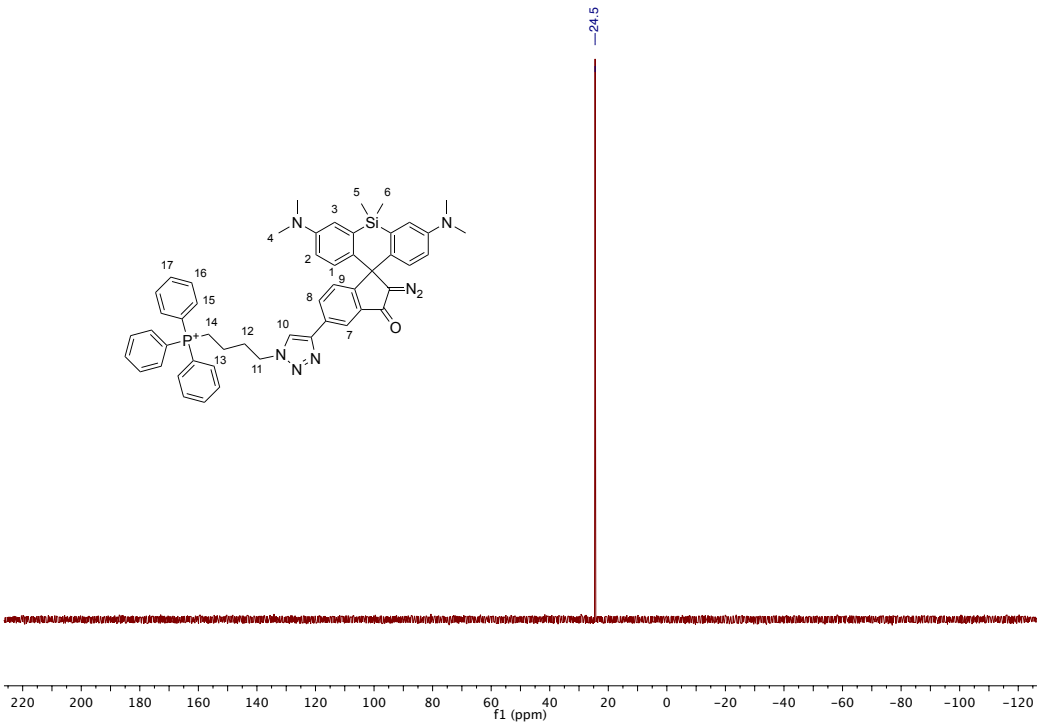

^{31}P NMR (202.5 MHz) of **5** in $CDCl_3$.

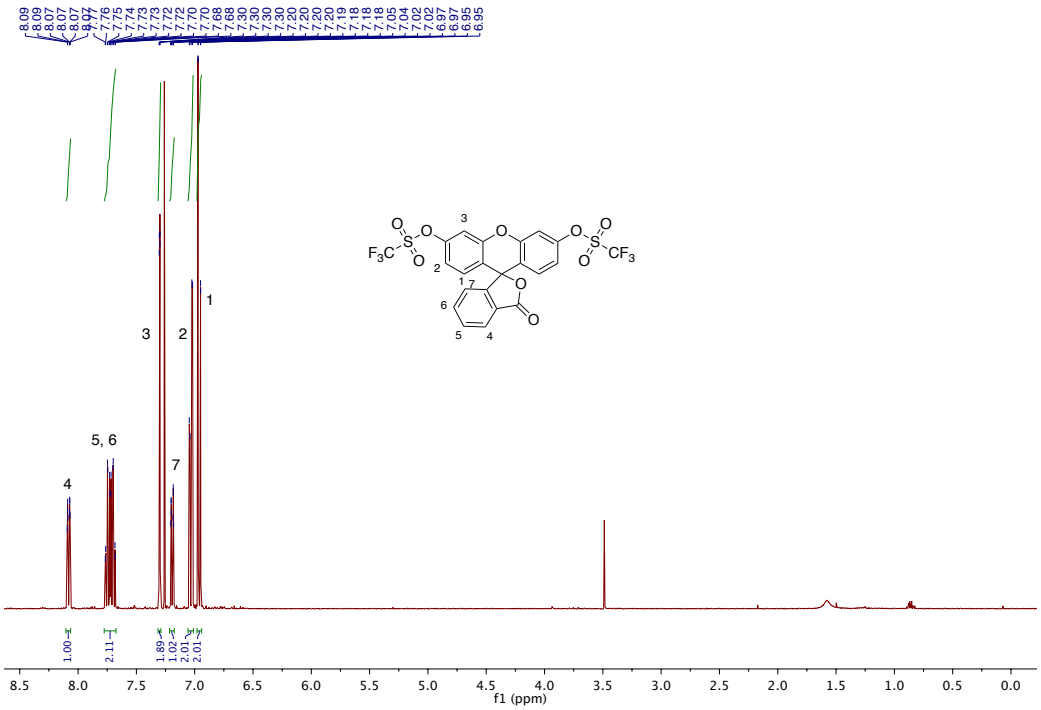

^{1}H NMR (400 MHz) of **S1** in $CDCl_3$.

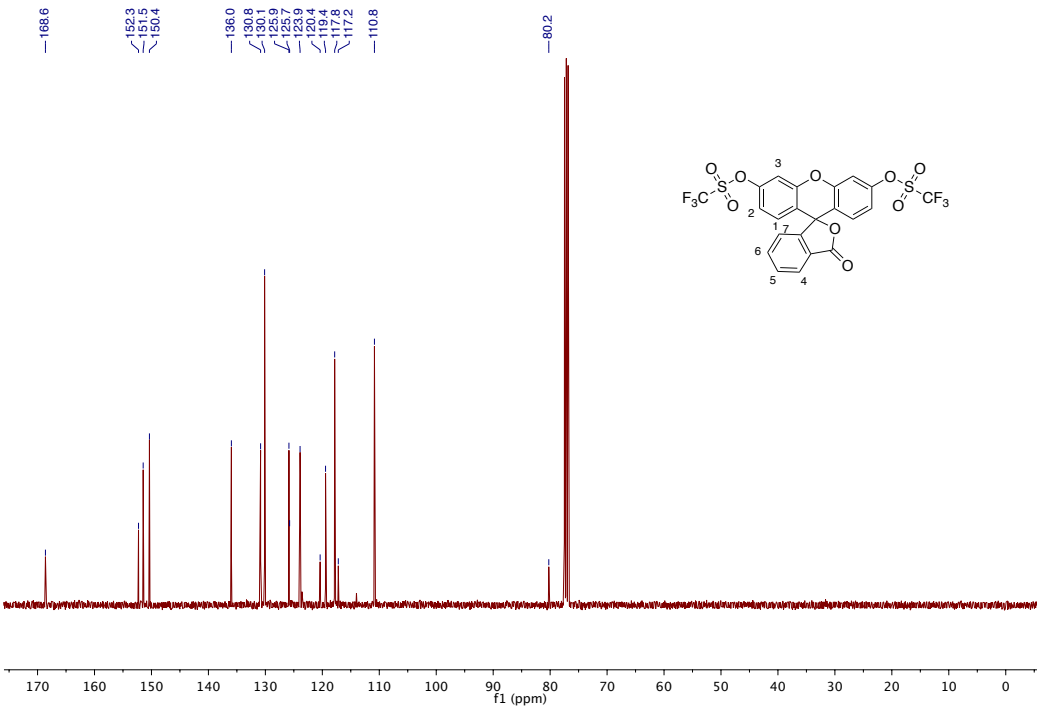

^{13}C NMR (101 MHz) of **S1** in $CDCl_3$.

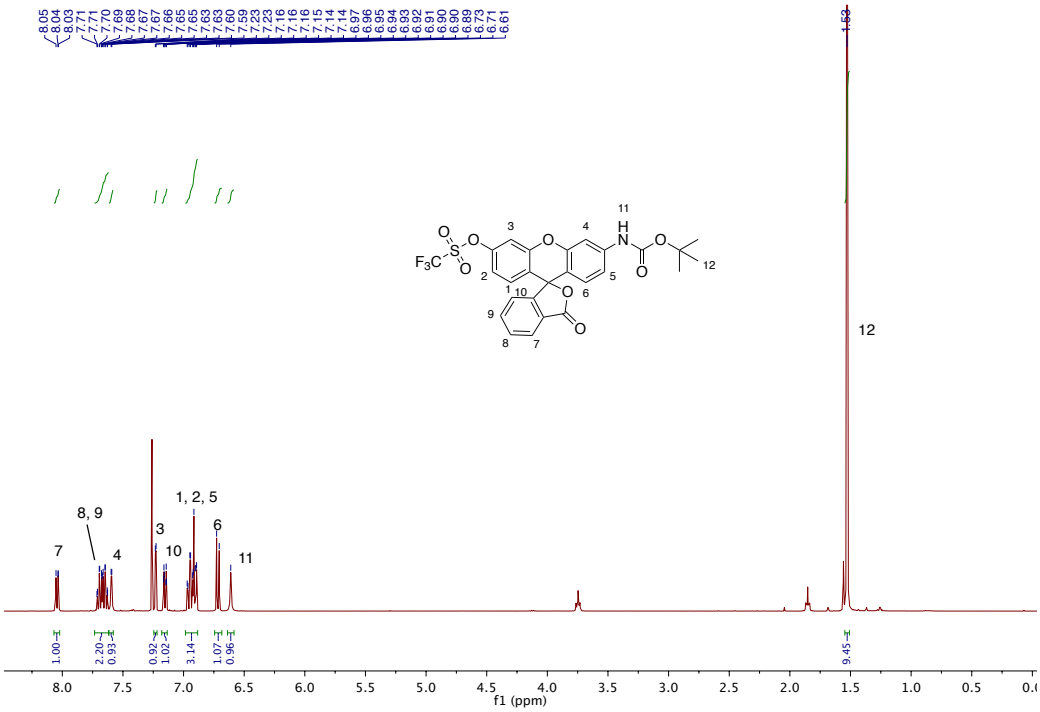

^{1}H NMR (400 MHz) of **S2** in $CDCl_3$.

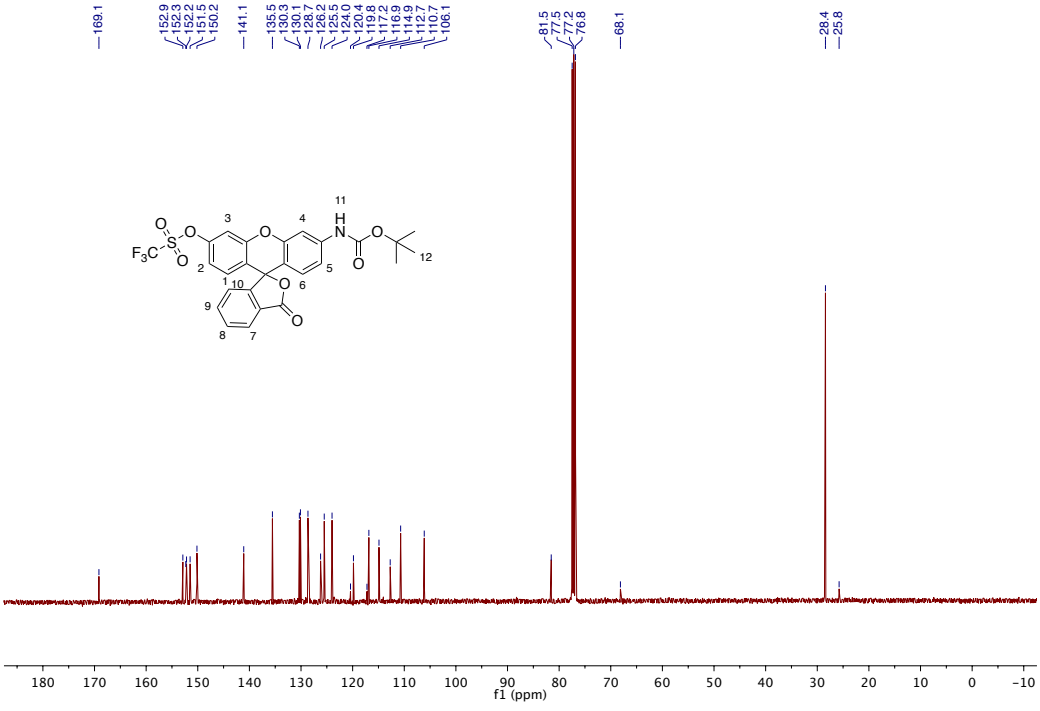

^{13}C NMR (101 MHz) of **S2** in $CDCl_3$.

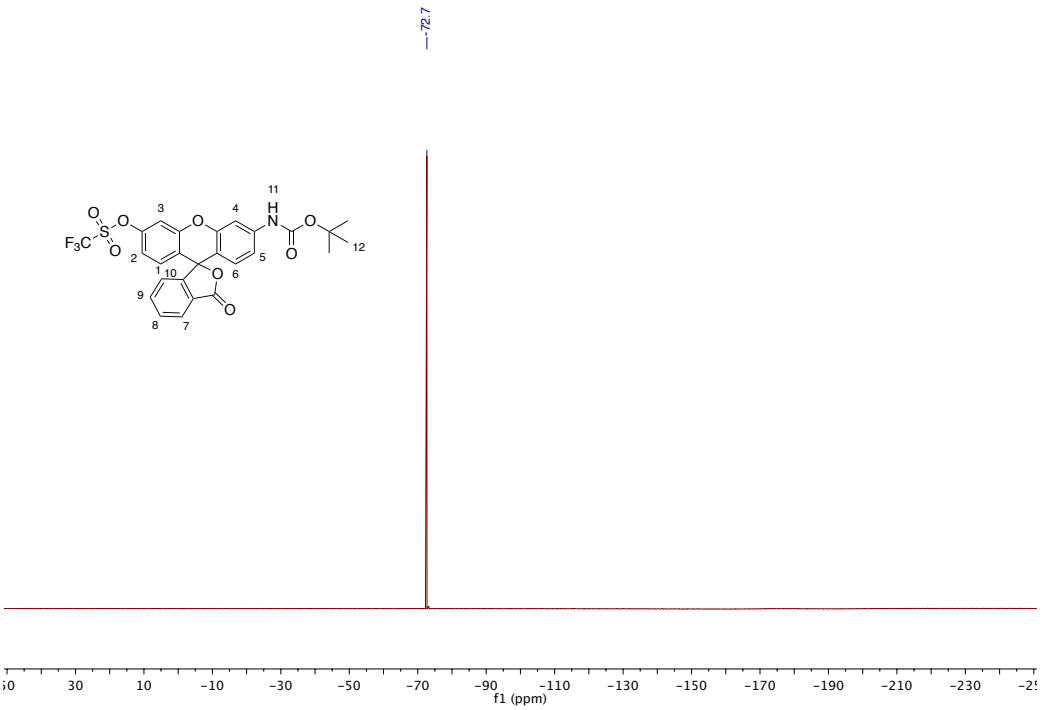

^{19}F NMR (377 MHz) of **S2** in $CDCl_3$.

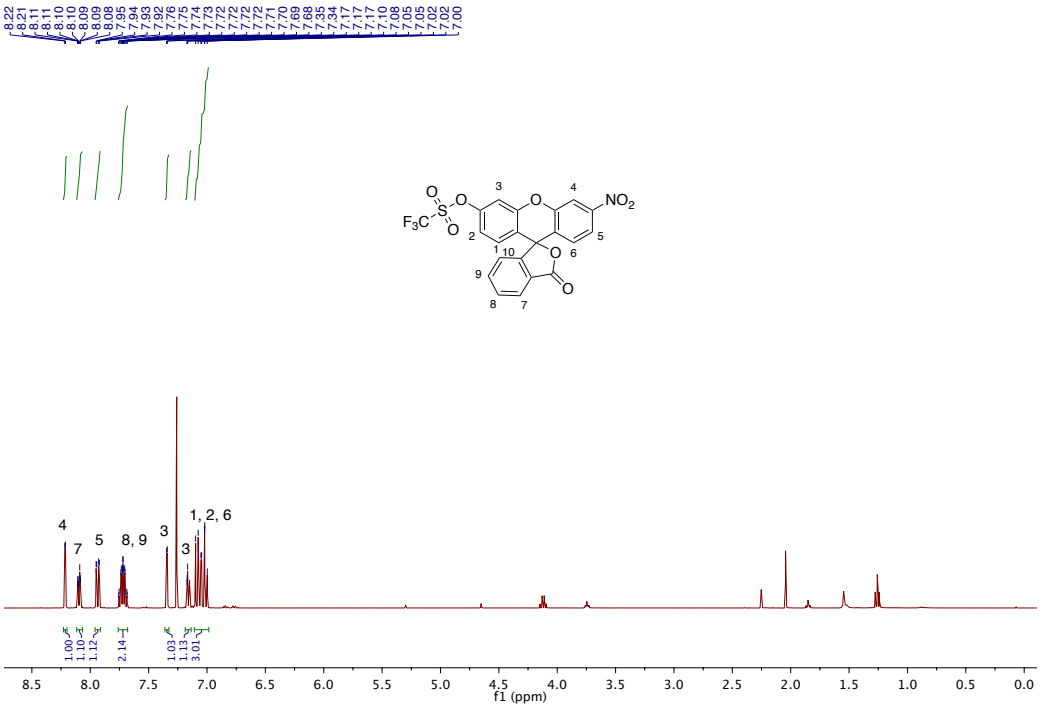

^{1}H NMR (300 MHz) of **S3** in $CDCl_3$.

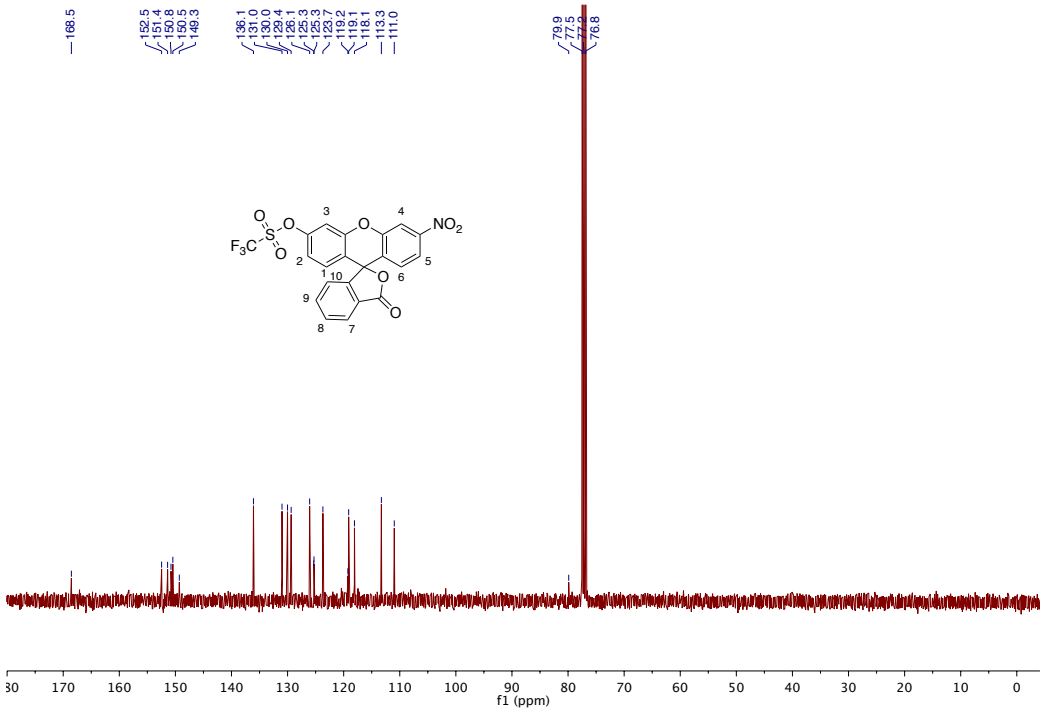

^{13}C NMR (101 MHz) of **S3** in $CDCl_3$.

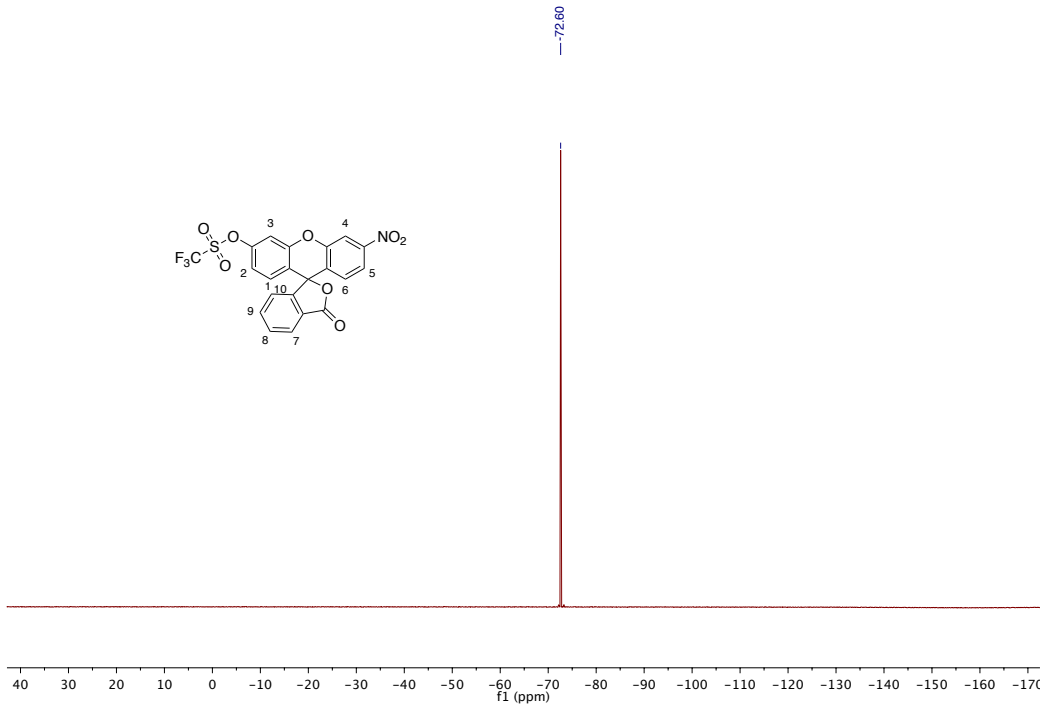

^{19}F NMR (282 MHz) of **S3** in $CDCl_3$.

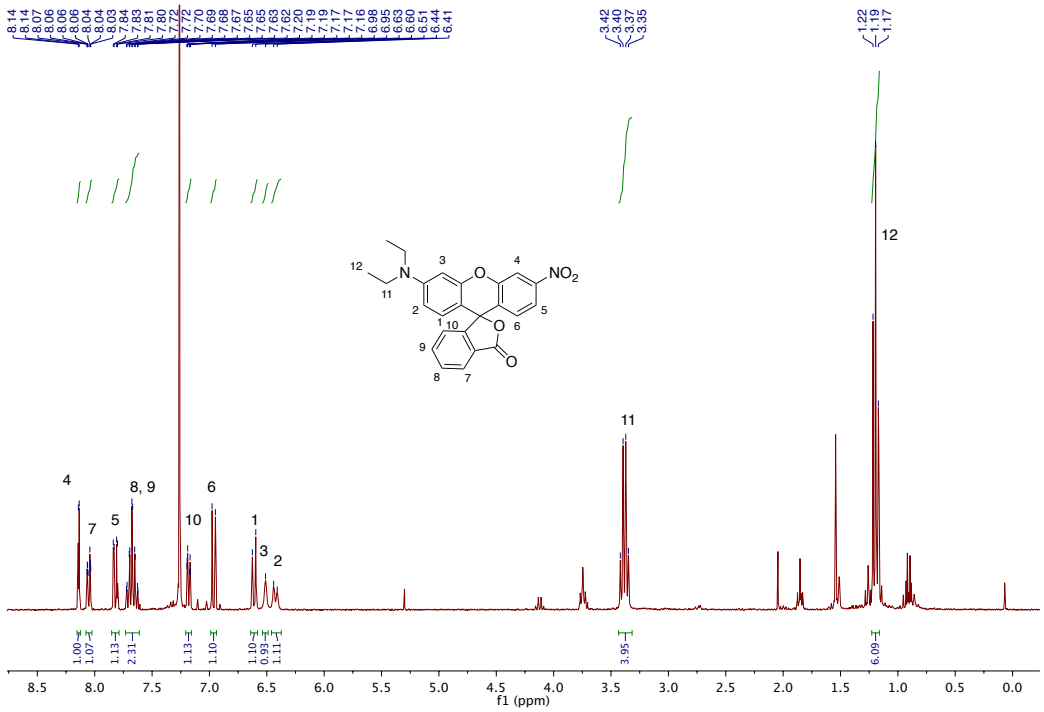

^{1}H NMR (300 MHz) of **S4** in $CDCl_3$.

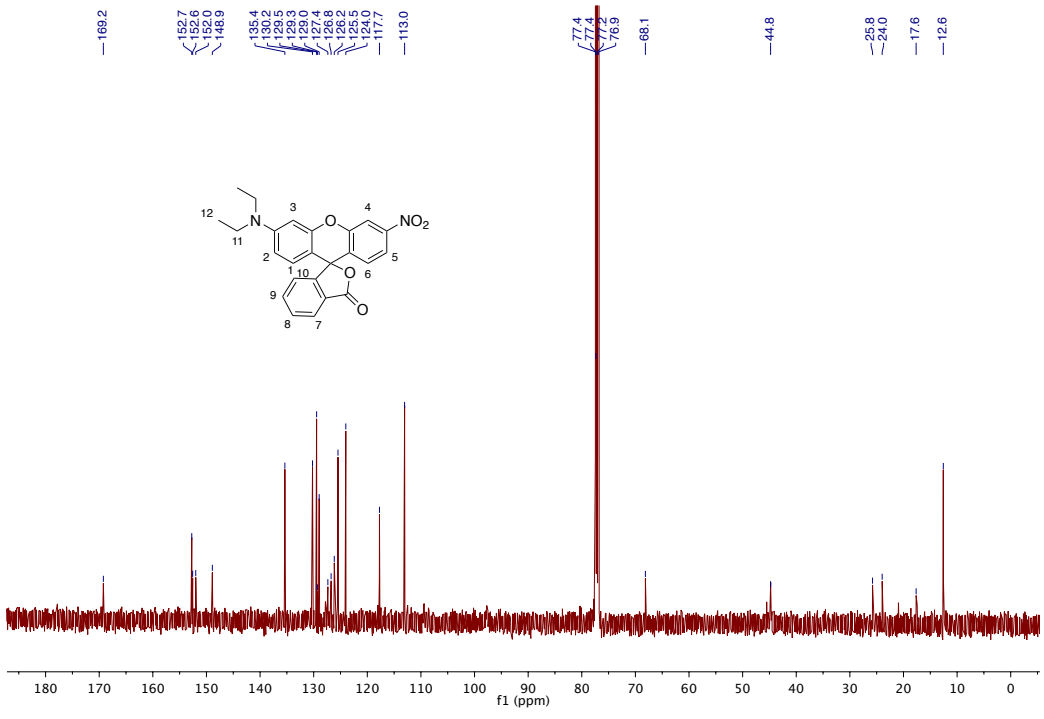

^{13}C NMR (126 MHz) of **S4** in $CDCl_3$.

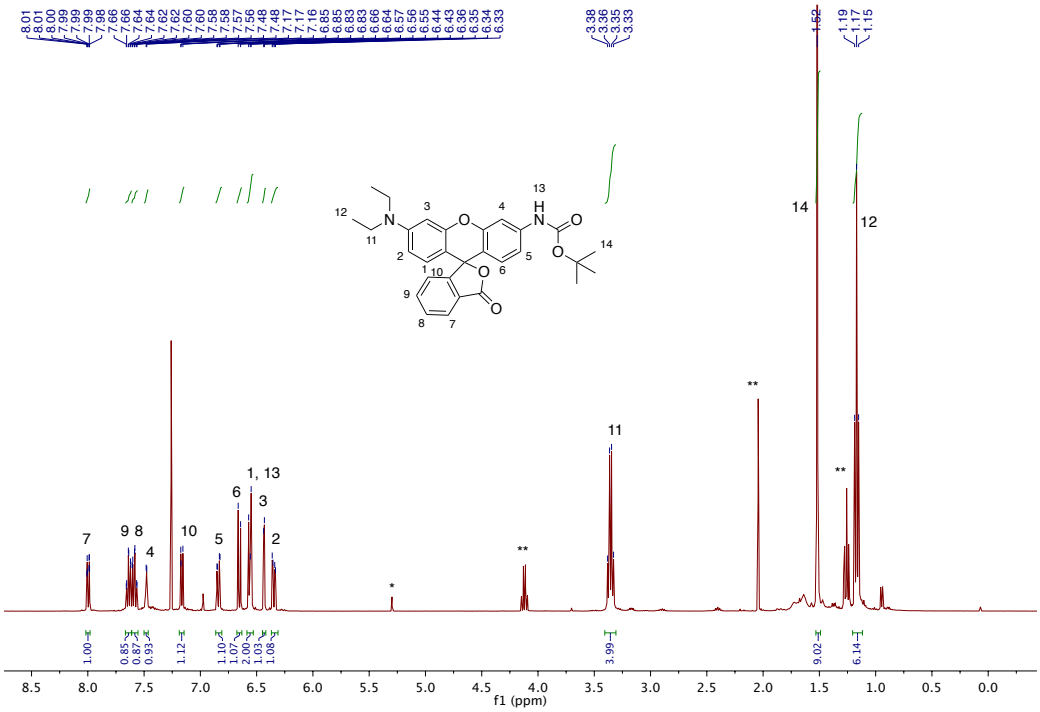

^{1}H NMR (400 MHz) of **S5** in $CDCl_3$. * CH_2Cl_2; ** ethyl acetate.

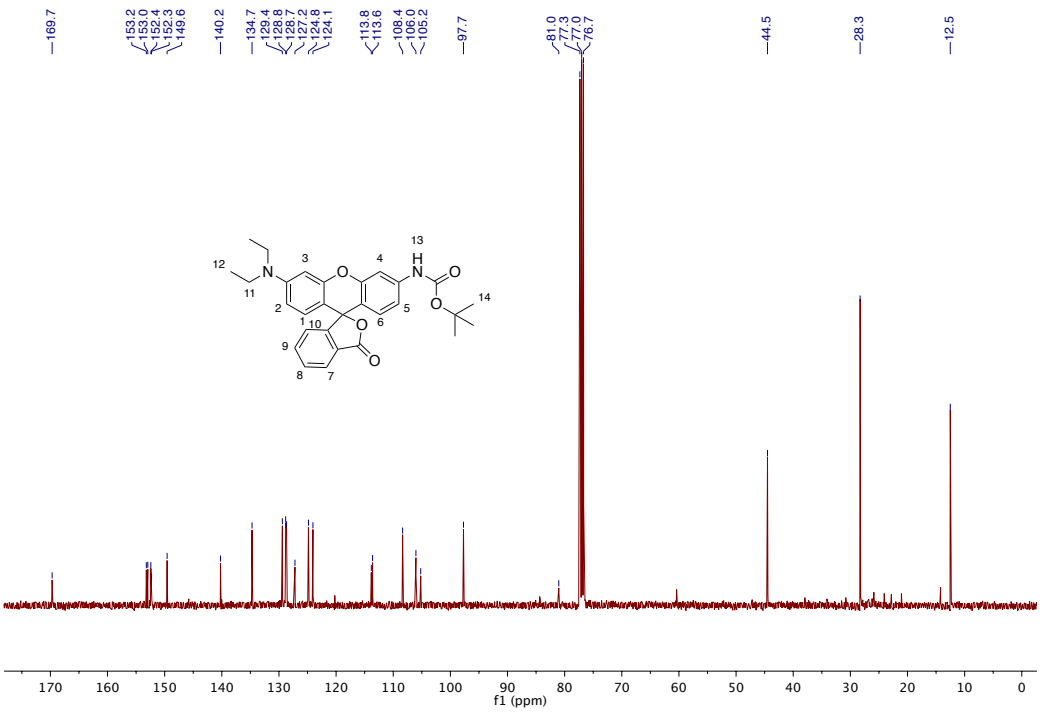

^{13}C NMR (101 MHz) of **S5** in $CDCl_3$..

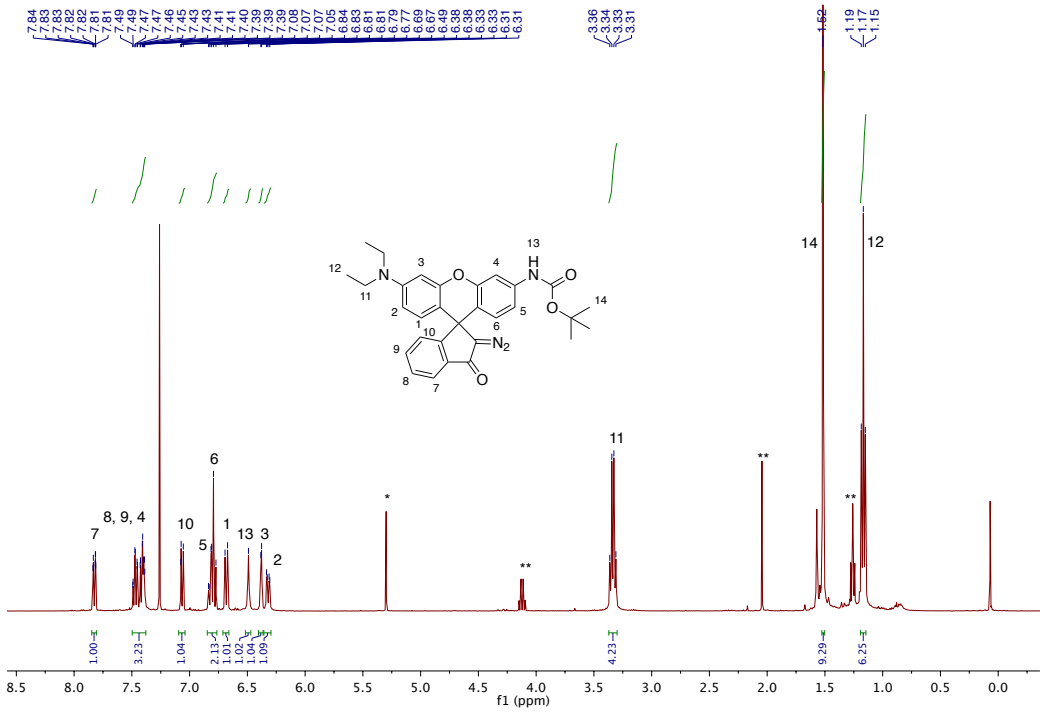

^{1}H NMR (400 MHz) of **S6** in $CDCl_3$. *CH_2Cl_2; **ethyl acetate.

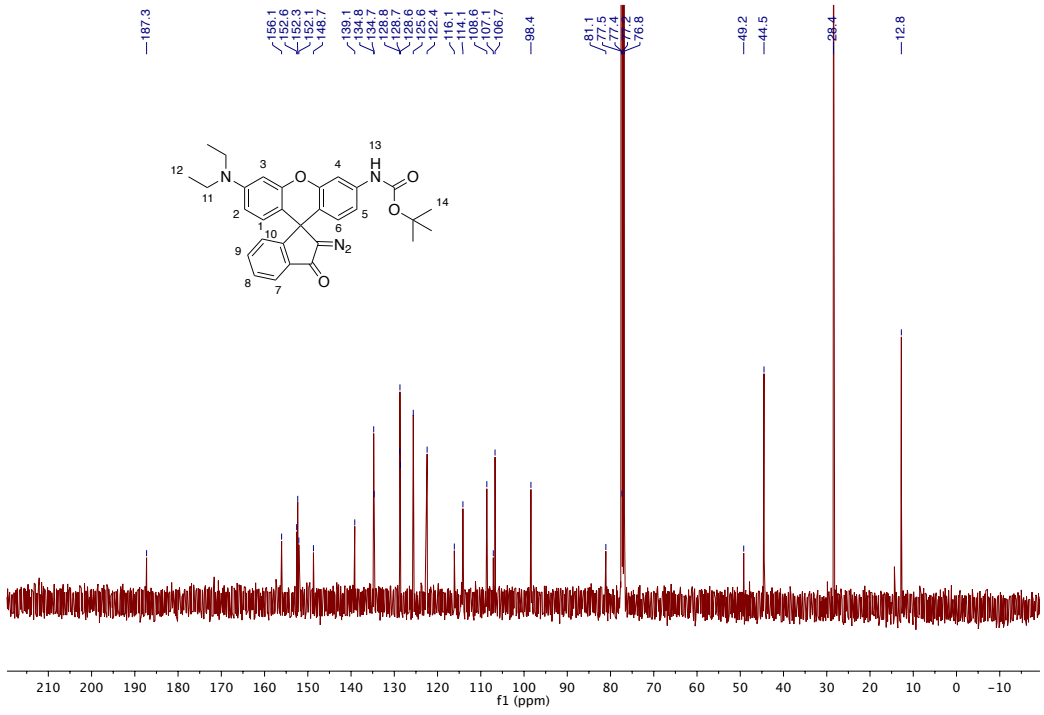

^{13}C NMR (101 MHz) of **S6** in $CDCl_3$.

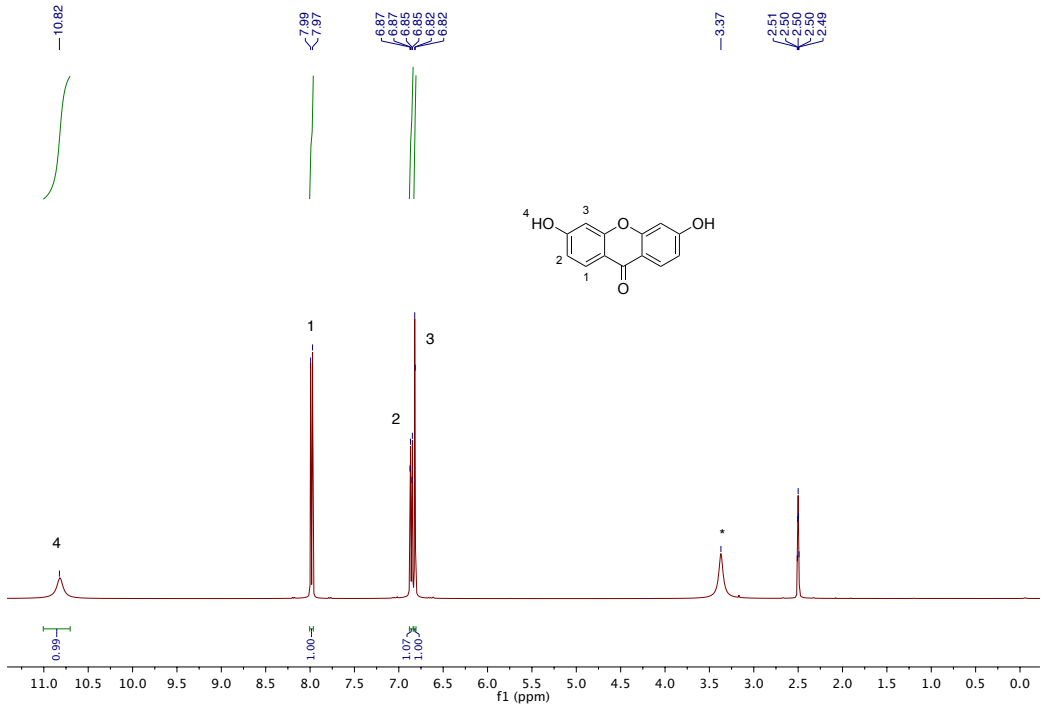

^{1}H NMR (400 MHz) of **S7** in $(CD_3)_2SO$. *H_2O.

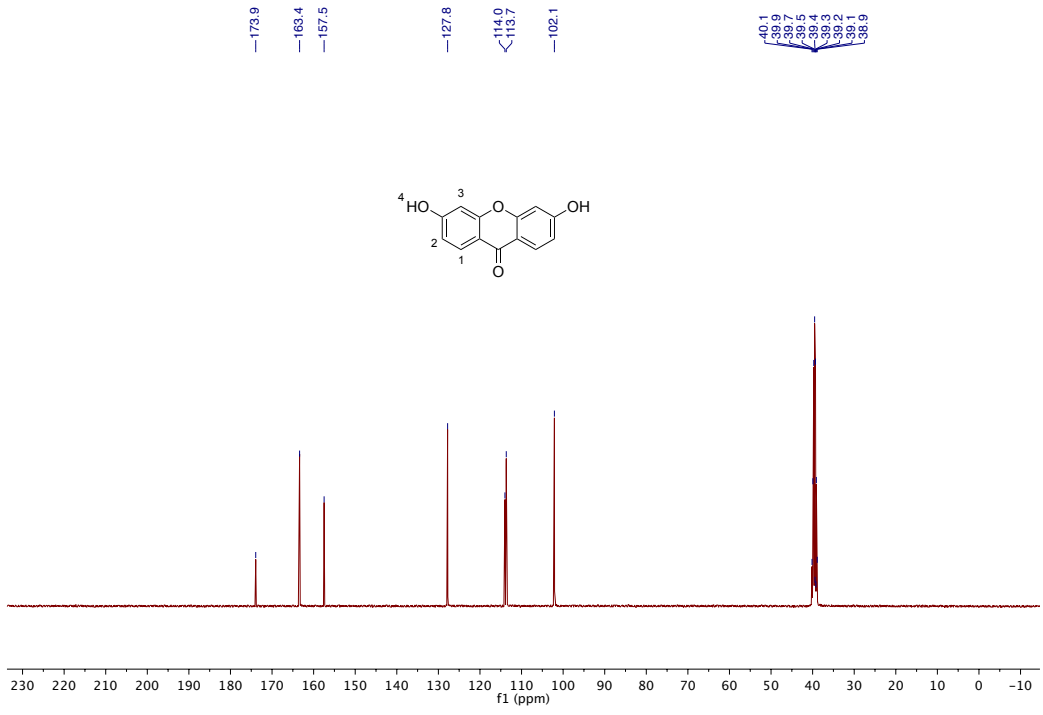

^{13}C NMR (101 MHz) of **S7** in $(CD_3)_2SO$.

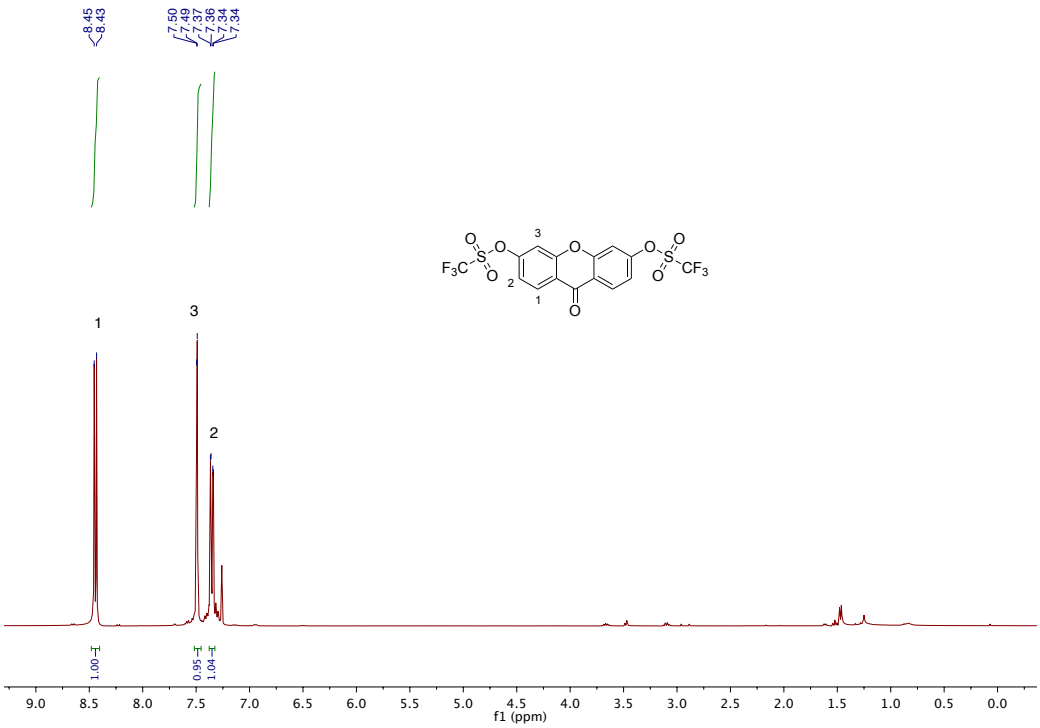

^{1}H NMR (400 MHz) of **S8** in $CDCl_3$.

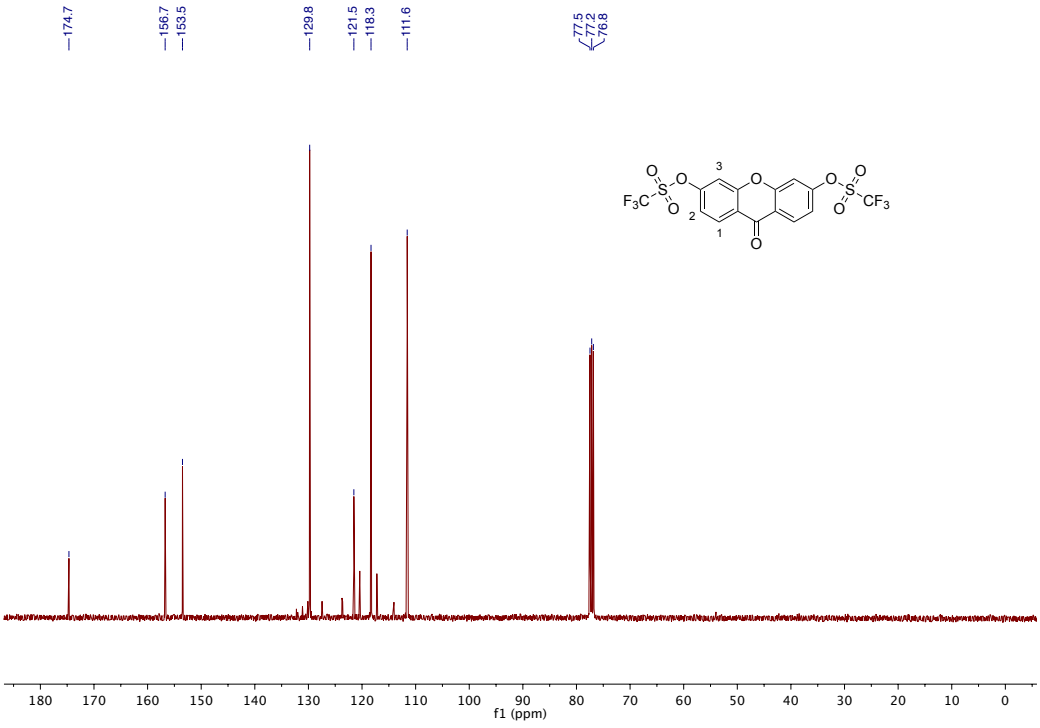

^{13}C NMR (101 MHz) of **S8** in $CDCl_3$.

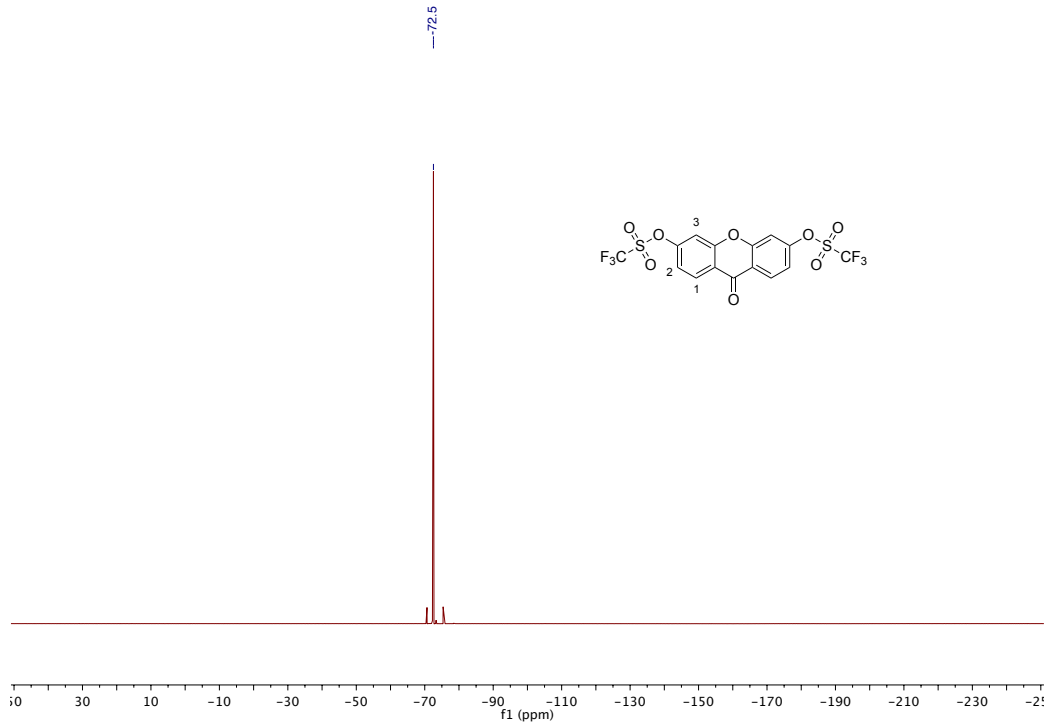

^{19}F (377 MHz) of **S8** in $CDCl_3$.

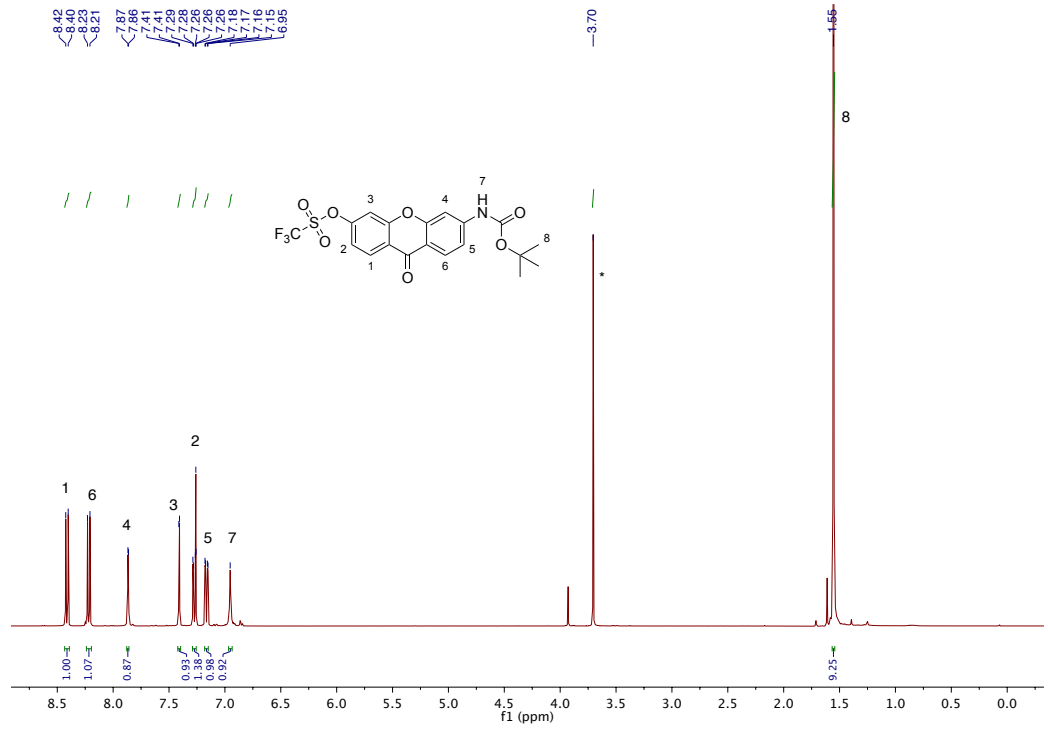

^{1}H NMR (400 MHz) of **S9** in $CDCl_3$. *Dioxane.

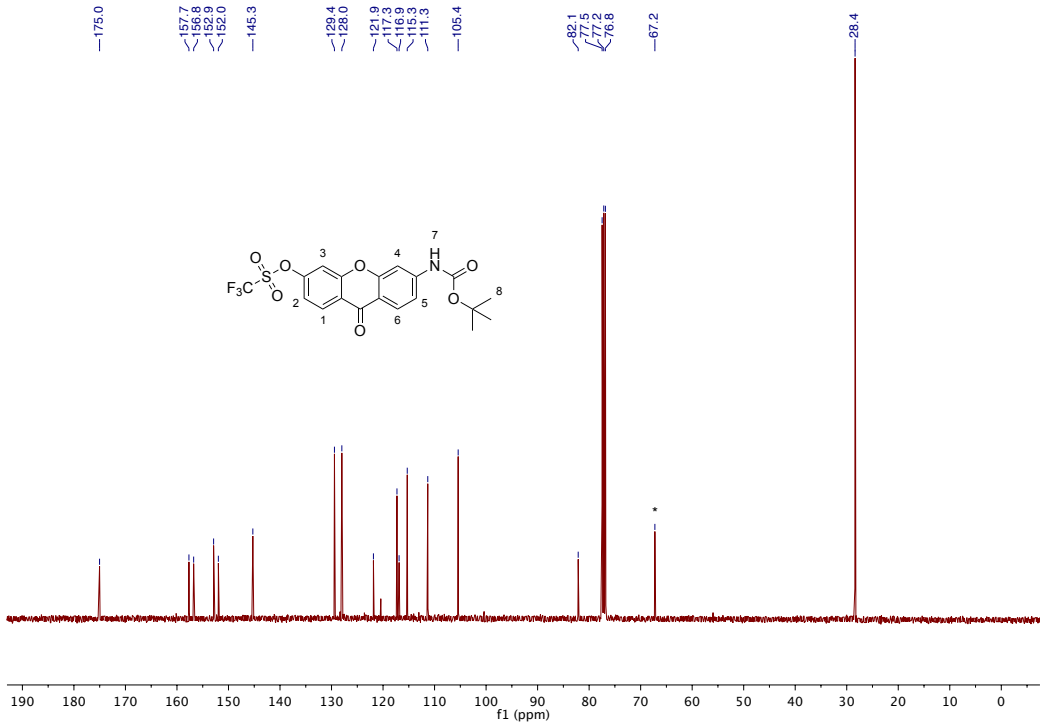

^{13}C NMR (101 MHz) of **S9** in $CDCl_3$. *Dioxane.

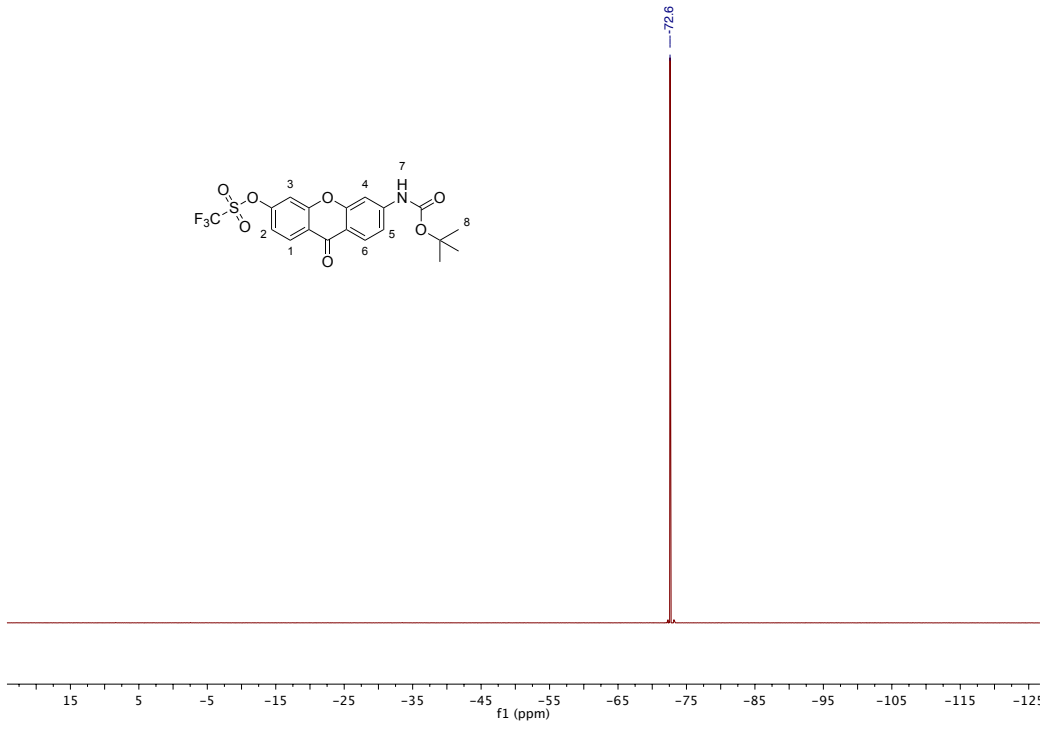

^{19}F (377 MHz) of **S9** in $CDCl_3$. *Dioxane.

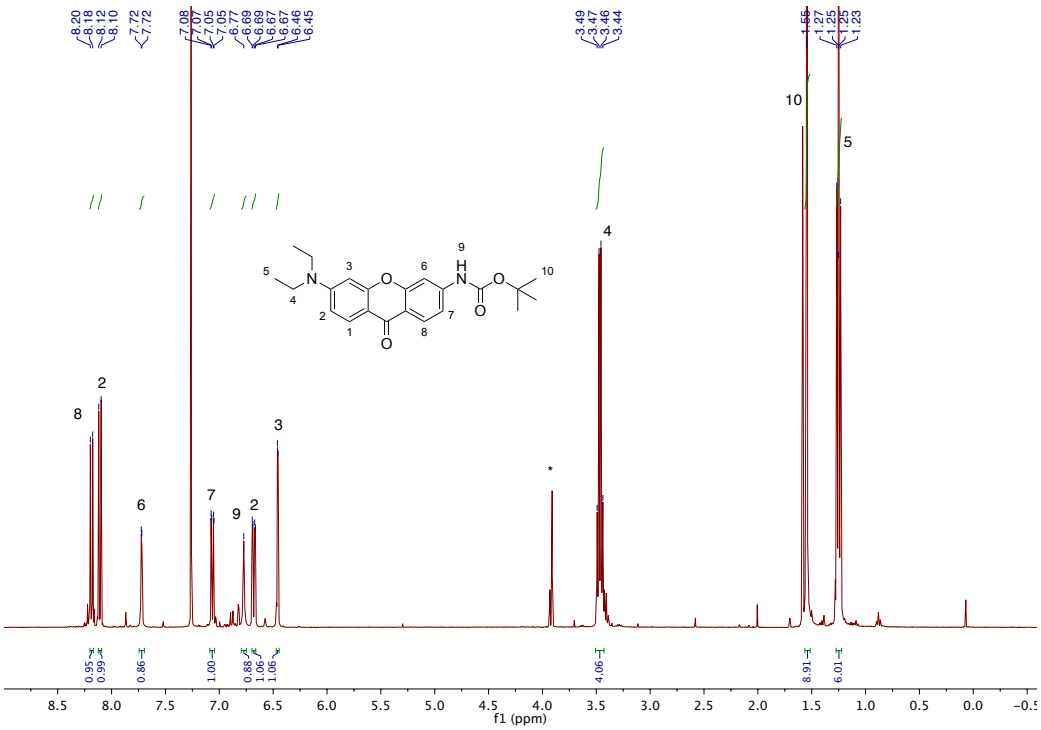

^{1}H NMR (400 MHz) of **S10** in $CDCl_3$. *Dioxane.

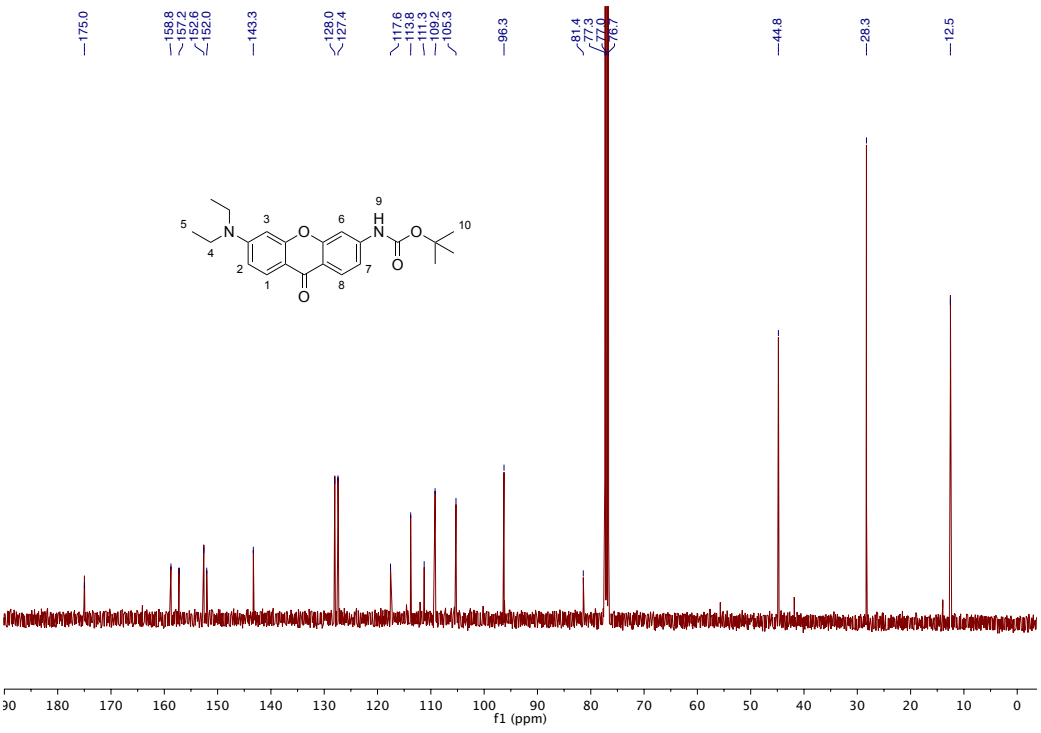

^{13}C NMR (101 MHz) of **S10** in $CDCl_3$. *Dioxane.

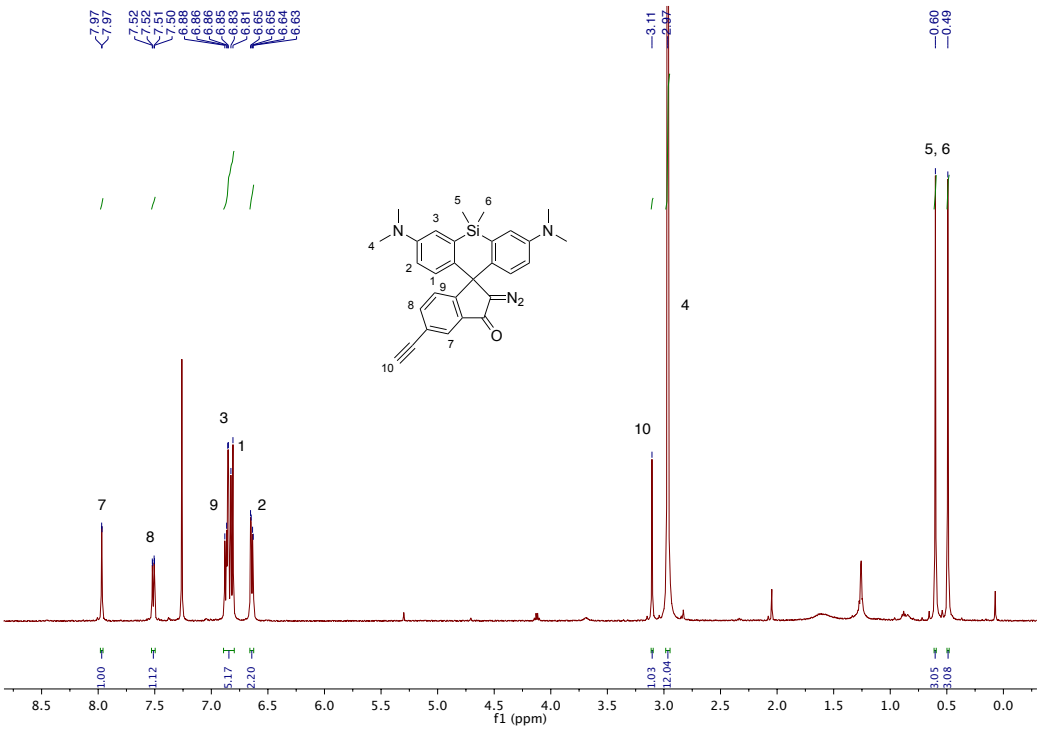

^{1}H NMR (500 MHz) of **S11** in $CDCl_3$.

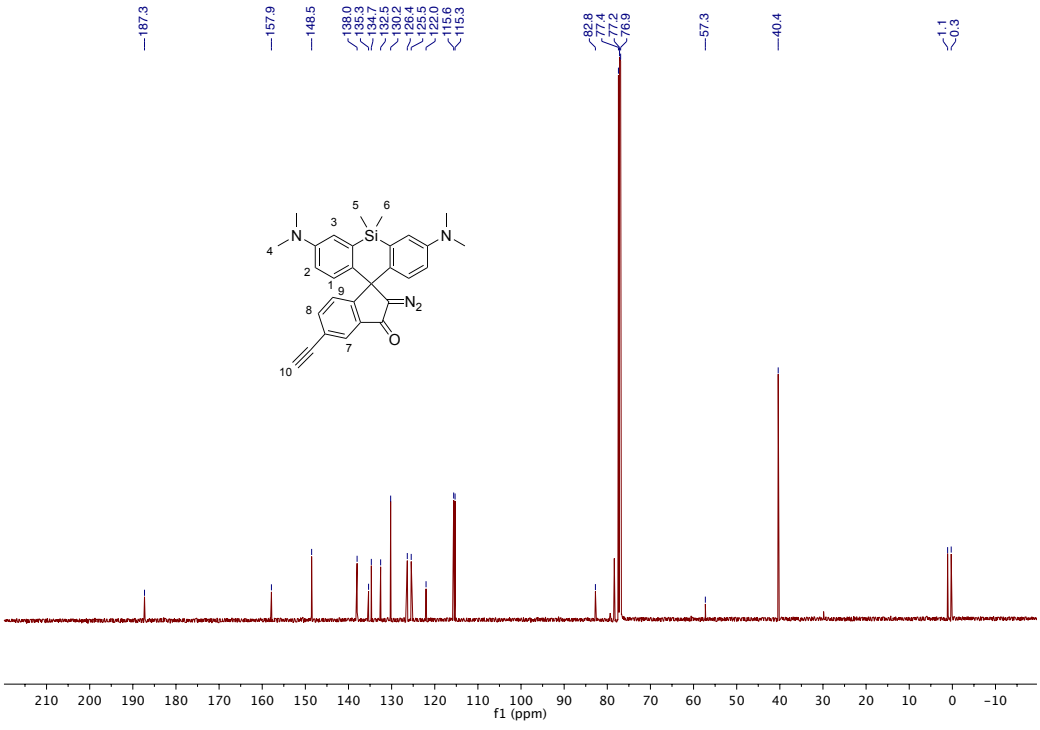

^{13}C NMR (126 MHz) of **S11** in $CDCl_3$.

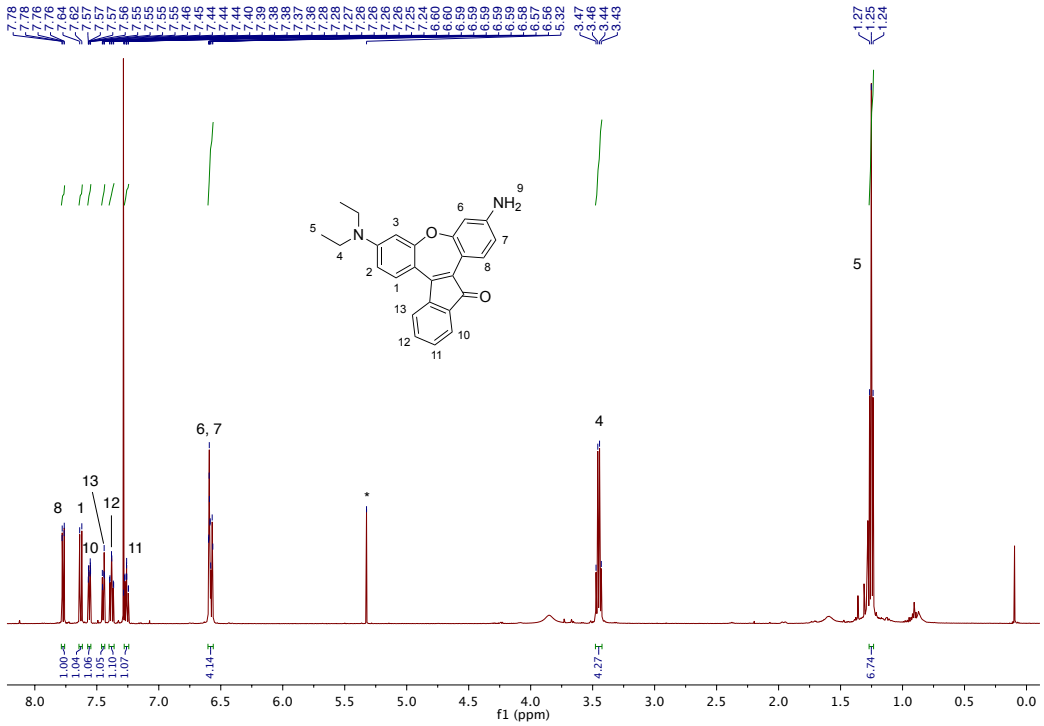

^{1}H NMR (500 MHz) of **S12** in $CDCl_3$.

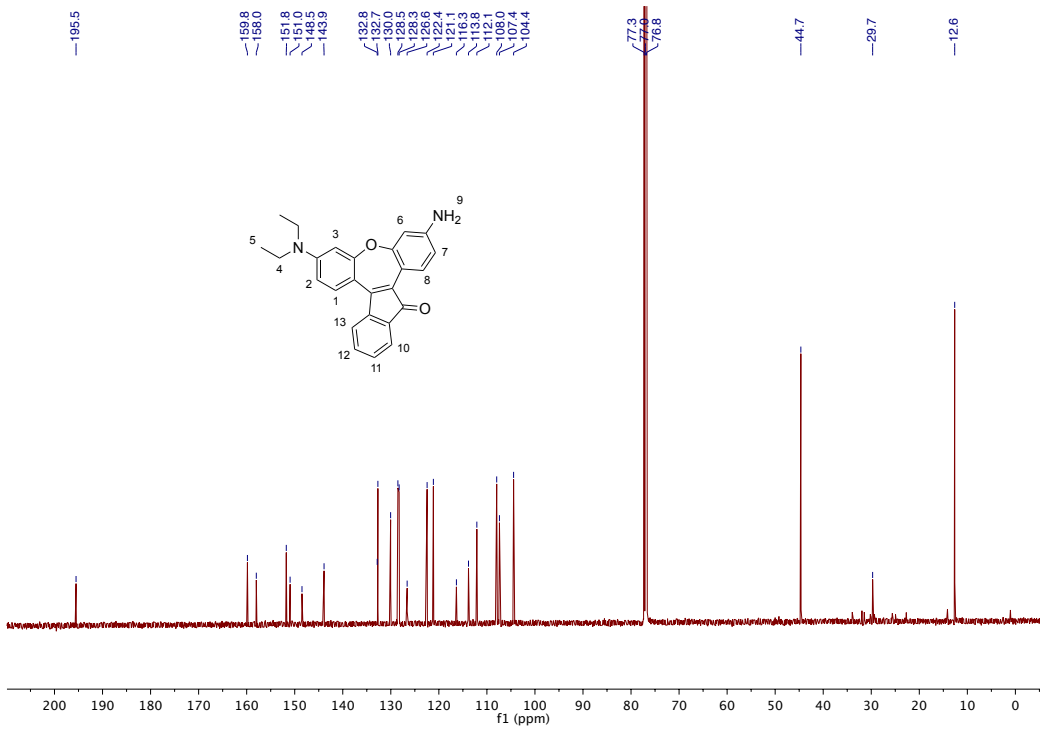

^{13}C NMR (126 MHz) of **S12** in $CDCl_3$.